

**EXPERIMENTAL AND ANALYTICAL STUDY TO MODEL
TEMPERATURE PROFILES AND STOICHIOMETRY
IN OXYGEN-ENRICHED IN-SITU COMBUSTION**

A Dissertation

by

JOSE RAMON RODRIGUEZ

Submitted to the Office of Graduate Studies of
Texas A&M University
in partial fulfillment of the requirements for the degree of

DOCTOR OF PHILOSOPHY

May 2004

Major Subject: Petroleum Engineering

**EXPERIMENTAL AND ANALYTICAL STUDY TO MODEL
TEMPERATURE PROFILES AND STOICHIOMETRY
IN OXYGEN-ENRICHED IN-SITU COMBUSTION**

A Dissertation

by

JOSE RAMON RODRIGUEZ

Submitted to the Office of Graduate Studies of
Texas A&M University
in partial fulfillment of the requirements for the degree of

DOCTOR OF PHILOSOPHY

Approved as to style and content by:

Daulat D. Mamora
(Chair of Committee)

Richard A. Startzman
(Member)

Jerome J. Schubert
(Member)

Brian J. Willis
(Member)

Stephen A. Holditch
(Head of Department)

May 2004

Major Subject: Petroleum Engineering

ABSTRACT

Experimental and Analytical Study to Model Temperature Profiles and Stoichiometry in Oxygen-Enriched In-Situ Combustion. (May 2004)

Jose Ramon Rodriguez, B.S., Universidad de Oriente, Venezuela;

M.S., Texas A&M University

Chair of Advisory Committee: Dr. Daulat D. Mamora

A new combustion zone analytical model has been developed in which the combustion front temperature may be calculated. The model describes in the combustion zone, the amount of fuel burned based on reaction kinetics, the fuel concentration and produced gas composition based on combustion stoichiometry, and the amount of heat generated based on a heat balance.

Six runs were performed in a 3-inch diameter, 40-inch long steel combustion tube with Jobo crude oil (9-11°API) from the Orinoco Belt in Venezuela. These runs were carried out with air containing three values of oxygen concentration, 21%, 30%, and 40%. The weight percentage of sand, clay, water, and oil in the sand mix was kept constant in all runs at 86.6%, 4.7%, 4.0%, and 4.7% respectively. Injection air rates (3 L/min) as well as the production pressure (300 psig) were kept constant in all runs.

The results indicate that the calculated combustion zone temperatures and temperature profiles are in good agreement with the experimental data, for the range of oxygen concentration in the injected air. The use of oxygen-enriched air slightly increased the combustion front temperature from 440°C in a 21 mole % O_2 concentration to a maximum of 475°C for air with 40 mole % O_2 concentration.

Oxygen-enriched air injection also increased the combustion front velocity from 13.4 cm/hr (for 21% oxygen) to 24.7 cm/hr (for 40% oxygen), thus reducing the start of oil production from 3.3 hours (for 21% oxygen) to 1.8 hours (for 40% oxygen). In the field, the use of oxygen-enriched air injection could translate into earlier oil production compared to not-enriched air injection.

The new analytical model for the combustion zone developed in this study will be beneficial to future researchers in understanding the effect of oxygen-enriched in-situ combustion and its implications on the combustion front temperature and combustion front thickness.

DEDICATION

To GOD, my guide

*To my wife Yadira, my daughters, Yadelys and Marielys, and my son Alejandro
for their companionship and patience during this period of time*

*To my parents, José Ramón and Ortensia. Their support and love have
always given me the strength to achieve my goals*

To my sister, Jenny

To all my aunts and cousins who were also my teachers at home

God bless you all

ACKNOWLEDGEMENTS

I would like to acknowledge and thank the following organizations and people:

PDVSA-CIED for sponsoring my graduate studies

Universidad de Oriente (UDO) for granting permission to enhance my academic background

My research advisor and *amigo*, Dr. Daulat D. Mamora, for his invaluable guidance and advice throughout this research at Texas A&M University

Dr. Richard Startzman, Dr. Jerome Schubert, and Dr. Brian Willis, for serving as committee members, and my external advisor Dr. Gonzalo Rojas (UDO), for their helpful comments, suggestions and insights

Jose Rivero, Delmira Ravago, Marco Ramirez, Angel Granado, Joyce Plazas, Cesar Valera, Carlos Rueda, Claudia Soto, Arief Hendroyono, Marpriansyah, Wan Dedi Yudistira, and Jeong Gyu Seo, my friends in the oil thermal recovery research group, for making my graduate years enjoyable and memorable

Texas A&M University for providing the facilities and resources in the Petroleum Engineering Department

Yadira, my wife, for being a part and giving me the most precious gift of all: a family with two daughters, Yadelys, and Marielys and one son, Alejandro; and for supporting me during the most challenging difficulties during my studies at Texas A&M University

TABLE OF CONTENTS

	Page
ABSTRACT	iii
DEDICATION	v
ACKNOWLEDGEMENTS	vi
TABLE OF CONTENTS	vii
LIST OF FIGURES	ix
LIST OF TABLES	xiii
CHAPTER	
I INTRODUCTION	1
1.1 Research objectives	3
II LITERATURE REVIEW	5
III EXPERIMENTAL APPARATUS AND PROCEDURE	12
3.1 Experimental apparatus	12
3.1.1 Fluid injection system	12
3.1.1.1 Nitrogen injection	12
3.1.1.2 Gas injection	12
3.1.2 Combustion tube	13
3.1.3 Fluid production system	18
3.1.4 Gas chromatograph and wet test meter system	24
3.1.5 Data measurement and recording system	24
3.2 Experimental procedure	24
IV EXPERIMENTAL RESULTS	30
4.1 Combustion run no. 2 (21% oxygen)	30
4.2 Combustion run no. 7 (21% oxygen)	42
4.3 Combustion run no. 3 (30% oxygen)	53
4.4 Combustion run no. 4 (30% oxygen)	64
4.5 Combustion run no. 5 (40% oxygen)	75
4.6 Combustion run no. 6 (40% oxygen)	86
V NEW COMBUSTION ZONE ANALYTICAL MODEL	97
5.1 Temperature profiles behind and ahead of the combustion zone	97
5.2 Combustion zone thickness model	99
5.3 Heat generated and lost in the combustion zone	102
5.4 Verification of model	105
5.4.1 Run no. 2 (21% oxygen)	105

CHAPTER	Page
5.4.2 Run no. 7 (21% oxygen).....	105
5.4.3 Run no. 3 (30% oxygen).....	105
5.4.4 Run no. 4 (30% oxygen).....	106
5.4.5 Run no. 5 (40% oxygen).....	106
5.4.6 Run no. 6 (40% oxygen).....	106
5.5 Summary of experimental results	119
VI STOICHIOMETRIC ANALYSIS	120
VII SUMMARY, CONCLUSIONS, AND RECOMMENDATIONS.....	126
7.1 Summary.....	126
7.2 Conclusions.....	126
7.3 Recommendations.....	127
NOMENCLATURE	128
REFERENCES	131
APPENDIX	135
VITA	150

LIST OF FIGURES

	Page
Fig. 1.1 Heat of combustion as a function of the H/C ratio, F_{HC} , of the fuel and the CO/CO_2 ratio in the produced gases.....	3
Fig. 2.1 Temperature and saturation profiles and the various zones formed during dry forward combustion.....	5
Fig. 3.1 Schematic diagram of experimental apparatus.....	14
Fig. 3.2 Combustion tube.....	15
Fig. 3.3 Dual-thermowell assembly.....	16
Fig. 3.4 Vacuum jacket.....	17
Fig. 3.5 Thermocouple sheaths.....	19
Fig. 3.6 Backpressure regulator.....	20
Fig. 3.7 Two-stage separation.....	21
Fig. 3.8 Condenser unit.....	22
Fig. 3.9 Acid scrubber and drierite columns.....	23
Fig. 3.10 HP 5890 Series II gas chromatograph and wet test meter.....	26
Fig. 3.11 Data logger and PC.....	27
Fig. 3.12 Complete view of the apparatus.....	28
Fig. 4.1 Combustion gas composition (run no. 2, 21% oxygen).....	32
Fig. 4.2 F_{HC} , CO_2/CO , and $CO/(CO+CO_2)$ ratios (run no. 2, 21% oxygen).....	33
Fig. 4.3 Temperature profiles (run no. 2, 21% oxygen).....	34
Fig. 4.4 Combustion front velocity (run no. 2, 21% oxygen).....	35
Fig. 4.5 Cumulative oil and water production (run no. 2, 21% oxygen).....	36
Fig. 4.6 Oil recovery (run no. 2, 21% oxygen).....	37
Fig. 4.7 Injection and production pressures, and injection rate (run no. 2, 21% oxygen).....	38
Fig. 4.8 Cumulative volume and produced gas rate (run no. 2, 21% oxygen).....	39
Fig. 4.9 Produced oil gravity (run no. 2, 21% oxygen).....	40
Fig. 4.10 Produced oil viscosity (run no. 2, 21% oxygen).....	41
Fig. 4.11 Combustion gas composition (run no. 7, 21% oxygen).....	43

	Page
Fig. 4.12 F_{HC} , CO_2/CO , and $CO/(CO+CO_2)$ ratios (run no. 7, 21% oxygen).	44
Fig. 4.13 Temperature profiles (run no. 7, 21% oxygen).	45
Fig. 4.14 Combustion front velocity (run no. 7, 21% oxygen).	46
Fig. 4.15 Cumulative oil and water production (run no. 7, 21% oxygen).	47
Fig. 4.16 Oil recovery (run no. 7, 21% oxygen).	48
Fig. 4.17 Injection and production pressures, and gas injection rate (run no. 7, 21% oxygen).	49
Fig. 4.18 Cumulative volume and produced gas rate (run no. 7, 21% oxygen).	50
Fig. 4.19 Produced oil gravity (run no. 7, 21% oxygen).	51
Fig. 4.20 Produced oil viscosity (run no. 7, 21% oxygen).	52
Fig. 4.21 Combustion gas composition (run no. 3, 30% oxygen).	54
Fig. 4.22 F_{HC} , CO_2/CO , and $CO/(CO+CO_2)$ ratios (run no. 3, 30% oxygen).	55
Fig. 4.23 Temperature profiles (run no. 3, 30% oxygen).	56
Fig. 4.24 Combustion front velocity (run no. 3, 30% oxygen).	57
Fig. 4.25 Cumulative oil and water production (run no. 3, 30% oxygen).	58
Fig. 4.26 Oil recovery (run no. 3, 30% oxygen).	59
Fig. 4.27 Injection and production pressures, and gas injection rate (run no. 3, 30% oxygen).	60
Fig. 4.28 Cumulative volume and produced gas rate (run no. 3, 30% oxygen).	61
Fig. 4.29 Produced oil gravity (run no. 3, 30% oxygen).	62
Fig. 4.30 Produced oil viscosity (run no. 3, 30% oxygen).	63
Fig. 4.31 Combustion gas composition (run no. 4, 30% oxygen).	65
Fig. 4.32 F_{HC} , CO_2/CO , and $CO/(CO+CO_2)$ ratios (run no. 4, 30% oxygen).	66
Fig. 4.33 Temperature profiles (run no. 4, 30% oxygen).	67
Fig. 4.34 Combustion front velocity (run no. 4, 30% oxygen).	68
Fig. 4.35 Cumulative oil and water production (run no. 4, 30% oxygen).	69
Fig. 4.36 Oil recovery (run no. 4, 30% oxygen).	70
Fig. 4.37 Injection and production pressures, and gas injection rate (run no. 4, 30% oxygen).	71

	Page
Fig. 4.38 Cumulative volume and produced gas rate (run no. 4, 30% oxygen).	72
Fig. 4.39 Produced oil gravity (run no. 4, 30% oxygen).	73
Fig. 4.40 Produced oil viscosity (run no. 4, 30% oxygen).....	74
Fig. 4.41 Combustion gas composition run (run no. 5, 40% oxygen).	76
Fig. 4.42 F_{HC} , CO_2/CO , and $CO/(CO+CO_2)$ ratios (run no. 5, 40% oxygen).	77
Fig. 4.43 Temperature profiles (run no. 5, 40% oxygen).	78
Fig. 4.44 Combustion front velocity (run no. 5, 40% oxygen).....	79
Fig. 4.45 Cumulative oil and water production (run no. 5, 40% oxygen).	80
Fig. 4.46 Oil recovery (run no. 5, 40% oxygen).	81
Fig. 4.47 Injection and production pressures, and gas injection rate (run no. 5, 40% oxygen).	82
Fig. 4.48 Cumulative volume and produced gas rate (run no. 5, 40% oxygen).	83
Fig. 4.49 Produced oil gravity (run no. 5, 40% oxygen).	84
Fig. 4.50 Produced oil viscosity (run no. 5, 40% oxygen).....	85
Fig. 4.51 Combustion gas composition (run no. 6, 40% oxygen).	87
Fig. 4.52 F_{HC} , CO_2/CO , and $CO/(CO+CO_2)$ ratios (run no. 6, 40% oxygen).	88
Fig. 4.53 Temperature profiles (run no. 6, 40% oxygen).	89
Fig. 4.54 Combustion front velocity (run no. 6, 40% oxygen).....	90
Fig. 4.55 Cumulative oil and water production (run no. 6, 40% oxygen).	91
Fig. 4.56 Oil recovery (run no. 6, 40% oxygen).	92
Fig. 4.57 Injection and production pressures, and gas injection rate (run no. 6, 40% oxygen).	93
Fig. 4.58 Cumulative volume and produced gas rate (run no. 6, 40% oxygen).	94
Fig. 4.59 Produced oil gravity (run no. 6, 40% oxygen).	95
Fig. 4.60 Produced oil viscosity (run no. 6, 40% oxygen).....	96
Fig. 5.1 Schematic diagram of the combustion zone model.	101
Fig. 5.2 Schematic diagram of the combustion front temperature model.....	104
Fig. 5.3 Verification of the combustion zone model (run no. 2, 21% oxygen).	107
Fig. 5.4 Observed and estimated temperature profiles (run no. 2, 21% oxygen).	108

	Page
Fig. 5.5	Verification of the combustion zone model (run no. 7, 21% oxygen). 109
Fig. 5.6	Observed and estimated temperature profiles (run no. 7, 21% oxygen). 110
Fig. 5.7	Verification of the combustion zone model (run no. 3, 30% oxygen). 111
Fig. 5.8	Observed and estimated temperature profiles (run no. 3, 30% oxygen). 112
Fig. 5.9	Verification of the combustion zone model (run no. 4, 30% oxygen). 113
Fig. 5.10	Observed and estimated temperature profiles (run no. 4, 30% oxygen). 114
Fig. 5.11	Verification of the combustion zone model (run no. 5, 40% oxygen). 115
Fig. 5.12	Observed and estimated temperature profiles (run no. 5, 40% oxygen). 116
Fig. 5.13	Verification of the combustion zone model (run no. 6, 40% oxygen). 117
Fig. 5.14	Observed and estimated temperature profiles (run no. 6, 40% oxygen). 118
Fig. 6.1	Combustion front velocity for all runs. 122
Fig. 6.2	Oil recovery for all runs..... 123
Fig. 6.3	Average API gravity of produced oil for all runs..... 124
Fig. 6.4	Average produced oil viscosity at 60°C for all runs. 125

LIST OF TABLES

	Page
Table 4.1 Sand pack properties of the combustion tube runs	31
Table 5.1 Summary of experimental results	119

CHAPTER I

INTRODUCTION

The term thermal Enhanced Oil Recovery (EOR) comprises those techniques in which heat is purposely introduced into an oil-bearing formation primarily to reduce oil viscosity and therefore improve recovery of oil. Heat may be introduced into the oil-bearing formation as steam or hot water, or it may be generated in the reservoir by a process called in-situ combustion. Because the main objective of thermal EOR methods is to reduce oil viscosity, these are mostly applied to reservoirs containing viscous and heavy oils.

In-situ combustion was the first EOR process to be developed.¹ In-situ combustion tube laboratory experiments were conducted as early as 1947^{2,3}, and important field tests performed by 1958.⁴⁻⁶ The first commercial operation of the in-situ combustion process began in 1959.⁷

The advantages of in-situ combustion over other thermal recovery methods lay primarily in that the heat is generated within the reservoir, thus no heat losses occur at the wellbore. Furthermore, this attribute allows the application of this recovery method at greater depth than the use of steam or hot water, where heat is generated at the surface and has to travel along the wellbore into the reservoir. In-situ combustion also has higher energy transfer properties, as temperatures can reach well above 350°C.

In-situ combustion also carries inherent disadvantages over other thermal recovery methods such as safety issues that are magnified by the higher temperatures and chemical reactions occurring within the reservoir, and/or chemical reactions taking place in the tubing and casing of the injection or producing well. Corrosion can be a problem, when the injected gas has not been dehydrated, as well as flue gas with high sulfur content that can create corrosion problems in the production well. Air compressor reliability is also a factor to take into account; if a compressor stops, no gas is injected and the combustion front will eventually die.

This dissertation follows the style and format of the *Journal of Petroleum Technology*.

One form of in-situ combustion is dry, forward combustion. In this process, air is injected into an oil reservoir, igniting it in-situ and the resulting combustion front moves away from the injection well. The heat generated at the combustion front propagates, by conduction and convection, through the reservoir towards the production well, reducing the oil viscosity and thereby increasing the oil production rate and recovery.

Another form of in-situ combustion is wet combustion, in which air and water are injected concurrently or alternately. A third variation of the in-situ combustion process is called reverse combustion. In this technique, the combustion zone is initiated at the production well. The reverse combustion front travels countercurrent to the air towards the injection well, where air is injected. The oil flows towards the production well, through the combustion zone.

Initial models to describe the in-situ combustion process were analytical heat transfer models.⁸⁻¹⁴ Subsequent models have included the kinetics of lumped reactions: a steady-state model¹⁵ and a model for simulation of combustion tube experiments, which incorporates thermal cracking and low-temperature oxidation.^{16,17} Numerical simulation models have been developed in which the physical and chemical reactions are described by basic kinetic relationships.¹⁸⁻²⁰

A variation of the dry, forward combustion process is called in-situ combustion with oxygen-enriched air, which consists of the injection of air with an oxygen concentration greater than 21 mole %. The advantages of oxygen-enriched air injection to air injection are, amongst others, the increased heat released at the combustion front as a product of the decreased carbon monoxide to carbon dioxide ratio in the produced gases, the miscibility of a higher carbon dioxide concentration in the oil, and finally a lower oxygen partial pressure leading to lower compression costs. Oxygen-enriched air injection is expected to primarily increase the combustion front temperature and amount of heat released as the oxygen concentration in the injected gas increases, thus decreasing operational costs, and possibly affecting the combustion reaction stoichiometry; however, the cost of higher oxygen concentration is the main drawback.

The proposed research aims at developing a method to estimate the combustion front temperature based on the amount of heat released by the combustion front, the fuel concentration available to maintain a constant rate propagation of the front through the combustion tube, and on the ratio of carbon monoxide to carbon dioxide (CO/CO_2) in the produced gases. As can be noted in **Fig. 1.1**, the heat of combustion increases as the CO/CO_2 ratio, β , decreases. This is expected to occur when oxygen-enriched air is injected during the in-situ combustion process. Finally, an analytical model⁸⁻¹⁴ can be used to evaluate the temperature profile behind and ahead of the combustion front.

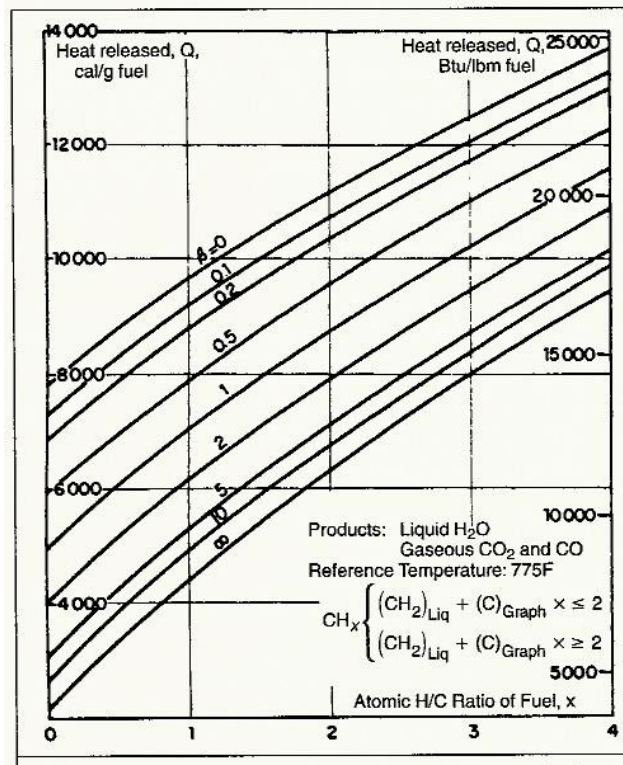


Fig. 1.1—Heat of combustion as a function of the H/C ratio, F_{HC} , of the fuel and the CO/CO_2 ratio in the produced gases.²¹

1.1 Research objectives

Experimental data will be acquired utilizing a vertical combustion tube containing a uniform mixture of sand, clay, oil and water. Upon ignition, air ($O_2 + N_2$) is injected at

the top of the cell and product gases and liquids (oil and water) are produced at the bottom of the cell. Volumes of produced fluids and gas composition are measured as well as temperature profiles in the combustion tube.

The main objectives of my research are as follows:

- A. Develop an analytical model of the combustion zone to determine the combustion temperature and combustion thickness.
- B. Describe the temperature profile ahead and behind the combustion front. This will be based on Penberthy's model,¹³ and will be linked to the combustion temperature model in objective A.
- C. Evaluate the effect of oxygen concentration in the injected gas on the stoichiometry of the combustion process.

This dissertation is presented in seven chapters as follows:

- I. The introduction summarizes thermal EOR and the research objectives.
- II. A literature review, which presents an examination of the dry-forward in-situ combustion process and previous experimental studies on oxygen-enriched in-situ combustion.
- III. Chapter on experimental apparatus and procedure, in which the experimental facility is described and the methodology used to acquire data is presented.
- IV. The experimental results are presented and discussed.
- V. The newly developed combustion front temperature model is described.
- VI. The stoichiometric analysis to describe the behavior of oxygen-enriched in-situ combustion is discussed.
- VII. The final chapter presents a summary of the work, and the conclusions and recommendations.

CHAPTER II

LITERATURE REVIEW

The representation of the temperature and saturation profiles and the various zones that are formed during dry, forward in-situ combustion are shown in **Fig. 2.1**.^{22,23}

As the temperature in a volume element of the reservoir rises, water and light hydrocarbons will be the first liquids to be vaporized. These vapors are carried along with the gas stream and will condense in colder regions ahead of the combustion front. The condensation of the water vapors will form a water bank (F), followed by an oil bank of the condensed light hydrocarbons (G). The steam-liquid, two-phase flow region is the steam plateau (E). The oil in the volume element can undergo a process called thermal cracking when the temperature is higher than 350°C. This thermal process will form a volatile fraction and a heavy residue (C and D). The volatile fraction is carried in the gas stream, while the heavy residue constitutes the fuel necessary to maintain the combustion

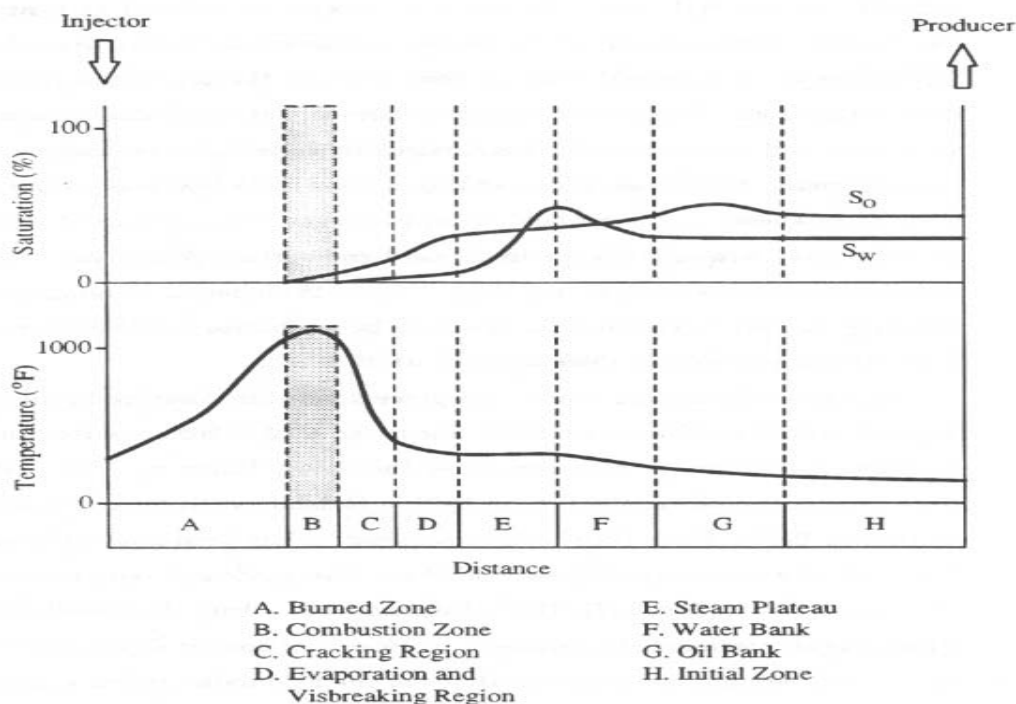


Fig. 2.1—Temperature and saturation profiles and the various zones formed during dry forward combustion.²³

front. The heat generated in this combustion zone (B) is conducted ahead through the formation matrix, and convected by the vapor and liquids. As the combustion front moves, a burned zone of clean sand is left behind where only the injection gas flows (A).

The use of wet combustion as an in-situ combustion process began at the moment in which it was recognized that much of the heat stored in the rock during the dry, forward combustion behind the combustion front was being lost to the adjacent formations. Thus wet combustion was developed to improve the efficiency of forward combustion by simultaneous or alternate injection of air and water during the combustion process. This process is called COFCAW, combination of forward combustion and water. When the injection of air and water occurs simultaneously, water initially will fill partly the region behind the combustion front. Water saturation will eventually increase and will be displaced into the heated regions where it will be converted to superheated steam. The additional energy provided by the superheated steam will mix with the combustion gases and volatile hydrocarbons ahead of the combustion front, where a large condensation zone will be formed. This condensation zone can travel up to three times faster than the combustion zone and can create an extended region of steam distillation ahead of the combustion front.

The main parameters required in the design of an in-situ combustion project are:²⁴ the fuel concentration per unit reservoir volume burned, the composition of the fuel, the amount of air required to burn the fuel, the volume of reservoir swept by the combustion zone, the required air-injection rates and pressures, the oil production rate and recovery, the investment, and operating costs.

Data from combustion tube experiments form the main basis for determining these design parameters. Nelson and McNeil²⁵ have described a method for calculating some of these parameters.

The rate of propagation of the combustion front, and therefore, the overall in-situ combustion process can be described by a simple reaction consisting of two competitive steps: fuel deposition, and fuel combustion.²⁶⁻²⁸ A third reaction, low-temperature

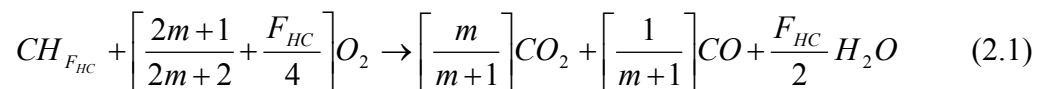
oxidation (LTO) may be involved if oxygen is present downstream of the combustion front.

In-situ combustion with oxygen-enriched air consists of the injection of air with an oxygen concentration greater than 21 mole %. Literature on this area is rather scarce, where there is a big gap in information from the mid '70s to the mid '80s for in-situ combustion in general.

Moss and Cady²⁹ conducted combustion tube experiments with oxygen-enriched air (94.33 mole % O_2) and air (21 mole % O_2) and obtained combustion front temperatures of 515 and 482°C respectively. Hansen *et al.*³⁰ carried out experimental work with light crude oil and found that as the oxygen concentration increased (40, 60, 80, and 95 mole % O_2), the CO_2 content and combustion front velocity increased. They also found that the time to produce the initial oil decreased. Shahani and Hansel³¹ found that for the heavy oil crude oil examined, high O_2 concentrations reduced the apparent coke loading and increased the rate of oil production.

Petit³² evaluated the effect of total pressure, oxygen partial pressure, and injected oxygen flux in combustion tube experiments with two different oils (specific gravities of 0.90 and 0.96). Fuel availability and the air requirement at the front were found to be slightly affected by the oxygen partial pressure at a constant oxygen flux at low pressure (145 psig). Petit³² also noted that an increase in oxygen concentration at higher total pressure (1015-1045 psig) and at constant oxygen flux caused a 40% reduction of oxygen requirement at the front for the lighter oil, but hardly affected the characteristics of combustion of the heavier oil.

Fuel combustion is described by Benham and Poettmann³³ in terms of the following stoichiometric equation:



where F_{HC} is atomic hydrogen-to-carbon ratio, m is the ratio of moles of CO_2 to CO produced, and $CH_{F_{HC}}$ is the fuel molecular weight.. They also derived an expression for

the combustion front velocity as a function of the air flux, fuel concentration, oxygen utilization efficiency, hydrogen to carbon ratio, and the ratio of CO_2 to CO produced, m ;

$$V_f = \frac{E_{O_2} O_{2i} U_a}{379 F_c} \frac{(12 + F_{HC})}{\left[\frac{2m+1}{2m+2} + \frac{F_{HC}}{4} \right]} \quad (2.2)$$

where E_{O_2} is the oxygen utilization efficiency, U_a is the injected air flux, O_{2i} is the injected oxygen concentration, and F_C is the fuel concentration.

The air requirement, a_R , is defined as the standard volume of air required to burn a unit volume of reservoir. The combustion front can advance only if it consumes fuel; therefore air requirement is directly proportional to fuel availability. Mathematically, air requirement is defined as:

$$a_R = \frac{379}{E_{O_2} O_{2i}} \left[\frac{2m+1}{2m+2} + \frac{F_{HC}}{4} \right] \frac{F_c}{(12 + F_{HC})} \quad (2.3)$$

Note then, that the combustion front velocity is:

$$V_f = \frac{U_a}{a_R} \quad (2.4)$$

Fuel concentration, F_C , is the mass of burned fuel per unit volume of reservoir, where the mass of fuel burned can be expressed in terms of combustion stoichiometry as:

$$m_f = (12 + F_{HC})(m+1)CO n_p \quad (2.5)$$

Here n_p represents the mass of moles produced during the combustion process, and it is estimated based on the total volume of produced gas. If this volume is given at standard conditions, then it will be necessary to convert volume to moles using the molar volume constant at standard conditions:

$$n_p = \frac{\text{Total Produced Volume [scf]}}{379 \left[\frac{\text{scf}}{\text{lbm mol}} \right]} \quad (2.6)$$

Kinetics reaction of in-situ combustion process, describe the rate of oxidation of crude oils in a porous media. The rate of oxygen consumption to the rate of crude oxidation can be written following Mamora as: ³⁴⁻³⁶

$$\frac{qO_{2c}}{AL} = ArP_{O_2}^m F_C^n \exp\left(-\frac{E}{RT}\right) \quad (2.7)$$

where q is the volumetric flow rate, O_{2c} is the molar concentration of oxygen consumed, A and L are the cross-sectional area and length of the sand mix in the combustion tube, Ar is the pre-Arrhenius constant, P_{O_2} is the oxygen partial pressure, E is the activation energy, R is the universal gas constant, T is the absolute temperature, and m and n are the reactions orders with respect to P_{O_2} and F_C respectively.

An important aspect of the above equation is that in the combustion zone the only parameters that are changing are O_{2c} and F_C . Therefore, under the assumption of same operating conditions in the combustion zone, the amount of oxygen consumed, O_{2c} , is directly proportional to the fuel concentration, F_C , and/or the mass of burned fuel, m_f , thus:

$$O_{2c} \propto m_f \quad (2.8)$$

Furthermore, oxygen consumption is also directly proportional to the concentration of injected oxygen, hence;

$$O_{2i} \propto m_f \quad (2.9)$$

Penberthy¹³ considered relevant characteristics of combustion tube experiments and assumed that:

1. The burning front moves axially at constant velocity and temperature under constant air flux.
2. The temperature is constant radially within the combustion tube but heat may be lost to the exterior.
3. Convection and conduction are important heat transfer events within the combustion tube.
4. The combustion front is considered planar (of zero thickness).
5. The convection coefficient between gas and the adjacent sand is infinitely large.
6. Thermal and physical properties are independent of temperature.

Under these assumptions Penberthy¹³ derived the following equation for the region ahead of the burning front:

$$\frac{k}{\rho_m C_m} \frac{\partial^2 T}{\partial x^2} + \left(V_f - \frac{\rho_g C_g U_a}{\rho_m C_m} \right) \frac{\partial T}{\partial x} - \frac{2U}{\rho_m C_m r_t} (T - T_a) = \frac{\partial T}{\partial t} \quad (2.10)$$

for the following initial and boundary conditions;

$$T(x, 0) = 0 \quad (2.11)$$

$$T(0, t) = T_c \quad (2.12)$$

$$\lim_{x_D \rightarrow \infty} \frac{\partial T_D}{\partial x_D} = 0 \quad (2.13)$$

where k is the thermal conductivity, C_f is the specific heat of the matrix, C_g is the specific heat of air, ρ_m is the density of the matrix, U_a is the air flux, T is the temperature, T_a is the ambient temperature, x is the distance from the burning front, U is the overall heat transfer coefficient through the annular insulation, r_t is the radius of the combustion tube, t is time, and V_f is the velocity of the burning front.

Again, the attention is drawn back to **Fig. 1.1**. Burger and Sahuquet²³ considered that the carbon deposited on the reservoir matrix was the product of the pyrolysis of crude oil:



From bond energies, Eq. 2.1 and Eq. 2.14, the heat generated during the combustion of the fuel is given by the following expression:

$$\Delta H_c = \frac{1800}{12 + F_{HC}} (94.0 - 67.9m' + 31.2F_{HC}) \quad (2.15)$$

Further considerations in stoichiometry of the combustion process will be given in chapters 5 and 6, as well as brief descriptions of the temperature profile model behind and ahead of the combustion zone.

Recently, the term air injection is being utilized to describe an enhanced oil recovery technique for light and heavy oils, in which air is injected into mainly deep reservoirs in

order to either create miscibility of nitrogen in the crude oil (if high pressures are required) and/or to expect for spontaneous ignition to occur. Since the process is mostly used in deep, high pressure fields, the high temperatures in the reservoir may provide sufficient energy to spontaneously ignite the crude oil, creating an in-situ combustion process under low temperature oxidation.

Greaves *et al.*³⁷ conducted kinetic and combustion tube experiments in different types of oils and concluded that the air injection under low temperature oxidation process can be considered for application to all light oils with sufficiently high reactivity.

Turta and Singhal³⁸ proposed a new classification for air injection processes taking into account the achievement of miscibility between oil and nitrogen and the dominance of high temperature oxidation or low temperature oxidation. According to this classification, in-situ combustion is an immiscible airflooding with high temperature oxidation associated to heavy oil exploitation.

CHAPTER III

EXPERIMENTAL APPARATUS AND PROCEDURE

3.1 Experimental apparatus

The experimental set-up is comprised of five main parts: fluid injection system, combustion tube, fluid production system, gas chromatograph and wet test meter system, and data recording system. A schematic diagram of the apparatus is shown in **Fig. 3.1**.

3.1.1 Fluid injection system

The fluid injection system consists of two parts: nitrogen injection, and air (normal or oxygen-enriched) injection. Both paths are independent (through 1/4 in. tubing) and are opened or closed to the system with valves in the control panel. The injected nitrogen or air rate is controlled by a mass flow controller, installed before the injection pressure transducer. The 1/4 in. tubing line is reduced with swagelok fittings to 1/8 in. tubing line, which is the gas inlet to the combustion tube.

3.1.1.1 Nitrogen injection

Nitrogen is used to flush the system before any combustion run allowing it to flow through the mass flow controller into the combustion tube. Nitrogen is also used to pressurize the combustion tube by closing the pressure regulator and the end of the production stream. At the end of the combustion run, nitrogen is injected into the system to flush and cool down the tube.

3.1.1.2 Gas injection

In this dissertation, the term air is used to refer to any mixture of oxygen and nitrogen. Air is injected at constant rate of 3 L/min throughout the combustion run. A cylinder with the desired oxygen concentration is connected to the injection system. When the temperature at the clean sand-mixture pack interface reaches approximately 570°F (300°C), air is allowed to flow at 3 L/min into the combustion tube to start ignition and to maintain combustion. The injection will continue until the front reaches the bottom

of the combustion tube (no more liquids are produced). At this instance, injection is switched to nitrogen.

3.1.2 Combustion tube

The combustion tube (**Fig. 3.2**) is a stainless steel cylinder with an external diameter of 3 in. (7.62 cm), a width of 1/16 in. (0.16 cm) and a length of 40-1/8 in. (101.92 cm). Sharp-edged flanges seal the ends of the cell to copper gaskets. A 12-1/2 in long x 3/4 in. tube was silver soldered to the center of the top flange, and a 1 in. x 3/4 in. swagelok fitting was machined and silver soldered to it. The assembly provided the path for the introduction of two 3/16 in. thermowells (**Fig. 3.3**), the one corresponding to a fixed set of thermocouples was 57-3/8 in. long, the other 56-1/2 in. long. Another tube, 10 in. long x 5/16 in. was soldered off-center on the top flange to allow air injection into the combustion tube through a reduction of swagelok fitting to a 1/8 in. inlet. A 10 in. long x 5/16 in. tubing was silver soldered to the bottom flange of the combustion tube to allow the collection of fluids in the production system.

The combustion tube is placed inside the vacuum jacket (**Fig. 3.4**), a 6-1/2 in. internal diameter tube (8 in. external diameter) 46 in. long. The jacket is wrapped with electric band heaters and covered with a one inch thick insulation. Flanges seal the end of the vacuum jacket to rubber o-rings. A connection installed at the top flange of the jacket provides electric current to the resistance igniter, and drilled holes allow the insertion of the top tubing end of the combustion cell. The bottom flange also allows the insertion of the bottom end of the combustion cell and also provides a tubing connection for vacuum purposes. The vacuum jacket is isolated from the combustion cell with Teflon ferrules installed in both flange ends. The exterior of the vacuum jacket is an aluminum cover with respective aluminum end caps. The center of the jacket is connected to a swivel that allows it to be rotated from the horizontal to vertical position.

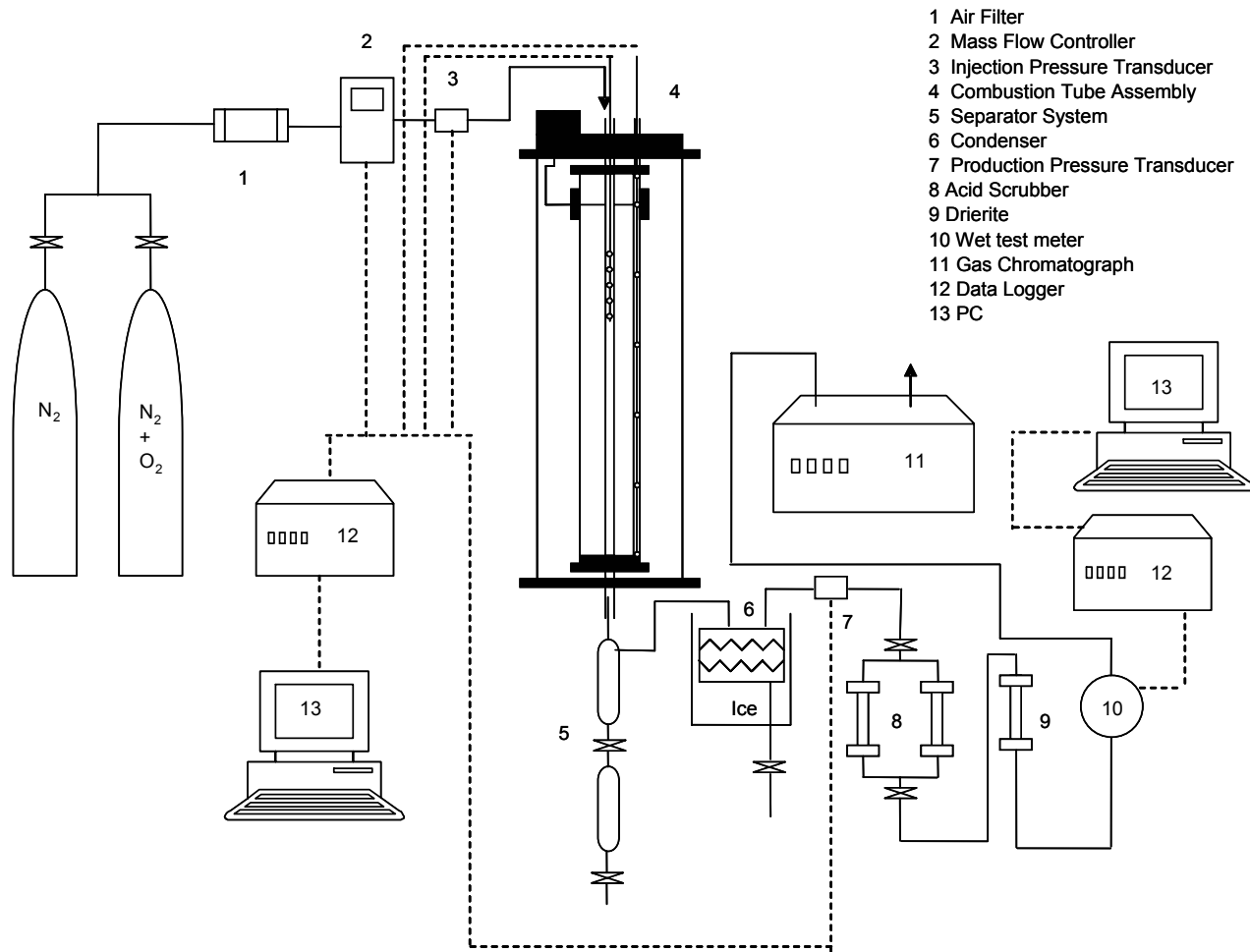


Fig. 3.1—Schematic diagram of experimental apparatus.



Fig. 3.2—Combustion tube.



Fig. 3.3—Dual-thermowell assembly.

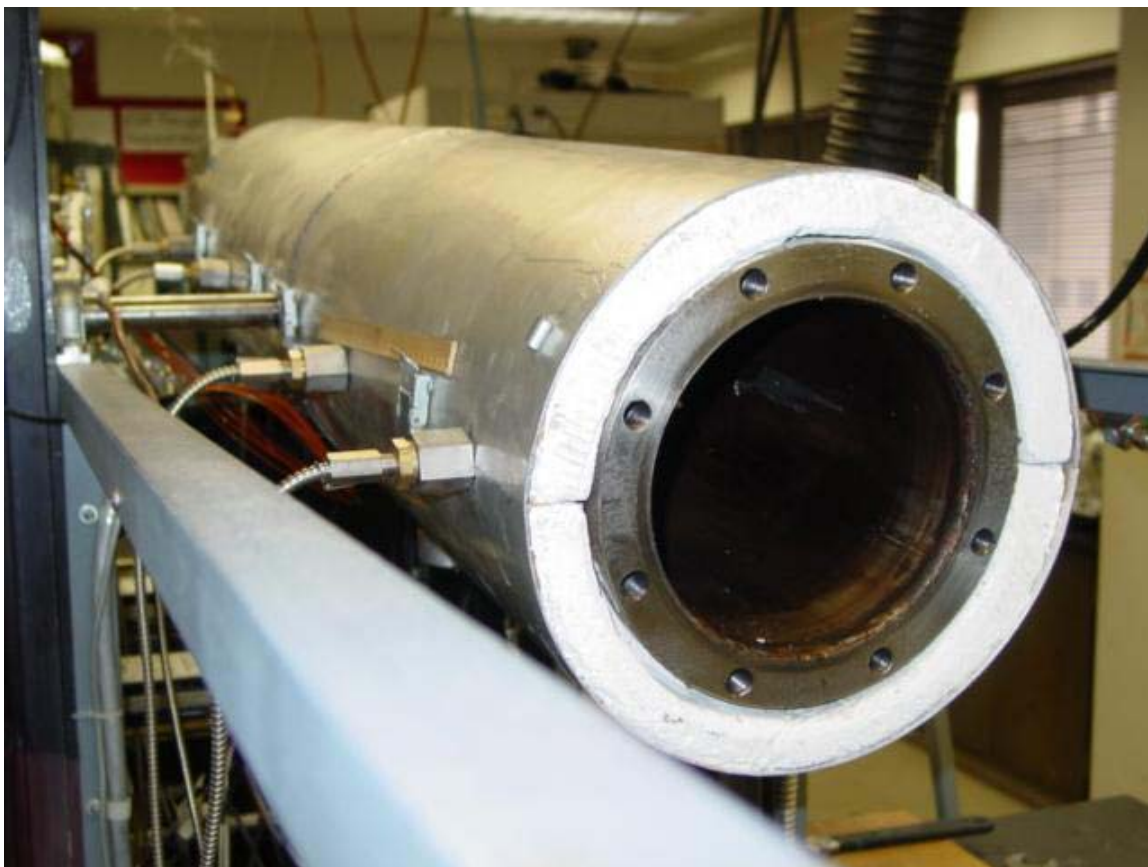


Fig. 3.4—Vacuum jacket.

One set of eight fixed J-type thermocouples (spaced 14.1 cm apart) runs through the assigned thermowell end and a set of six movable J-type thermocouples spaced 0.5 cm apart runs through the other end. All thermocouples used are 0.002 in. thick. The set of eight thermocouples was inserted inside a 1/8 in. diameter x 63-1/2 in. long thermocouple sheath (**Fig. 3.5**) at the following depths: 1.4, 11.0, 25.1, 53.3, 67.4, 81.5, and 95.6 cm respectively measured from the top of the combustion tube. The other set of thermocouples was inserted inside a 1/8 in diameter x 62-1/8 in long thermocouple sheath (**Fig. 3.5**). In this set the bottom thermocouple was set at 157.0 cm and the rest were spread 0.5 cm apart in a 2.5 cm length.

The combustion tube system is placed vertically and is secured to the production end and to the arm of the motor of the movable thermocouple set. Each one of the thermocouples is connected to its terminal to display or register its signal to the data logger and/or the control panel and/or PC monitor.

3.1.3 Fluid production system

A backpressure regulator (**Fig 3.6**) maintains the outlet pressure of the combustion tube at a constant predetermined level during the experiment. The liquids leaving the combustion tube pass through a two-stage separation where they are collected at the production outlet (**Fig. 3.7**). Gases pass through a condenser kept at low temperature to recover any volume of liquid in this stream (**Fig. 3.8**). In such case, an outlet end of the condensed unit is used.

Gases flowing toward the gas chromatograph are scrubbed of acid, using a column of permanganate, and dehydrated, using a column of calcium sulfite, before entering the next system (**Fig. 3.9**).

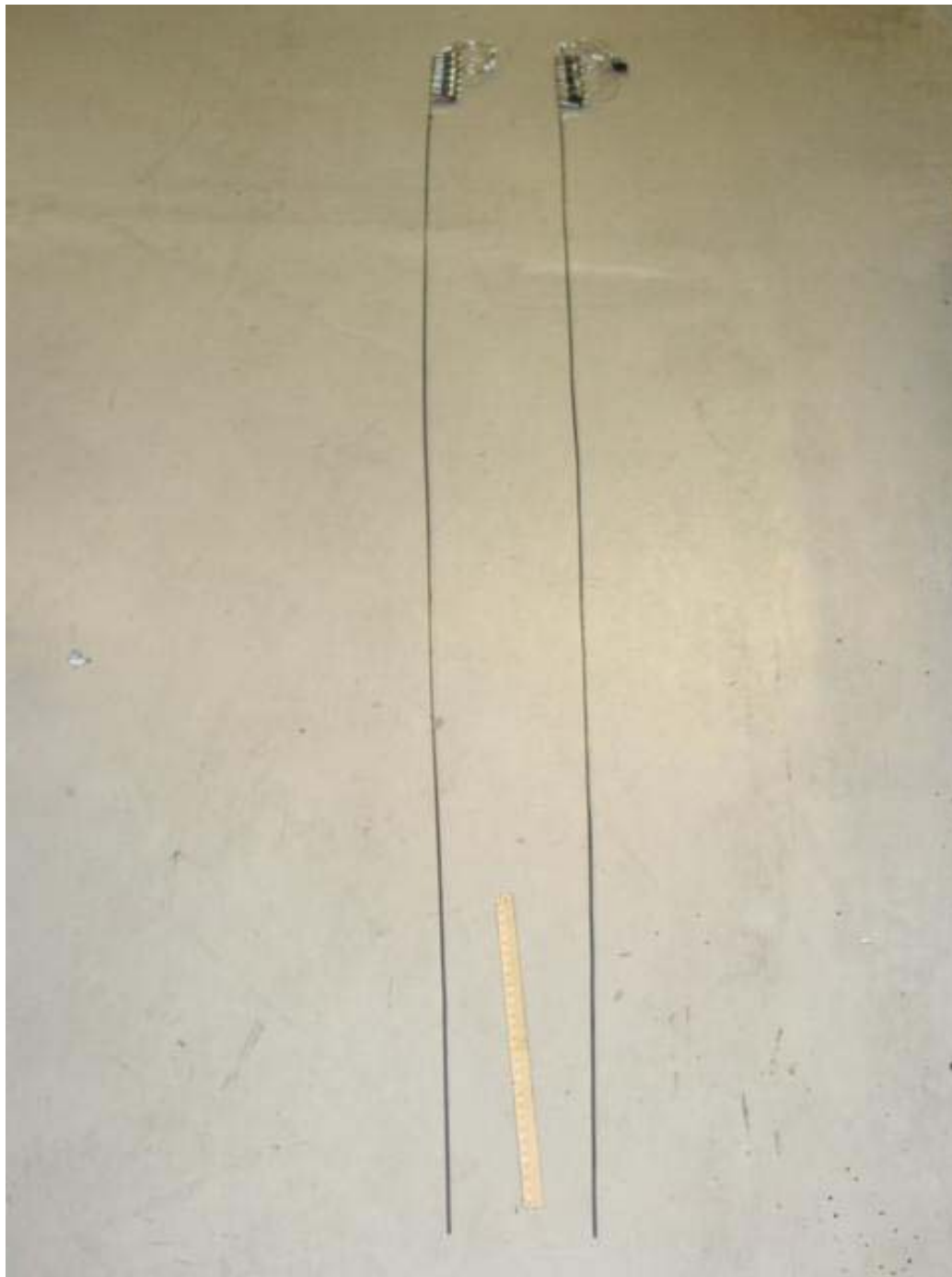


Fig. 3.5—Thermocouple sheaths.



Fig. 3.6—Backpressure regulator.



Fig. 3.7—Two-stage separation.



Fig. 3.8—Condenser unit.



Fig. 3.9—Acid scrubber and drierite columns.

3.1.4 Gas chromatograph and wet test meter system

A small fraction of produced gas is injected into the HP 5890 Series II gas chromatograph (**Fig. 3.10**) where the gas is analyzed for carbon dioxide, oxygen, nitrogen, and carbon monoxide every 15-20 minutes. This data is registered in a HP 3966A Integrator. A wet test meter installed before the gas chromatograph allows the measurement of the produced combustion gases, which is recorded in a PC (**Fig. 3.10**).

3.1.5 Data measurement and recording system

Two data loggers and two personal computers (**Fig. 3.11**) are used to record the following parameters: time, jacket temperatures, fixed thermocouple temperatures, movable thermocouple temperatures, injection pressure, production pressure, depth of bottom movable thermocouple, gas injection rate, average produced gas rate, cumulative gas rate. The parameters are recorded at 30-second intervals and most of them are displayed on the PC monitors for monitoring purposes. A complete view of the apparatus can be seen in **Fig. 3.12**.

3.2 Experimental procedure

First of all a mixture of sand, clay, water and oil was prepared in a large mixing bowl. About 6700 g. of sand and 350 g. of clay were thoroughly mixed using a small shovel. About 310 g. of water were also added to the sand-clay mixture and mixed until the mixture was evenly moist. Then, about 350 g. of oil were added and mixed thoroughly to obtain a uniform mixture. Finally, the mixture was weighted.

The bottom flange of the combustion tube was installed. Two 3/16 in. thermowells connected to meshed steel screens at the bottom, to prevent sand blocking, were introduced into the tube. Portions of about 200 g. of mixture were introduced into the tube once the combustion tube was safely fastened in a vertical position. A heavy metal plunger that passed through the thermowells was used to tamp the sample into the tube. The process of adding sample and tamping was repeated until the tube was filled to about 10 cm from the top. About 5 ml of linseed oil was placed on the top of the sample to accelerate ignition. The combustion tube was then filled to the top with clean sand. The

remaining mixture in the large mixing bowl was weighted to determine the amount of mixture placed in the combustion tube.

The top flange of the combustion tube was installed and the flange bolts fastened. The injection assembly was carefully installed, passing through the thermowells, and Teflon ferrules passed through them and tightened. Nitrogen was introduced at the injection inlet and with the outlet of the combustion tube plugged, the cell was pressure tested for leaks at 400 psig for 30 minutes. Once the pressure test was performed successfully, the outlet plug of the combustion cell was slowly opened and the pressure in the tube allowed to decrease to atmospheric. The injection assembly was uninstalled and an electric igniter was placed and tightened at the exterior of the combustion tube at the same depth where the linseed oil was placed. The tube was then placed carefully inside the vacuum jacket which was tilted to about 30° from the horizontal to allow better handling of the combustion tube. The bottom flange of the combustion tube was wrapped with insulation and the bottom flange of the vacuum jacket was installed. The electric igniter was connected to the ignition terminals of the top flange of the vacuum jacket and the latter was tightened. The injection assembly was replaced in its position and the fixed and movable thermocouple sheaths were inserted in their respective thermowells. Teflon ferrules were tightened to the outlet and injection assembly to seal the vacuum jacket from the combustion tube. The vacuum jacket was placed in a vertical position and the outlet of the combustion tube fastened to the production section. The movable thermocouple sheath was fixed to the motor arm and all thermocouples were connected to their terminals. The vacuum jacket was tested for one hour with a vacuum of about 28 mm Hg. The injection line was connected to the assembly, and the vacuum jacket heater was set to about 140°F (60°C) and left overnight to allow the temperature of the sand mix to stabilize.



Fig. 3.10—HP 5890 Series II gas chromatograph and wet test meter.



Fig. 3.11—Data logger and PC.



Fig. 3.12—Complete view of the apparatus.

Prior to the beginning of the experimental run, the mass flow controller was calibrated to the injection rate, the gas chromatograph was also calibrated, the bottom of the movable thermocouple sheath was raised to the linseed oil depth, and the sand pack was pressurized with nitrogen to 300 psig. Electric current was gradually introduced into the igniter using a variable power transformer. Approximately 90 minutes later, the temperature in the combustion tube at the igniter level (movable thermowell placed at the linseed oil depth) reached about 570°F (300°C) and air injection was initiated at 3 L/min. A backpressure regulator was adjusted to maintain a production pressure of 300 psig. The movable thermocouple reading in the instruments panel and PC activated to record data was observed to increase rapidly to about 970°F (520°C), a clear indication that ignition occurred inside the combustion tube. Combustion gas composition was measured every 15-20 minutes; temperature profiles approximately every 6 in. (15 cm), and production liquids every 15-20 minutes. Accurate readings of temperature profiles were taken with the set of six movable thermocouples, spaced 0.5 cm from each other, which allowed the recording of 6 entries just behind and ahead of the combustion front. These entries were made by pressing an assigned key on the PC.

Initial water and oil production varied depending on the composition of the injected air. Liquids were collected in graduated sample bottles which were capped for subsequent analysis. The end of the combustion run occurred when no oil production was attained, in other words, the sand pack was burned to the bottom flange of the combustion tube. Combustion runs varied between 4-7.5 hours, depending on the composition of the air injected.

CHAPTER IV

EXPERIMENTAL RESULTS

The main goal of conducting combustion tube experiments in this study is to obtain the basic data necessary to estimate the amount of heat generated at the combustion front. For this purpose, the critical data are the composition of the combustion gases. Analysis of the combustion runs has been made and the results are presented in this chapter.

Six successful runs were performed with Jobo crude oil (9-11°API) from the Orinoco Belt in Venezuela. The conditions that were constant in these runs were the air injection rate (3 L/min) and production pressure (300 psig). Concentration by weight of oil, water, clay, and sand in the samples were approximately 4.6%, 4.0%, 4.6%, and 86.8% respectively (**Table 4.1**). However, the interest was set on varying the oxygen concentration in the injected air. Gas cylinders containing air with oxygen composition of 21, 30, and 40 mole % were available. The oxygen-enriched air was prepared by Portagas, Inc. of Houston.

In all runs, air injection was initiated when the temperature of the sand pack across the electric igniter reached 300°C. The igniter was switched off within 10 minutes after air injection started.

4.1 Combustion run no. 2 (21% oxygen)

The combustion gas composition during this run was observed to vary, which indicated that the combustion was not very stable (**Fig. 4.1**). During the run the average concentrations of the produced gases were: CO_2 , 12.41%; O_2 , 2.29%; N_2 , 81.22% and CO , 4.10%.

Apparent hydrogen/carbon ratio, F_{HC} , CO_2/CO , and, $CO/(CO+CO_2)$ ratios based on the combustion gas analysis are presented in **Fig. 4.2**. The instability of the produced gas composition makes F_{HC} fall below one in some instances. This may be explained by low temperature oxidation occurring ahead of the combustion front or injected air channeling through the center of the combustion tube where the thermowells are placed; however, the average F_{HC} , CO_2/CO , and, $CO/(CO+CO_2)$ ratios are 1.174, 3.029, and 0.248 respectively corresponding to a high temperature oxidation process.

	Run 2	Run 7	Run 3	Run 4	Run 5	Run 6
mole % O ₂	21	21	30	30	40	40
Length (cm)	89.92	90.92	91.52	92.32	92.32	92.52
Weight (g)	7084	7146	7204	7193	7194	7215
Oil (wt. %)	4.69	4.60	4.61	4.59	4.65	4.62
Water (wt.%)	4.04	4.02	4.11	4.02	3.99	4.01
Sand (wt. %)	86.60	86.79	86.53	86.80	86.77	86.77
Clay (wt. %)	4.67	4.60	4.61	4.60	4.60	4.61
S _o (%)	23.79	23.24	24.01	22.64	22.94	22.86
S _w (%)	25.26	22.08	22.46	21.43	21.28	21.40
S _g (%)	50.95	54.67	53.53	55.93	55.78	55.74
φ(%)	36.22	36.29	36.37	36.84	36.85	36.80

The average combustion temperature was 455°C (**Fig. 4.3**). The average combustion front velocity was 13.42 cm/hr (0.43 ft/hr) as observed in **Fig. 4.4**.

Fig. 4.5 shows the cumulative volumes of produced oil and water, with an initial water production occurring at 2.25 hrs. The initial oil production occurred at 3.25 hrs. **Fig. 4.6** shows an oil recovery of 80.6% of original oil in the tube.

Fig. 4.7 is the representation of the injected gas rate, held at 3 L/min, production pressure maintained at 300 psig, and the injection pressure showing a high of approximately 335 psig at which oil production began. The concave shape of the injection pressure profile is the result of the formation of the oil bank inside the combustion cell. **Fig. 4.8** shows the accumulative gas injected volume, and an average gas production rate of 2.773 L/min.

Produced oil gravity at the end of the combustion run was 2.4°API higher than that of the original crude oil (**Fig. 4.9**). Viscosity of the produced oil dropped to 123 cp at 60°C from its original value of 568 cp (**Fig. 4.10**).

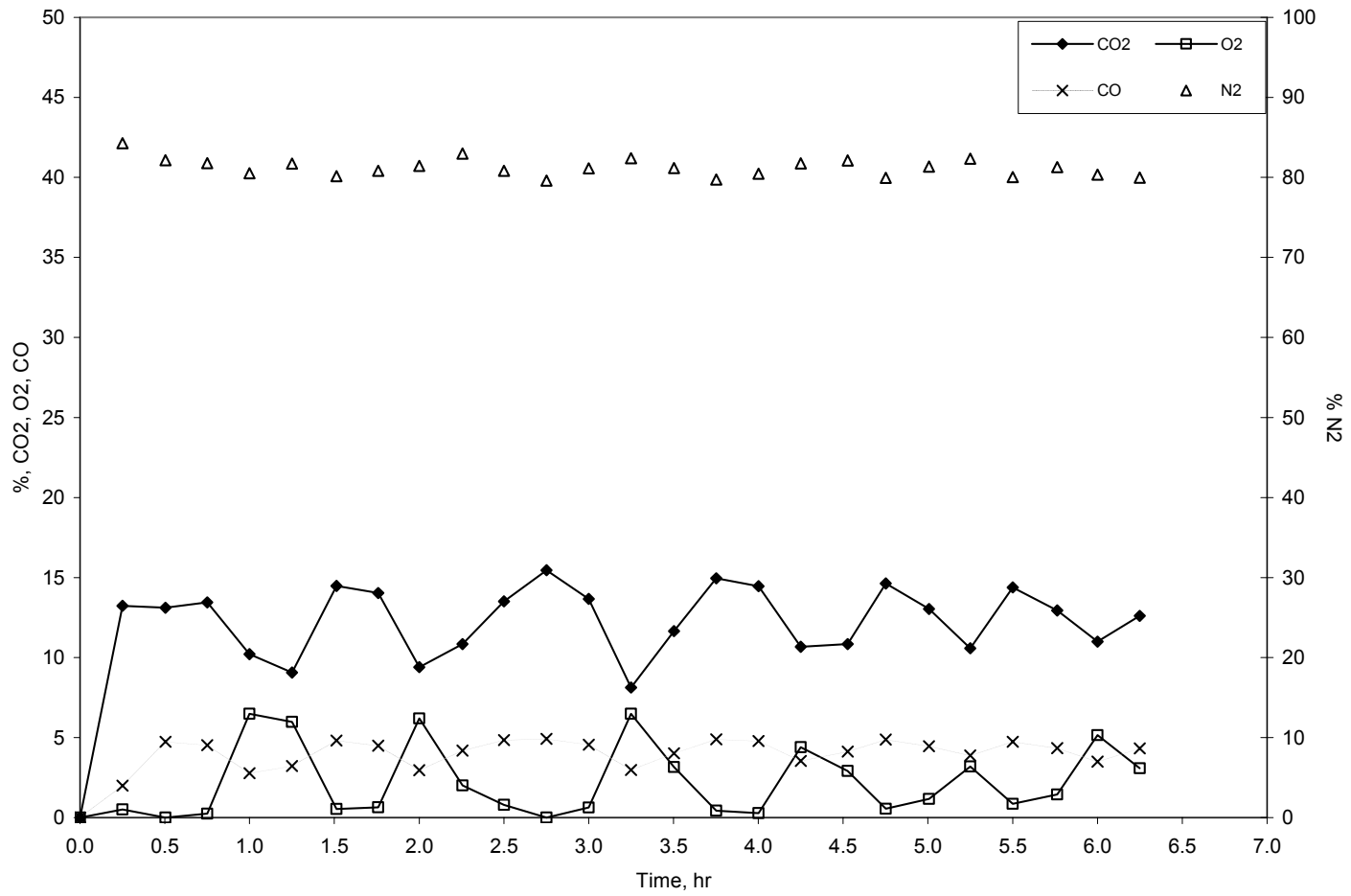


Fig. 4.1—Combustion gas composition (run no. 2, 21% oxygen).

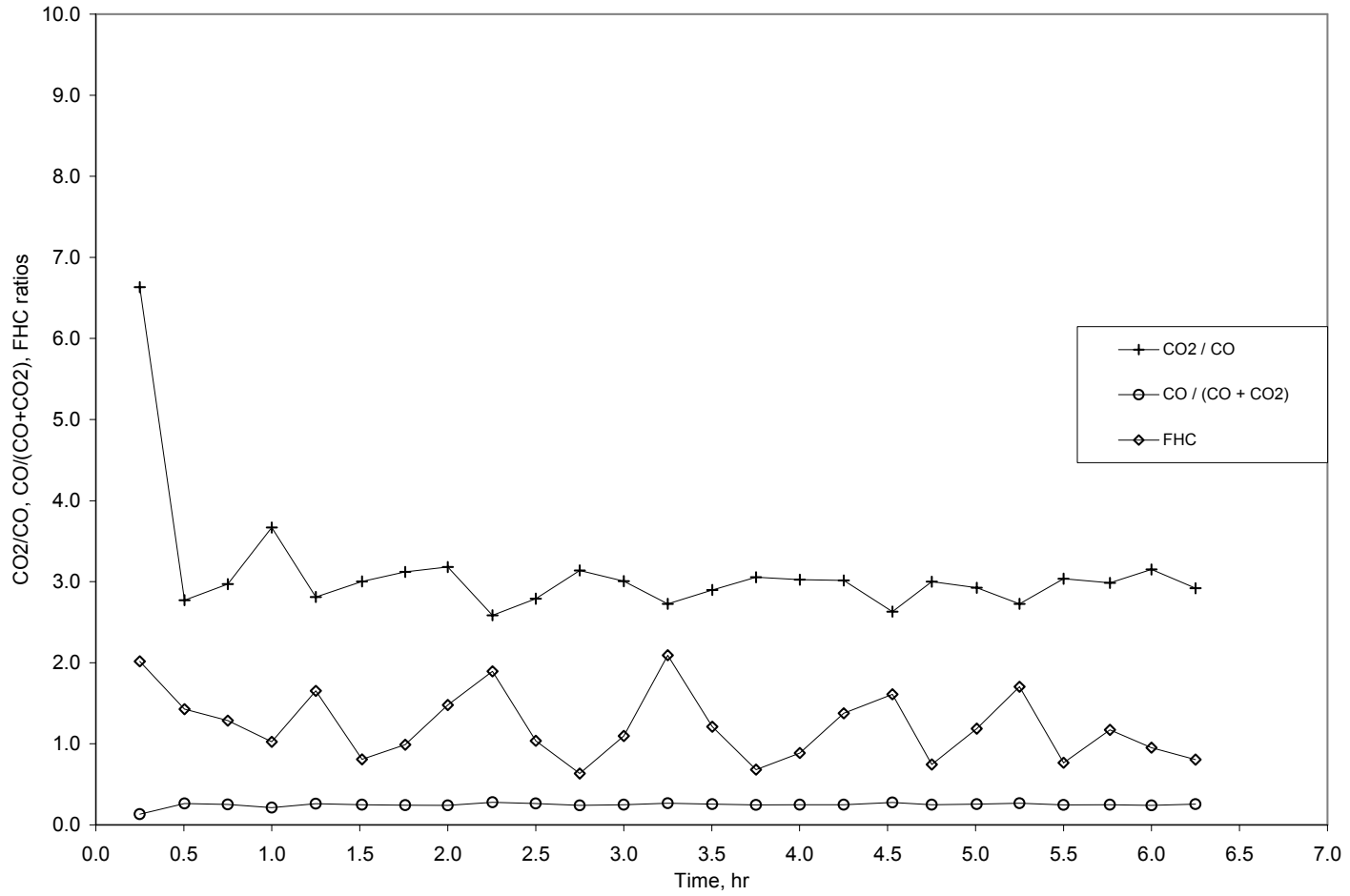


Fig. 4.2— F_{HC} , CO_2/CO , and $CO/(CO+CO_2)$ ratios (run no. 2, 21% oxygen).

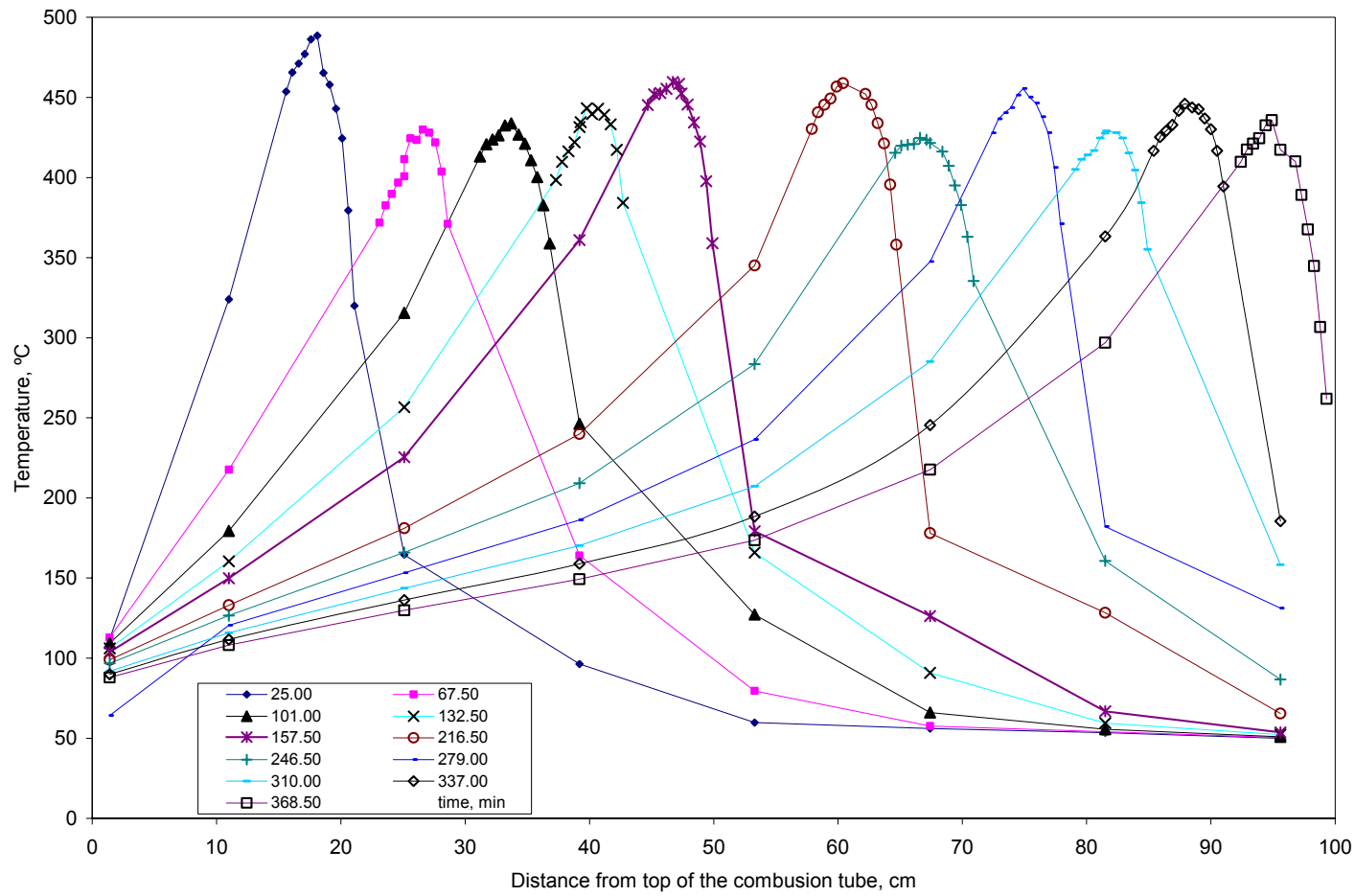


Fig. 4.3—Temperature profiles (run no. 2, 21% oxygen).

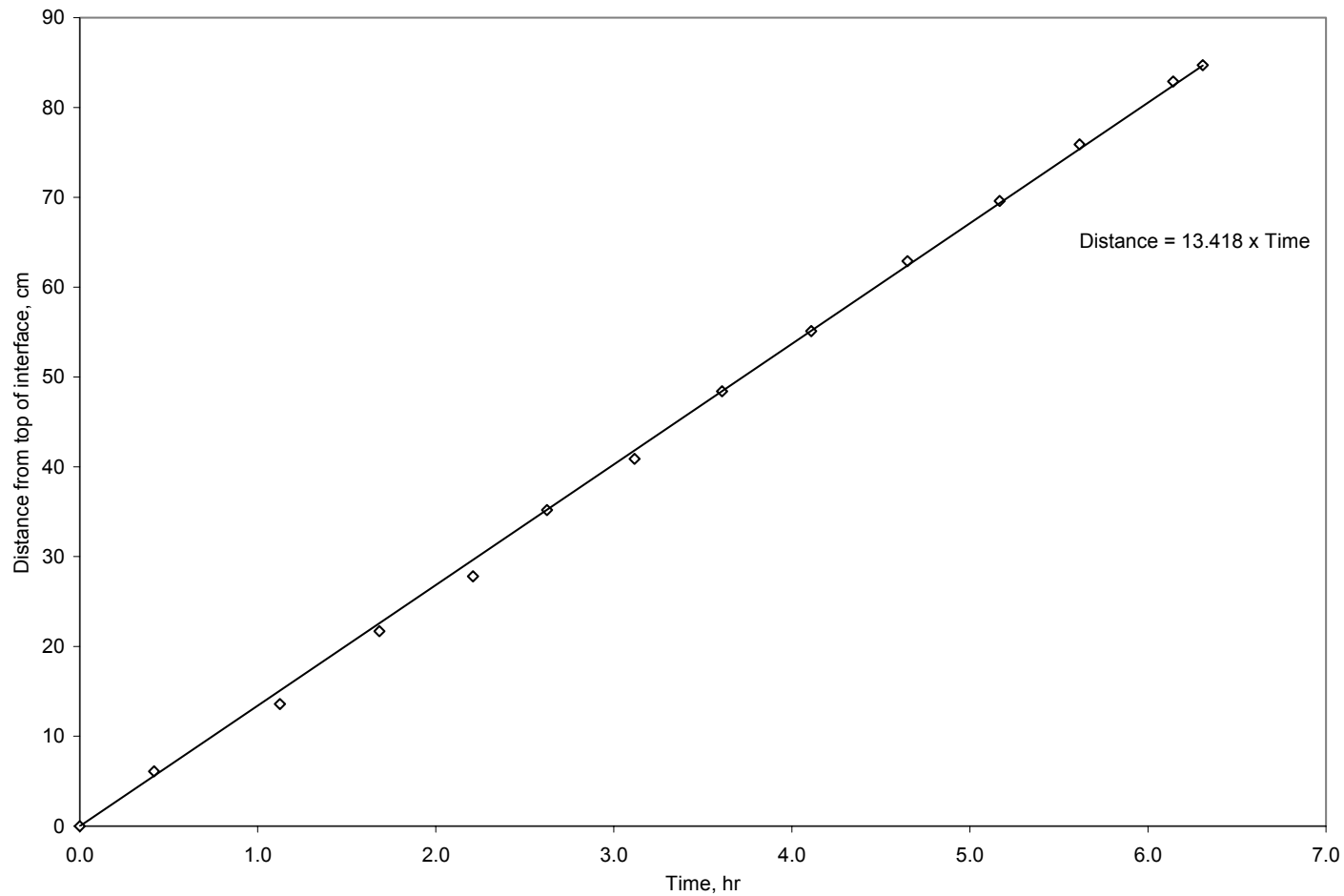


Fig. 4.4—Combustion front velocity (run no. 2, 21% oxygen).

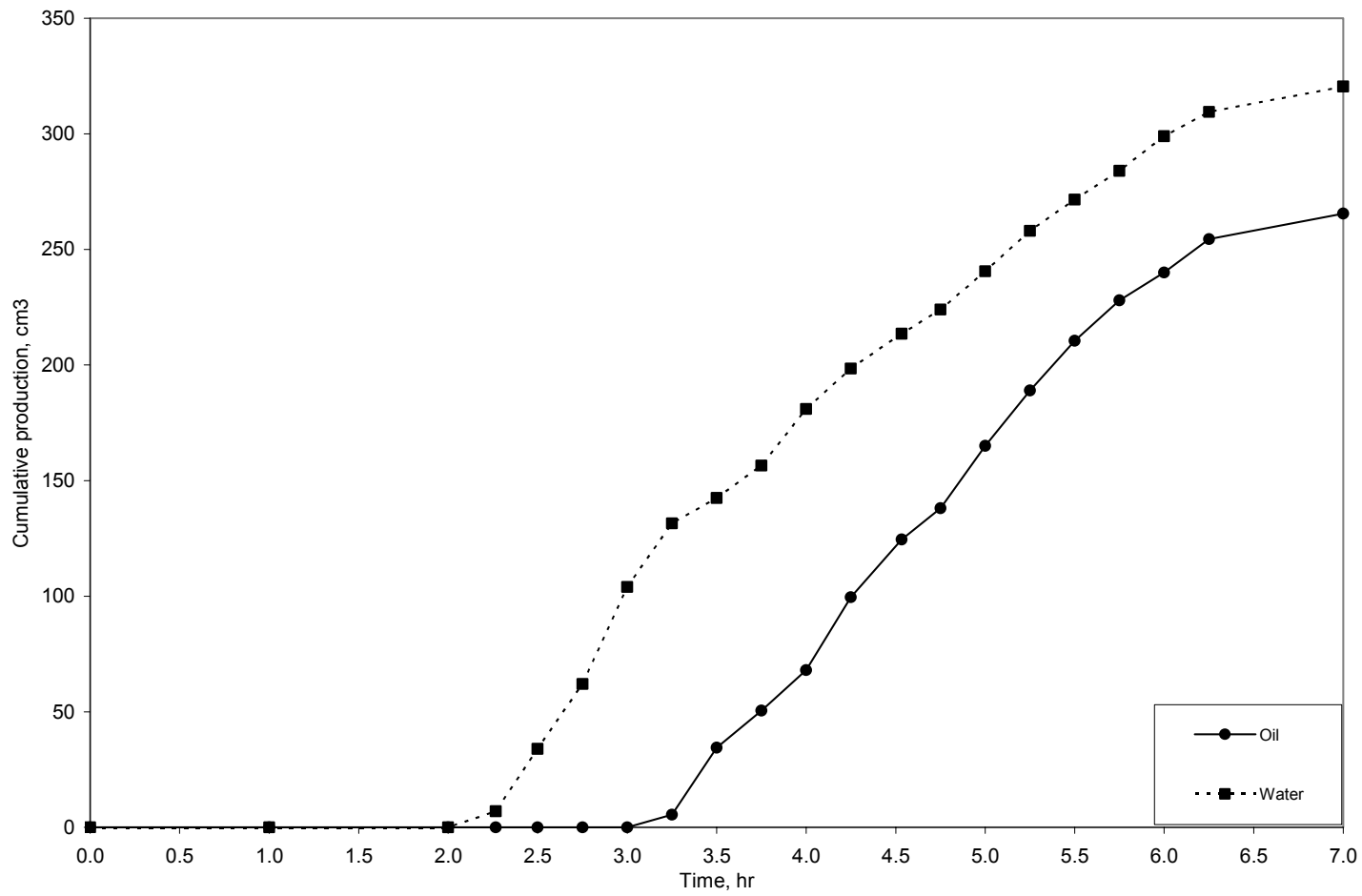


Fig. 4.5—Cumulative oil and water production (run no. 2, 21% oxygen).

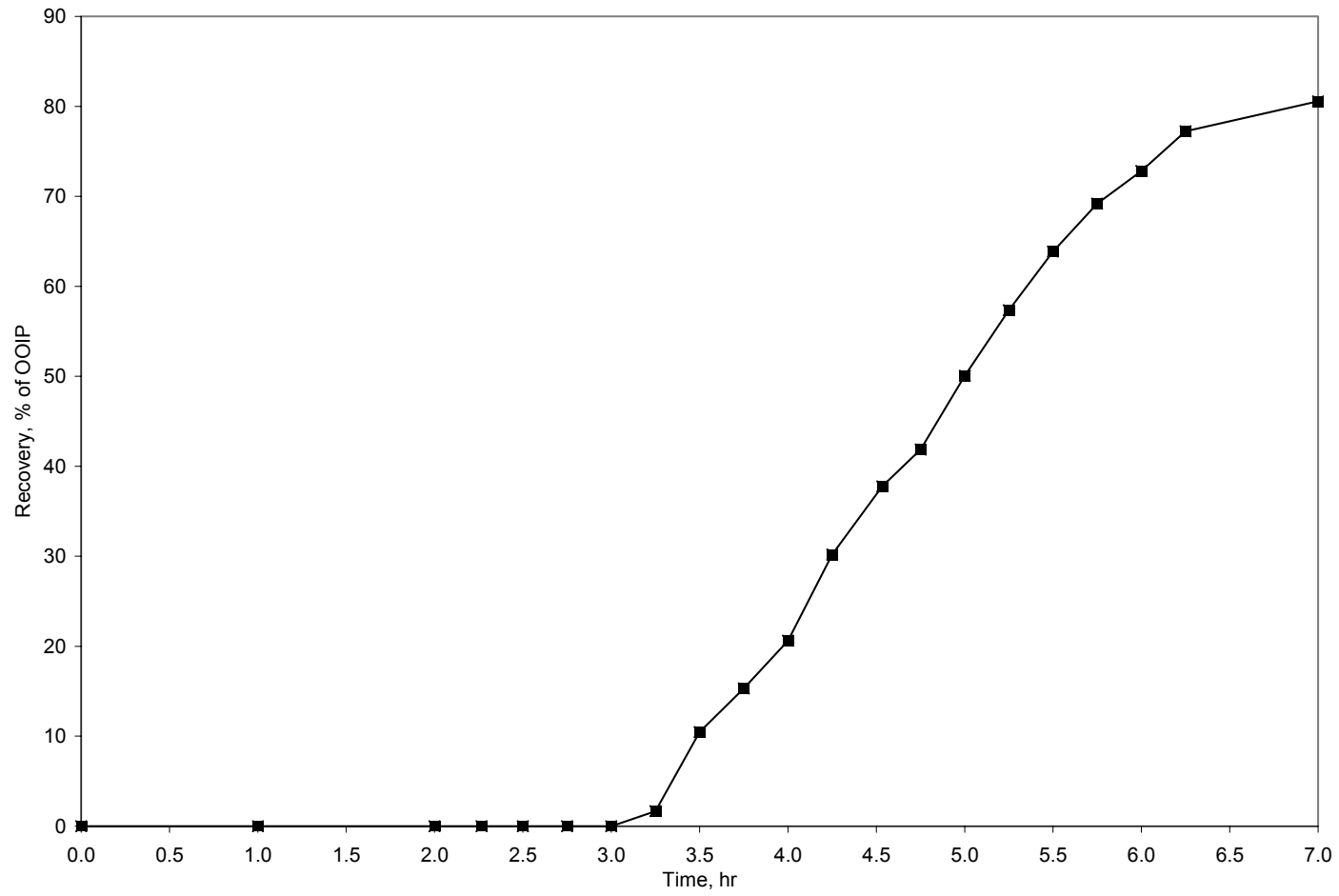


Fig. 4.6—Oil recovery (run no. 2, 21% oxygen).

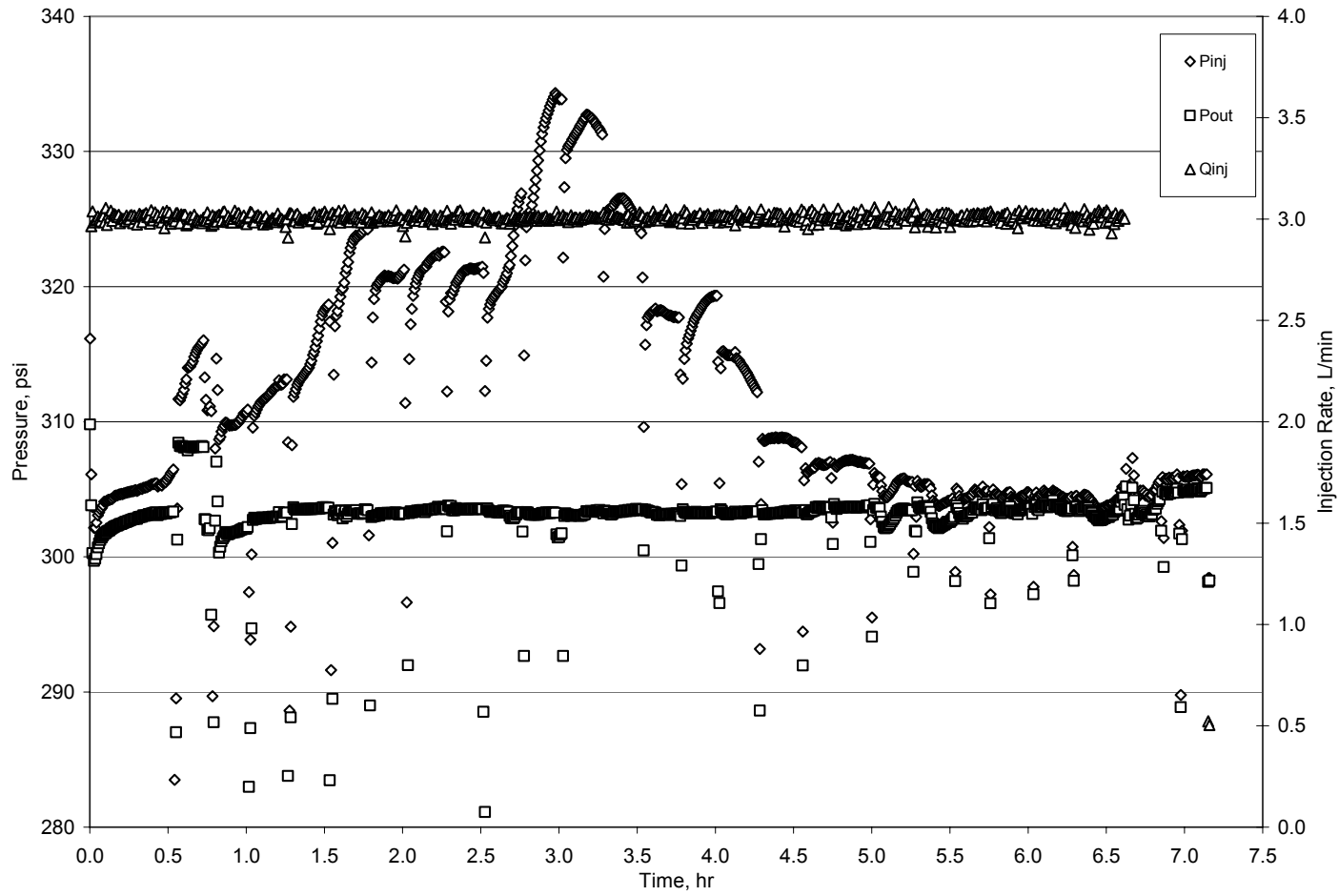


Fig. 4.7—Injection and production pressures, and injection rate (run no. 2, 21% oxygen).

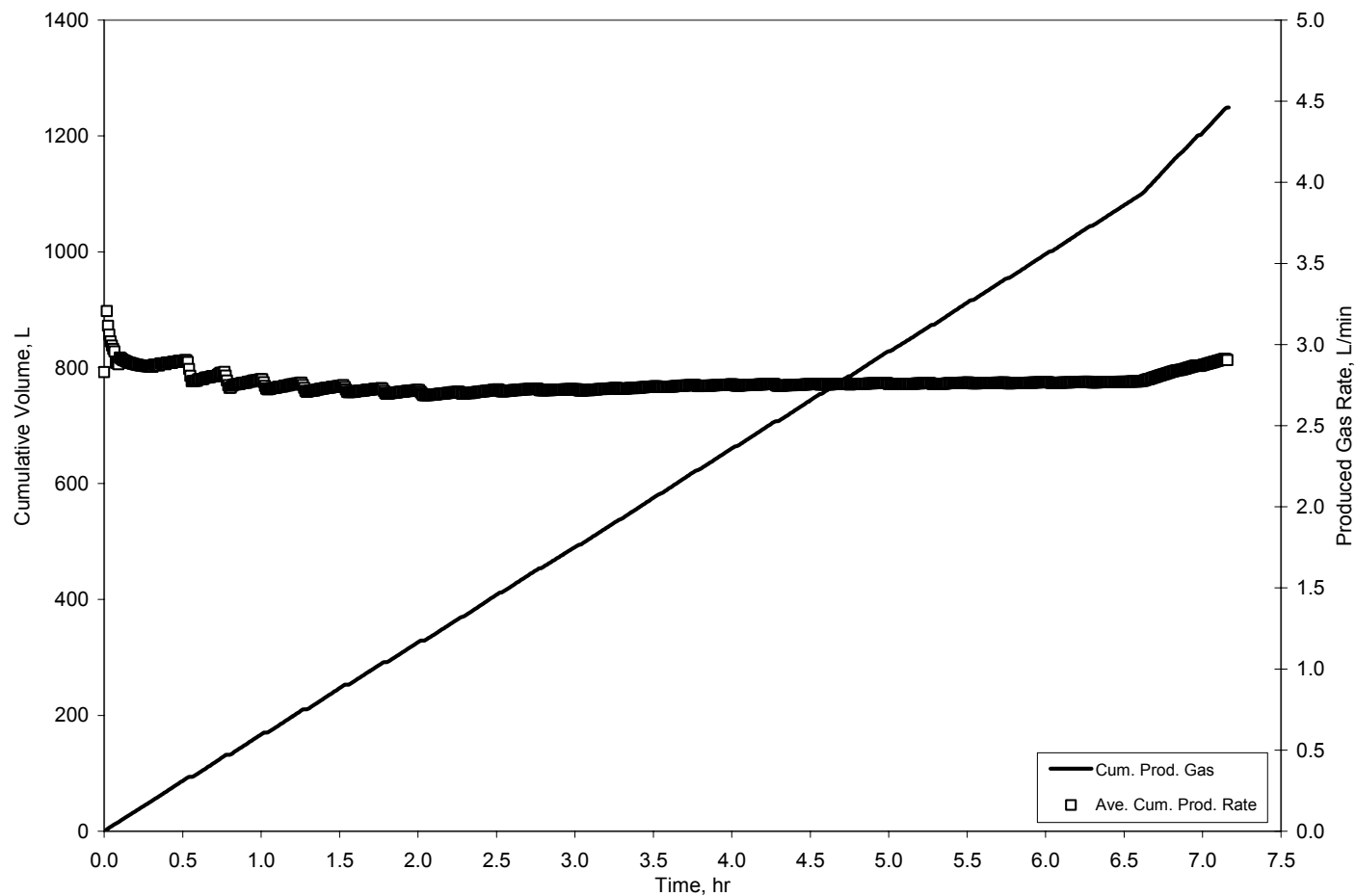


Fig. 4.8—Cumulative volume and produced gas rate (run no. 2, 21% oxygen).

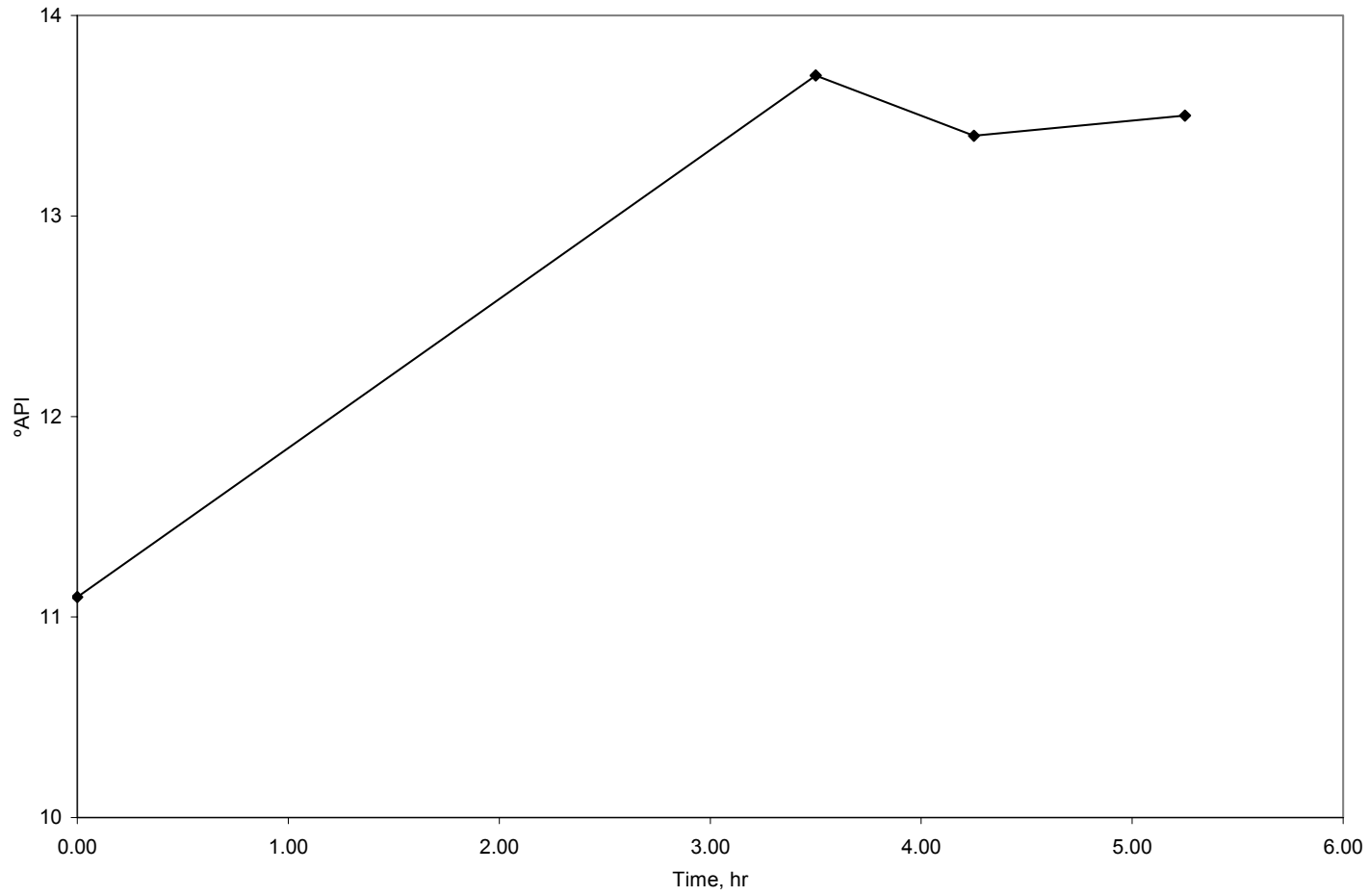


Fig. 4.9—Produced oil gravity (run no. 2, 21% oxygen).

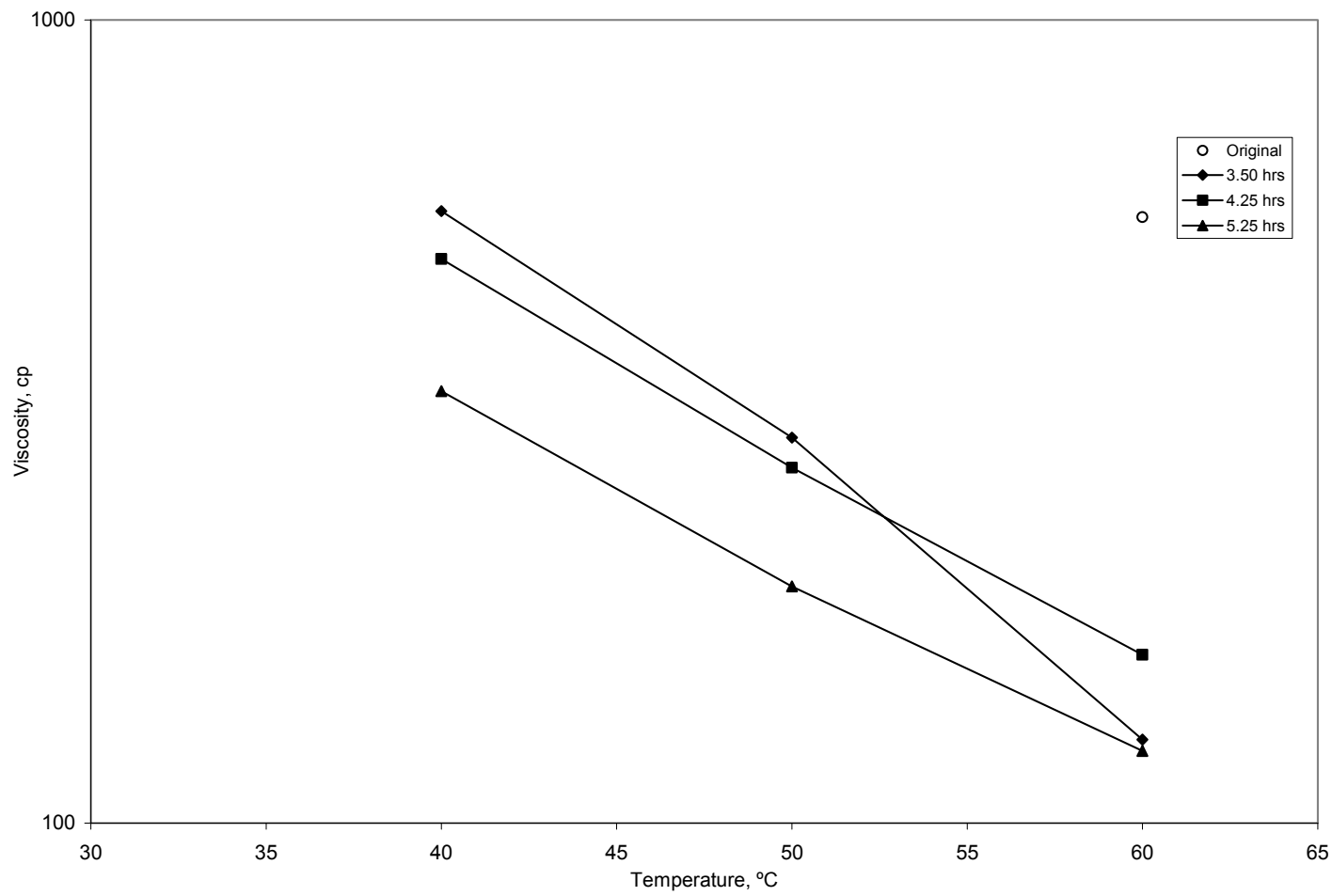


Fig. 4.10—Produced oil viscosity (run no. 2, 21% oxygen).

4.2 Combustion run no. 7 (21% oxygen)

More stable readings of combustion gas composition were observed during this run (**Fig. 4.11**), in which the average concentrations of the produced gases were: CO_2 , 10.30%; O_2 , 2.09%; N_2 , 83.55% and CO , 4.07%.

Apparent hydrogen/carbon ratio, F_{HC} , CO_2/CO , and $CO/(CO+CO_2)$ ratios based on the combustion gas analysis presented in **Fig. 4.12**. The average F_{HC} , CO_2/CO , and $CO/(CO+CO_2)$ ratios are 2.230, 2.537, and 0.283.

The average combustion temperature was 440 °C (**Fig. 4.13**) and the combustion front velocity was 13.46 cm/hr (0.58 ft/hr) as observed in **Fig. 4.14**

Cumulative volumes of produced oil and water (**Fig. 4.15**) show initial water production occurring at 2.10 hrs and initial oil production at 3.08 hrs, which are similar to those observed in the previous run. Oil recovery (**Fig. 4.16**) is a little higher than run no. 2 with a final production of 81.9% of the original oil in place.

The injected gas rate, constant at 3 L/min, production pressure maintained at about 300 psig, and the injection pressure showing a high of approximately 330 psig are observed in **Fig. 4.17**. An increase of the injection pressure is seen again as a product of the formation of the oil bank inside the combustion cell. **Fig. 4.18** shows the accumulative gas injected volume, and an average gas production rate of 2.627 L/min.

Produced oil gravity at the end of the combustion run was 8.7°API higher than that of the original crude oil (**Fig. 4.19**). Viscosity of the produced oil dropped to 9 cp at 60°C from its original value of 568 cp (**Fig. 4.20**).

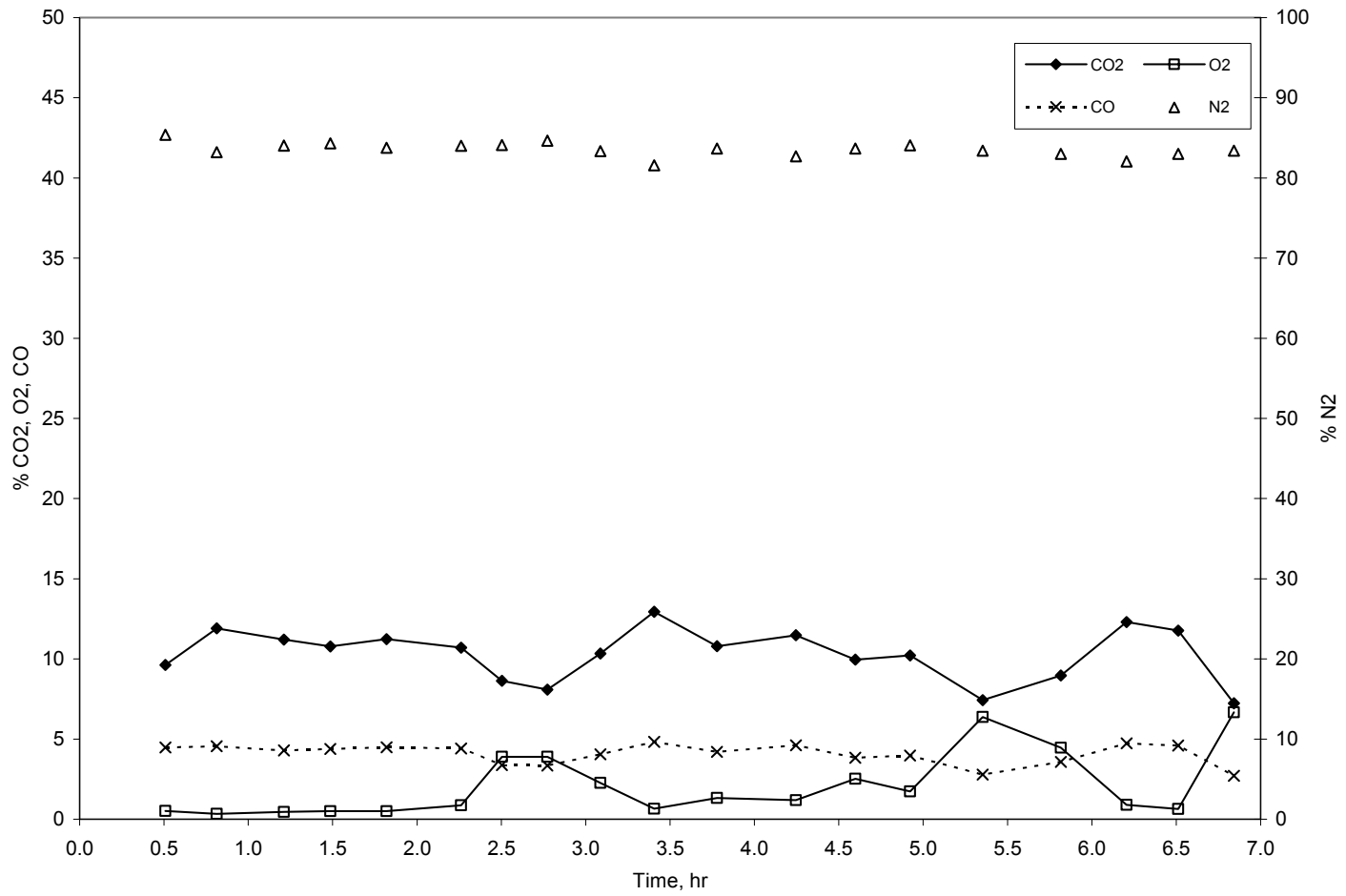


Fig. 4.11—Combustion gas composition (run no. 7, 21% oxygen).

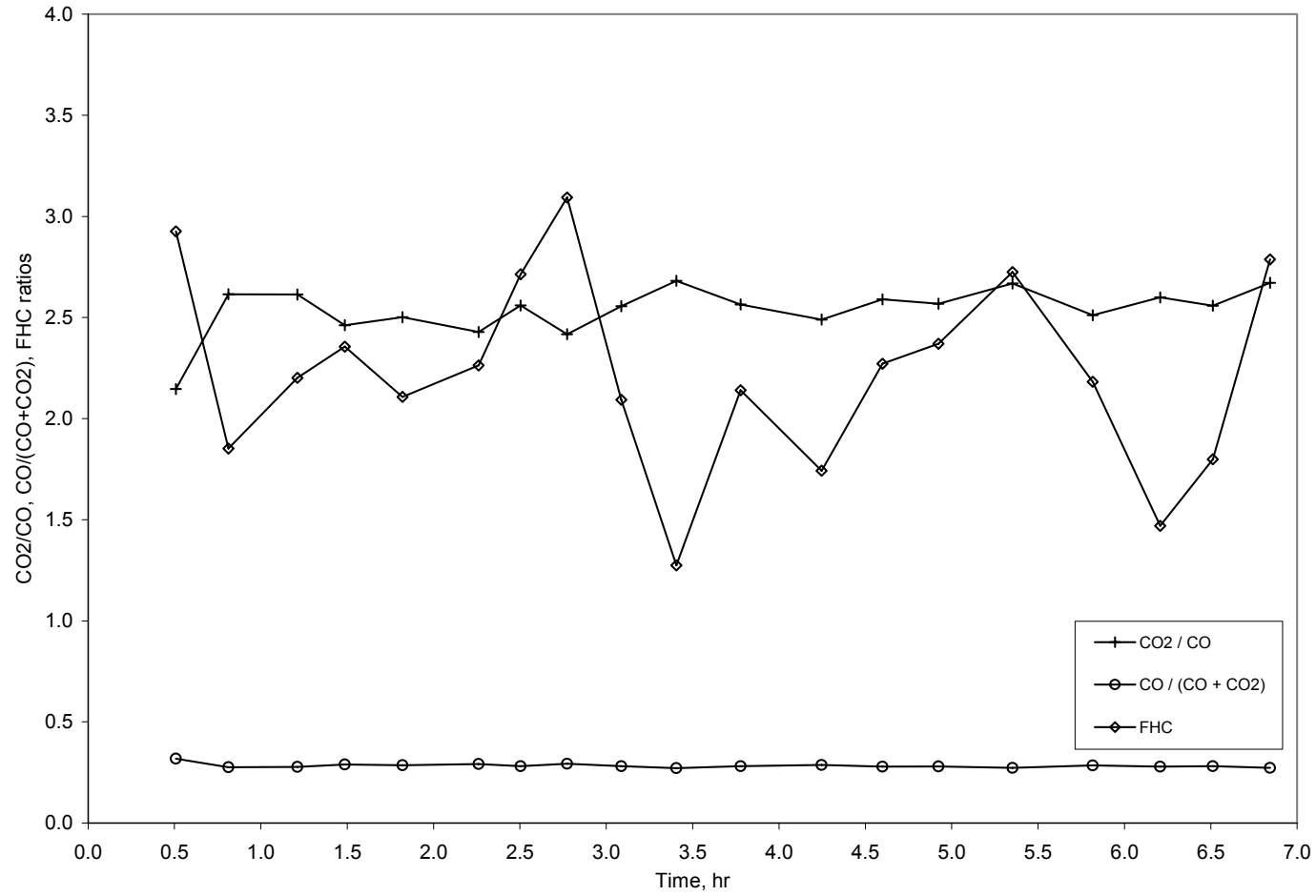


Fig. 4.12— F_{HC} , CO_2/CO , and $CO/(CO+CO_2)$ ratios (run no. 7, 21% oxygen).

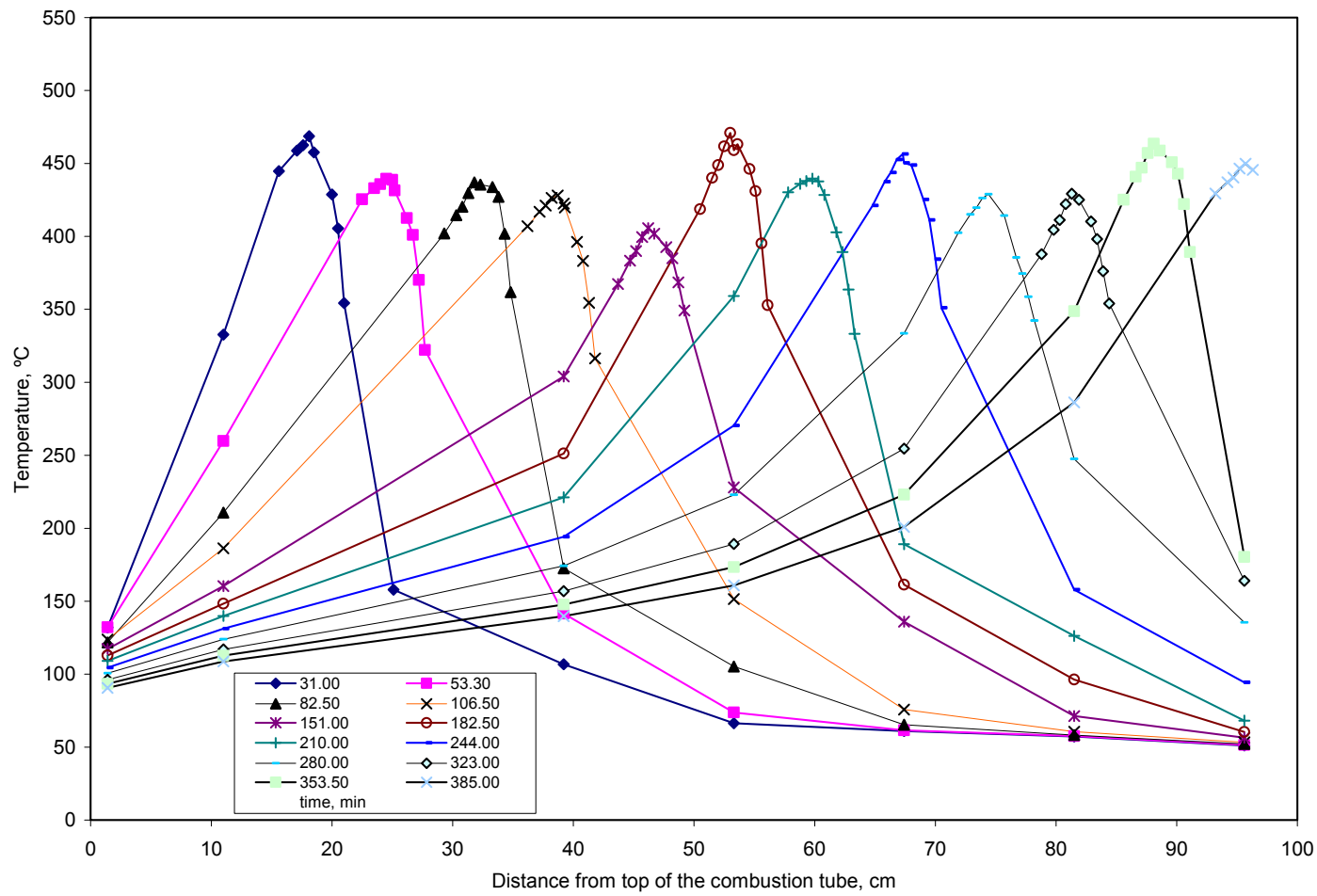


Fig. 4.13—Temperature profiles (run no. 7, 21% oxygen).

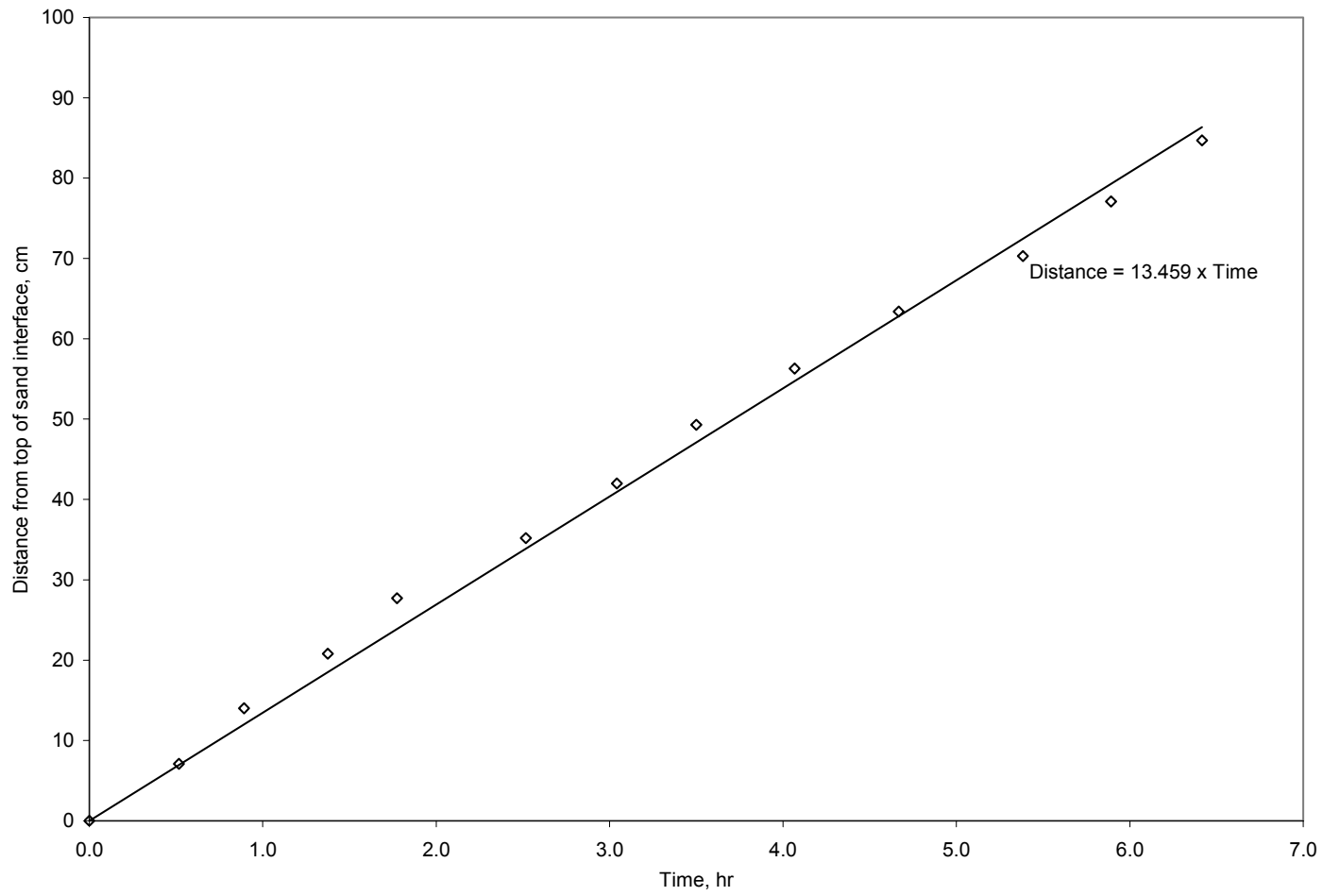


Fig. 4.14—Combustion front velocity (run no. 7, 21% oxygen).

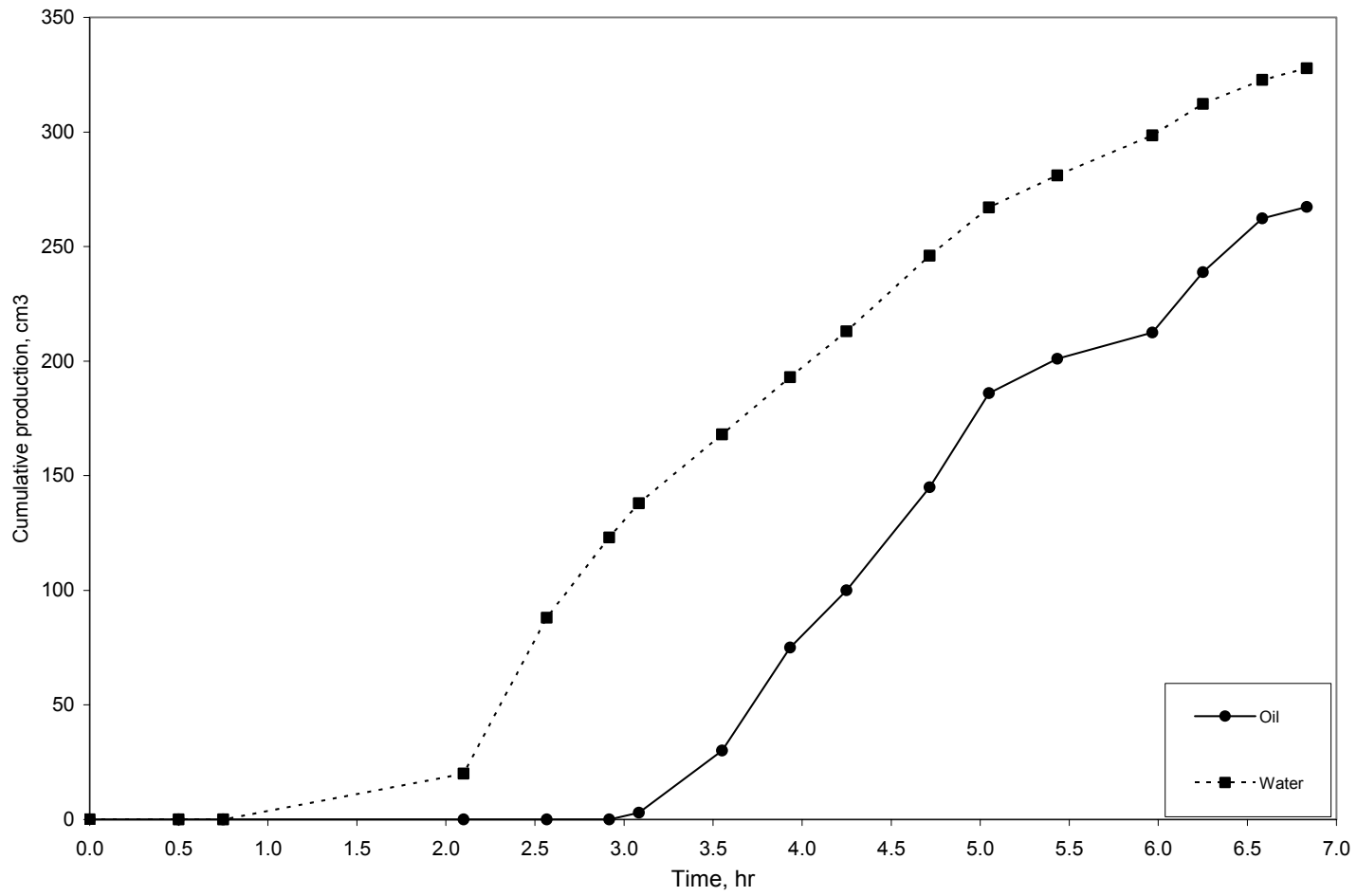


Fig. 4.15—Cumulative oil and water production (run no. 7, 21% oxygen).

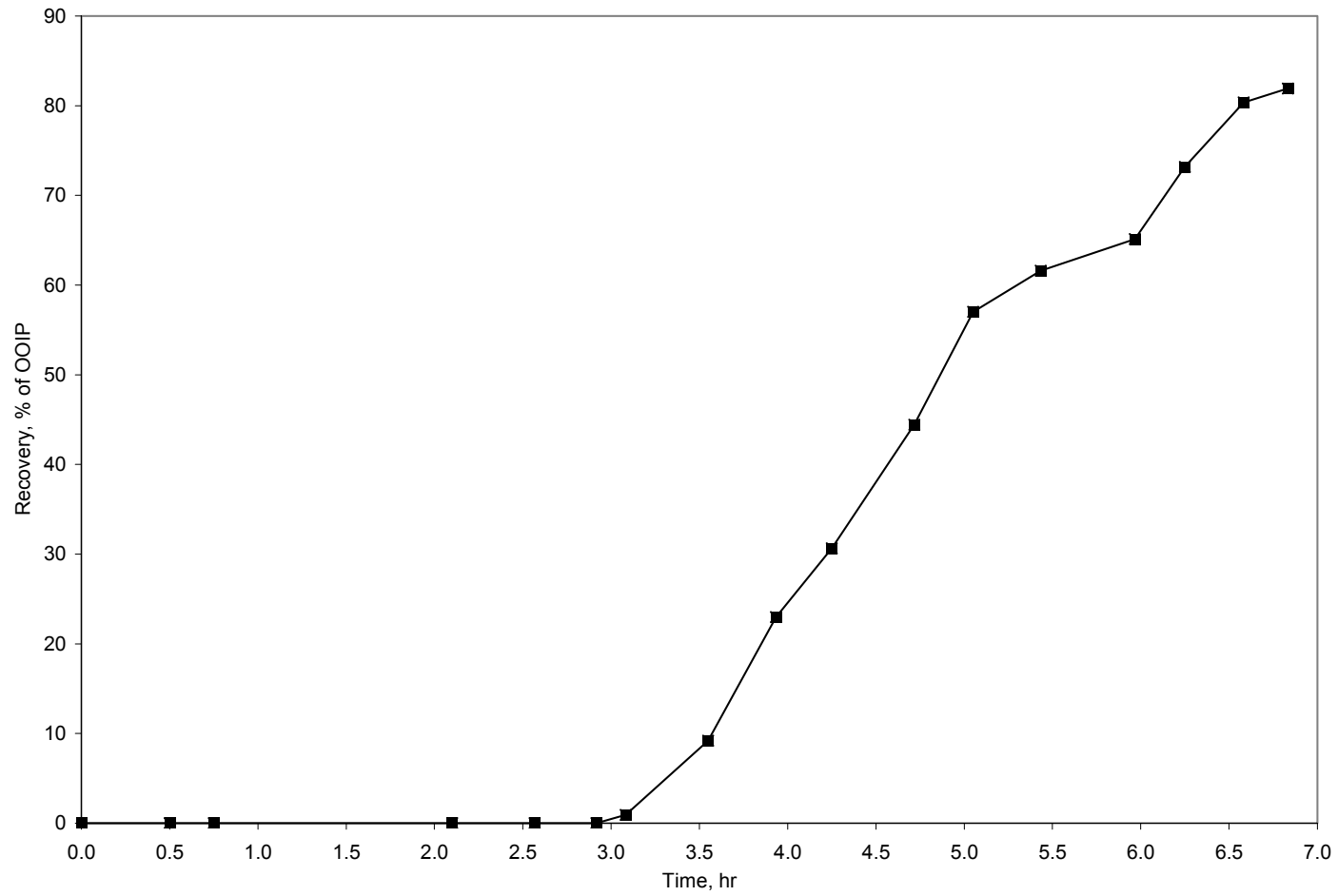


Fig. 4.16—Oil recovery (run no. 7, 21% oxygen).

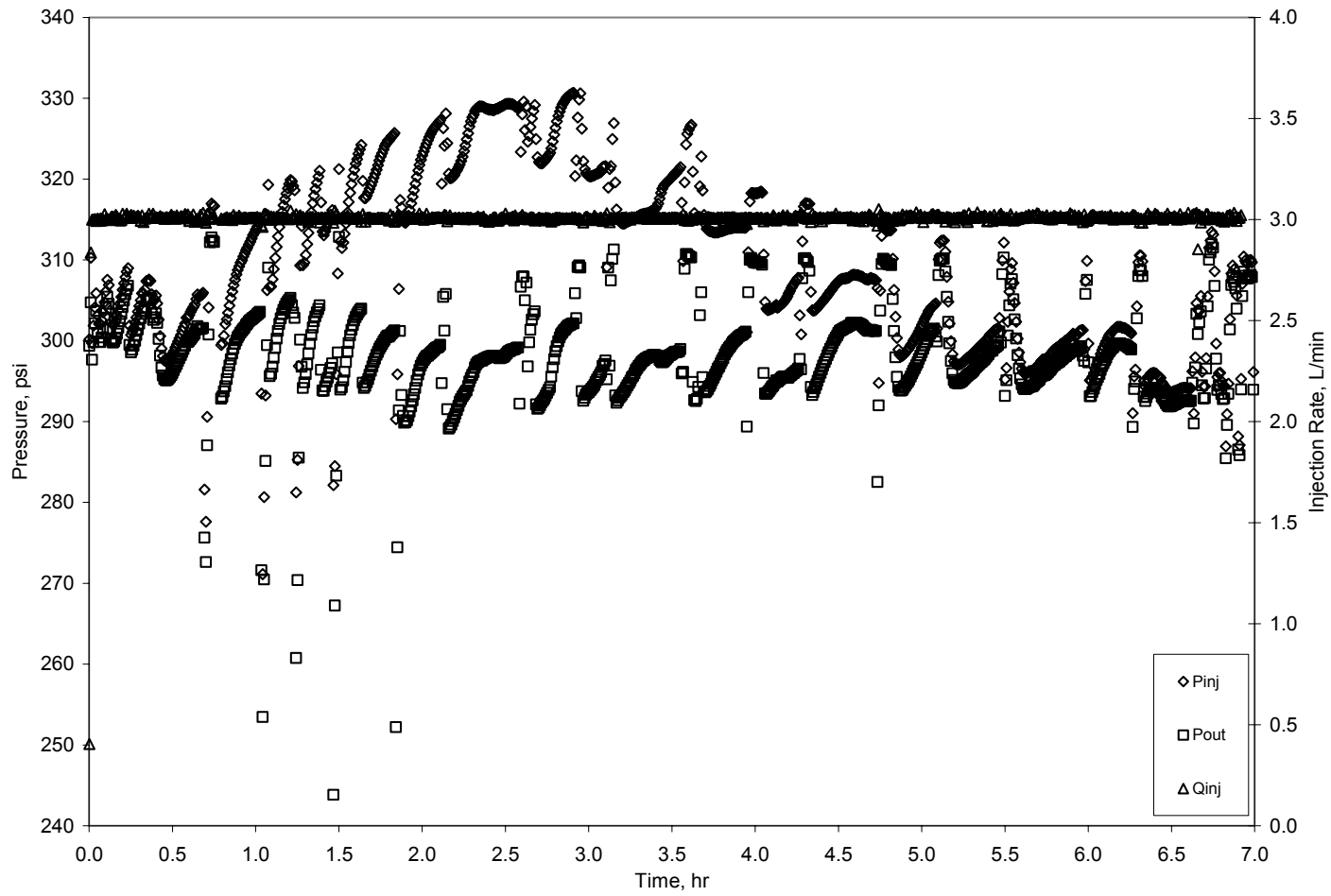


Fig. 4.17—Injection and production pressures, and gas injection rate (run no. 7, 21% oxygen).

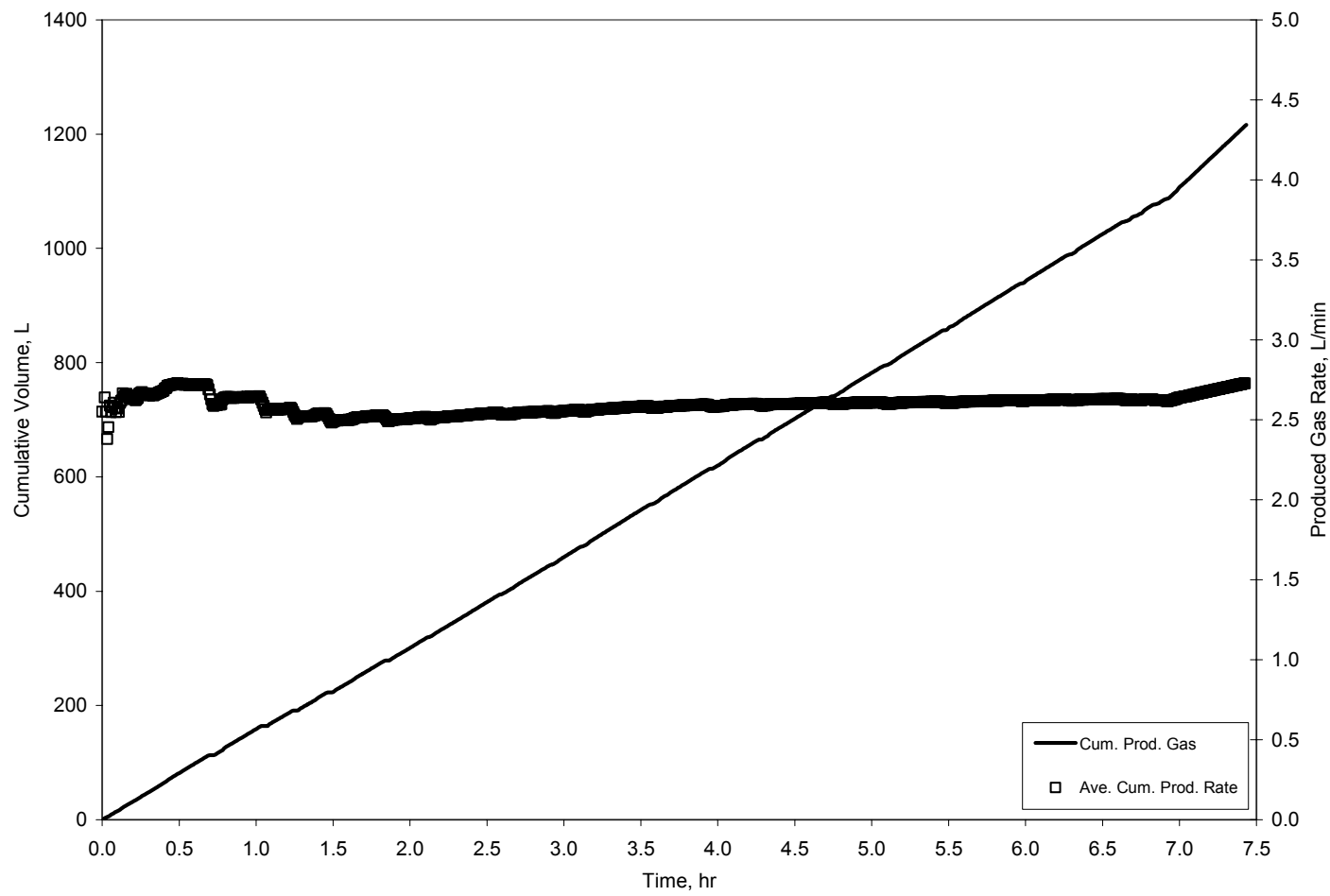


Fig. 4.18—Cumulative volume and produced gas rate (run no. 7, 21% oxygen).

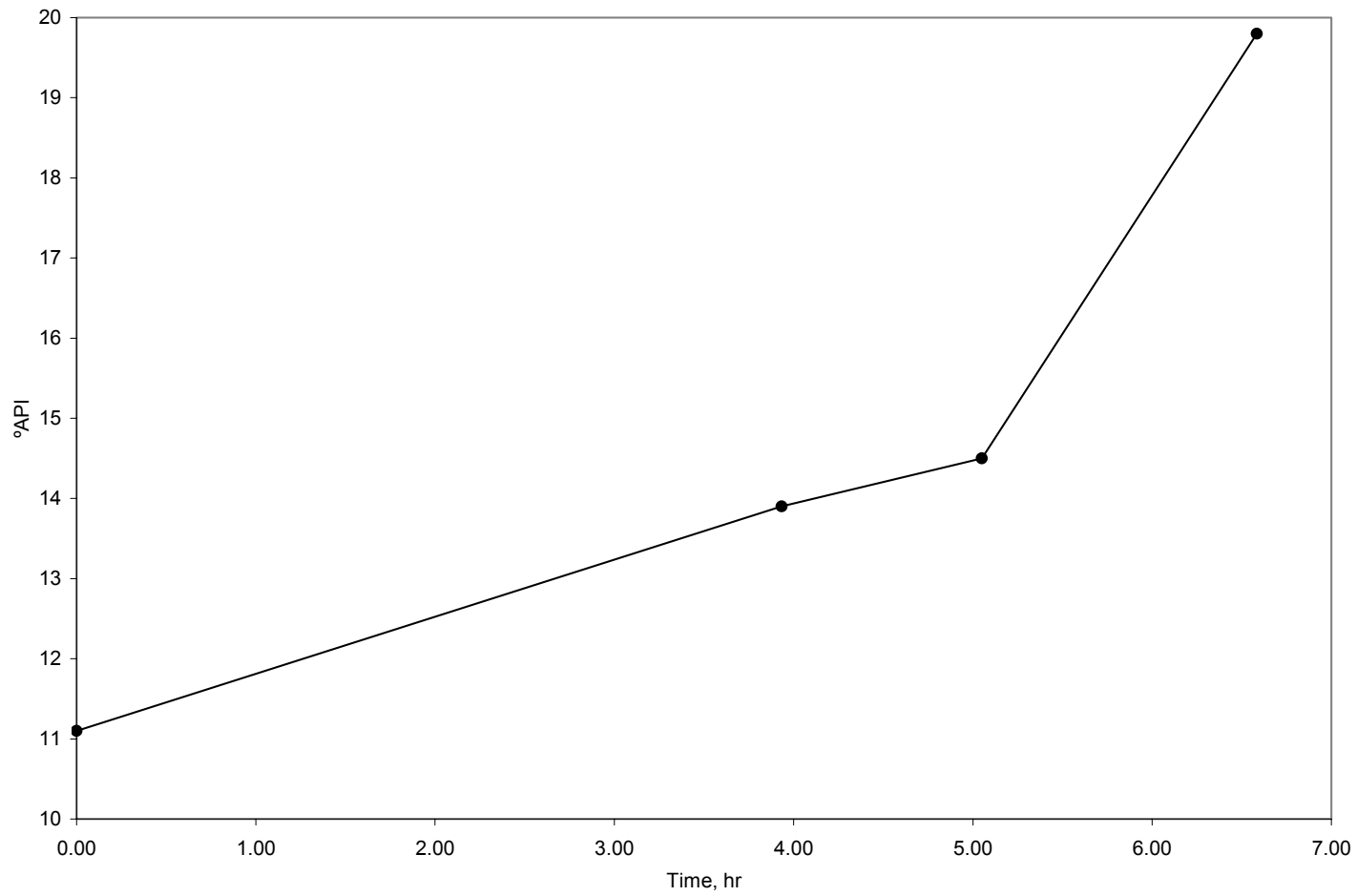


Fig. 4.19—Produced oil gravity (run no. 7, 21% oxygen).

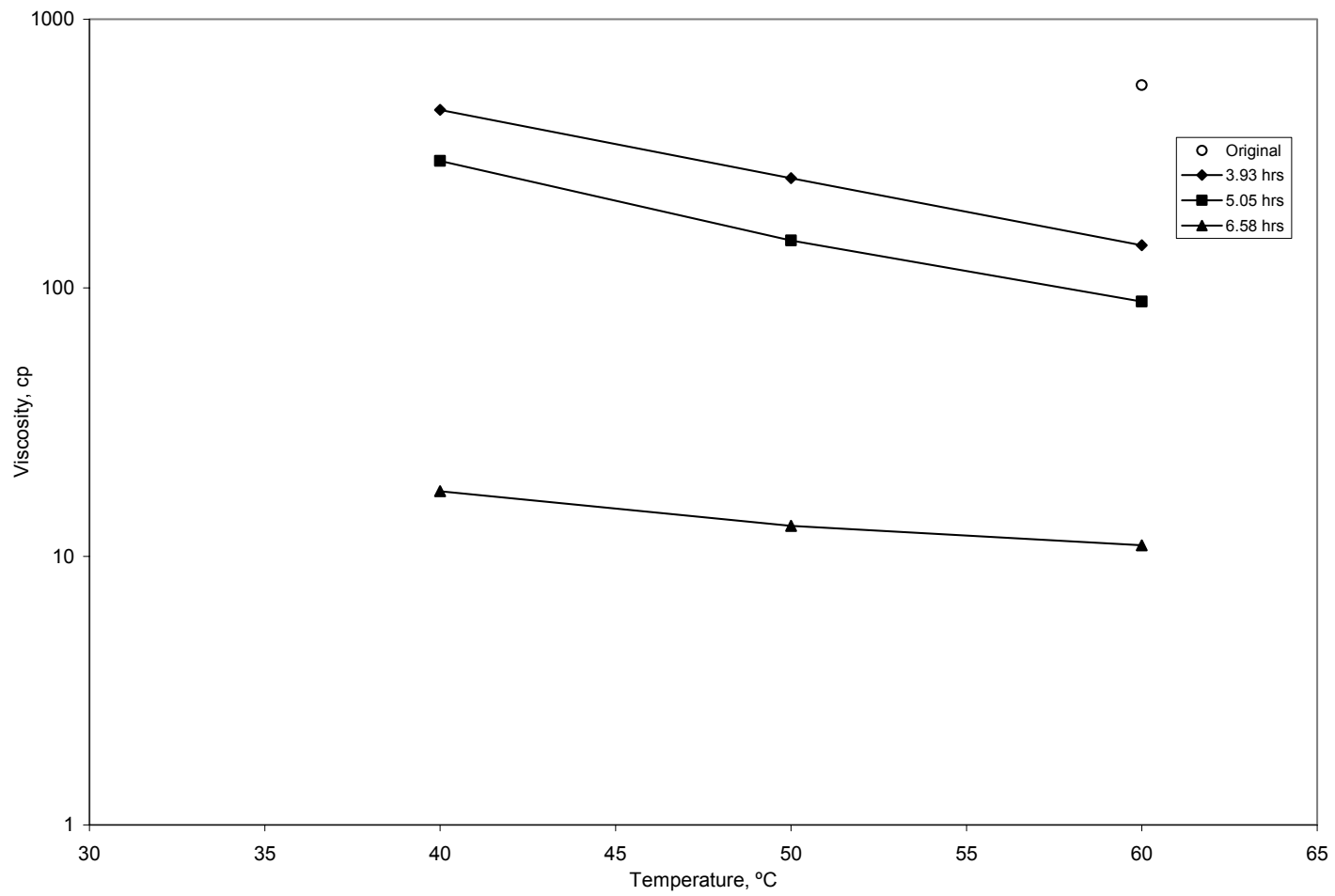


Fig. 4.20—Produced oil viscosity (run no. 7, 21% oxygen).

4.3 Combustion run no. 3 (30% oxygen)

Stable combustion gas composition readings were observed during this run (**Fig. 4.21**), in which the average concentrations of the produced gases were: CO_2 , 15.90%; O_2 , 5.14%; N_2 , 73.73% and CO , 5.21%.

Apparent hydrogen/carbon ratio, F_{HC} , CO_2/CO , and $CO/(CO+CO_2)$ ratios based on the combustion gas analysis presented in **Fig. 4.22** are quite constant during the first two hours of the combustion run. After this period some instability is observed and F_{HC} falls below one, and climbs back to an average value similar to that observed during the first period. This unstable behavior may be due to low temperature oxidation occurring ahead of the combustion front or injection air channeling through the center of the combustion tube where the thermowells are placed. The average F_{HC} , CO_2/CO , and $CO/(CO+CO_2)$ ratios are 1.509, 3.054, and 0.247.

The average combustion temperature was 460 °C (**Fig. 4.23**) and the combustion front velocity was 17.55 cm/hr (0.58 ft/hr) as observed in **Fig. 4.24**. Both values show an increase with respect to the combustion run no. 2 and no. 3 (21% oxygen), something that was expected since the oxygen concentration in the injected air is higher (30% oxygen).

Cumulative volumes of produced oil and water (**Fig. 4.25**) show initial water production occurring at 2.25 hrs and initial oil production at 3.00 hrs., which is slightly lower than that observed in the previous run. Oil recovery (**Fig.4.26**) is a little higher than in the previous runs with a final production of 85.0% of the original oil in place.

The representation of the injected gas rate, held at 3 L/min, production pressure maintained at about 300 psig, and the injection pressure showing a high of approximately 360 psig is observed in **Fig. 4.27**. An increase of the injection pressure is observed as a result of the formation of the oil bank inside the combustion cell. **Fig. 4.28** shows the accumulative gas injected volume, and an average gas production rate of 2.600 L/min.

Produced oil gravity at the end of the combustion run was 8.3°API higher than that of the original crude oil (**Fig. 4.29**). Viscosity of the produced oil dropped to 2.7 cp at 60°C from its original value of 568 cp (**Fig. 4.30**).

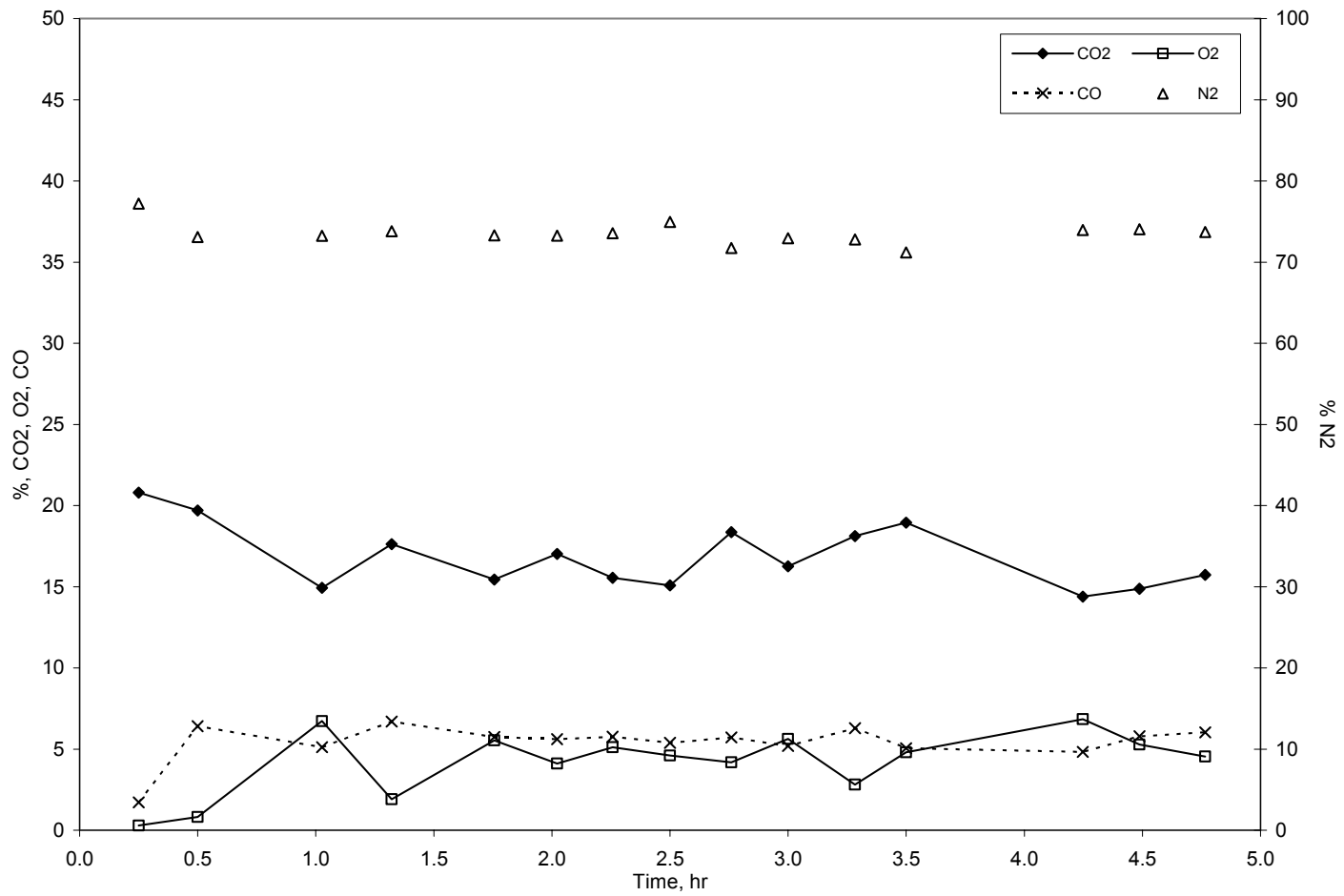


Fig. 4.21—Combustion gas composition (run no. 3, 30% oxygen).

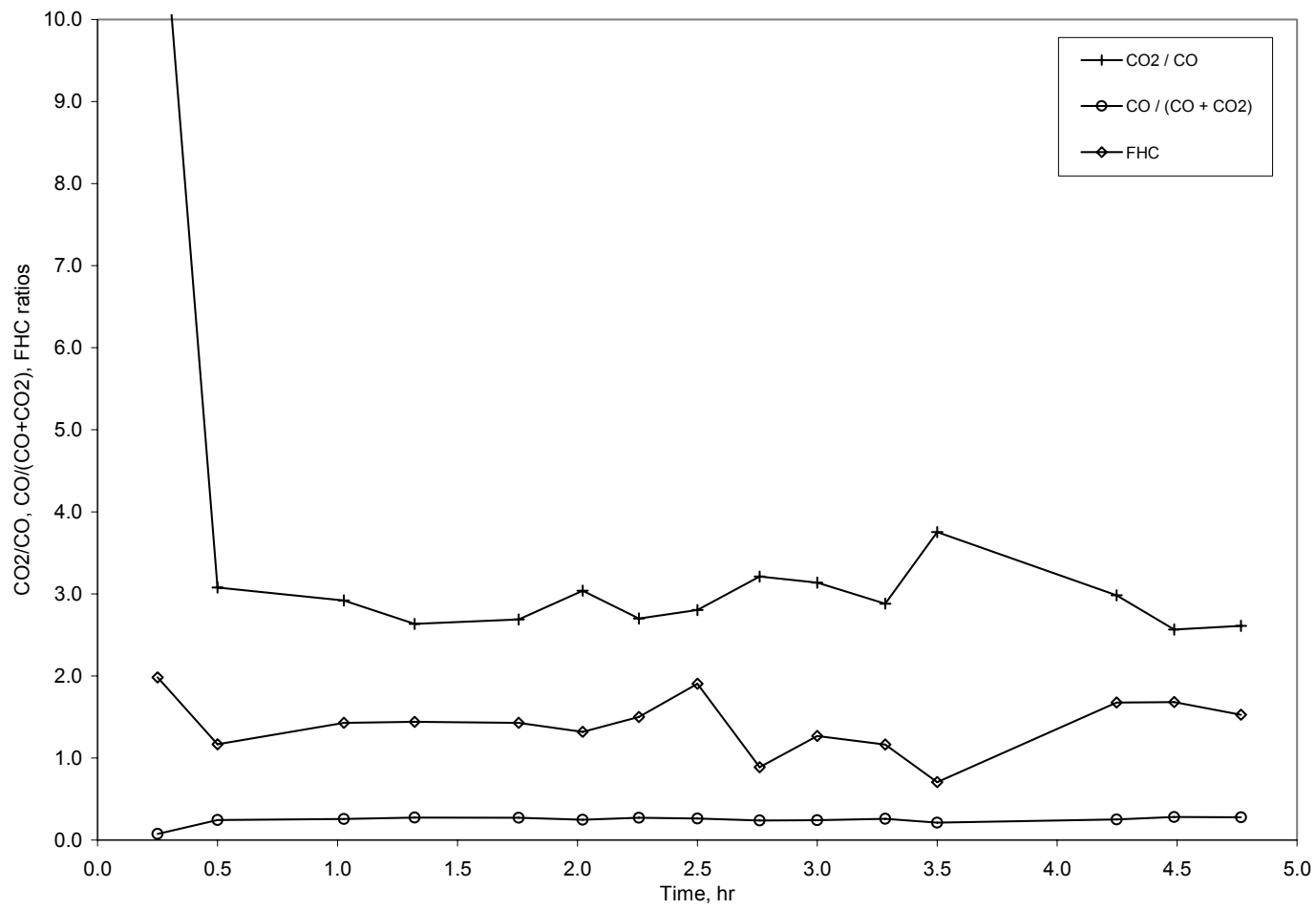


Fig. 4.22— F_{HC} , CO_2/CO , and $CO/(CO+CO_2)$ ratios (run no. 3, 30% oxygen).

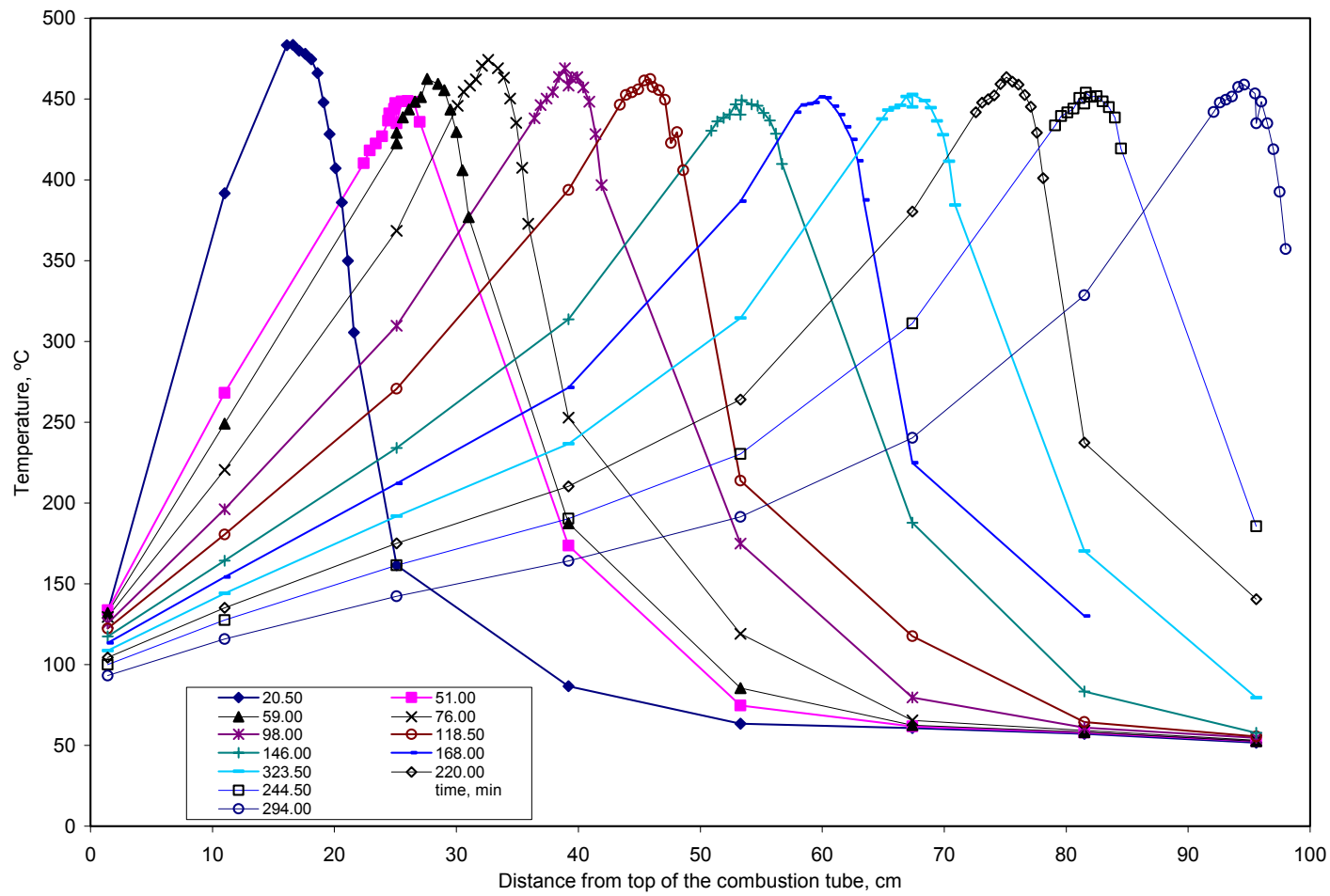


Fig. 4.23—Temperature profiles (run no. 3, 30% oxygen).

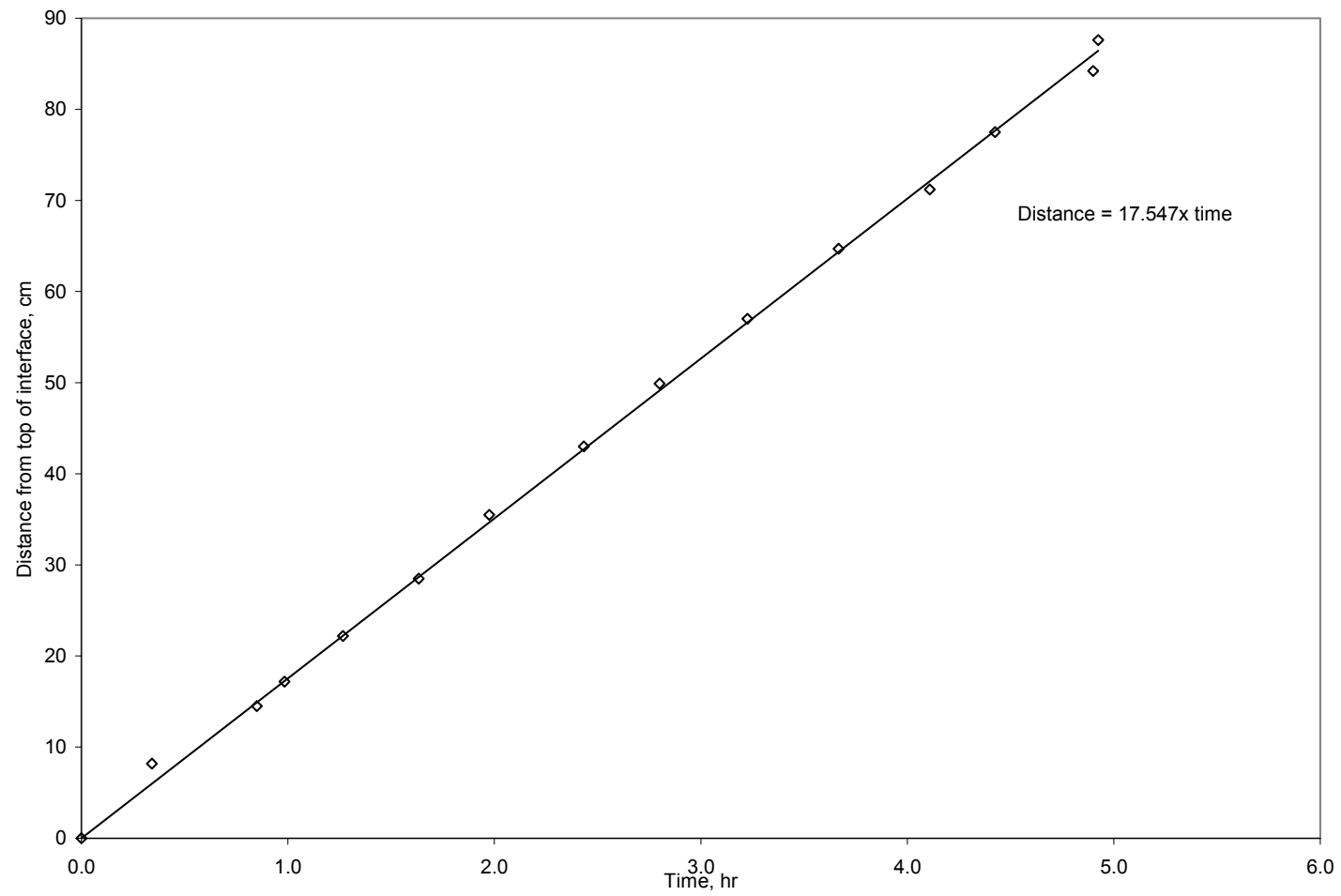


Fig. 4.24—Combustion front velocity (run no. 3, 30% oxygen).

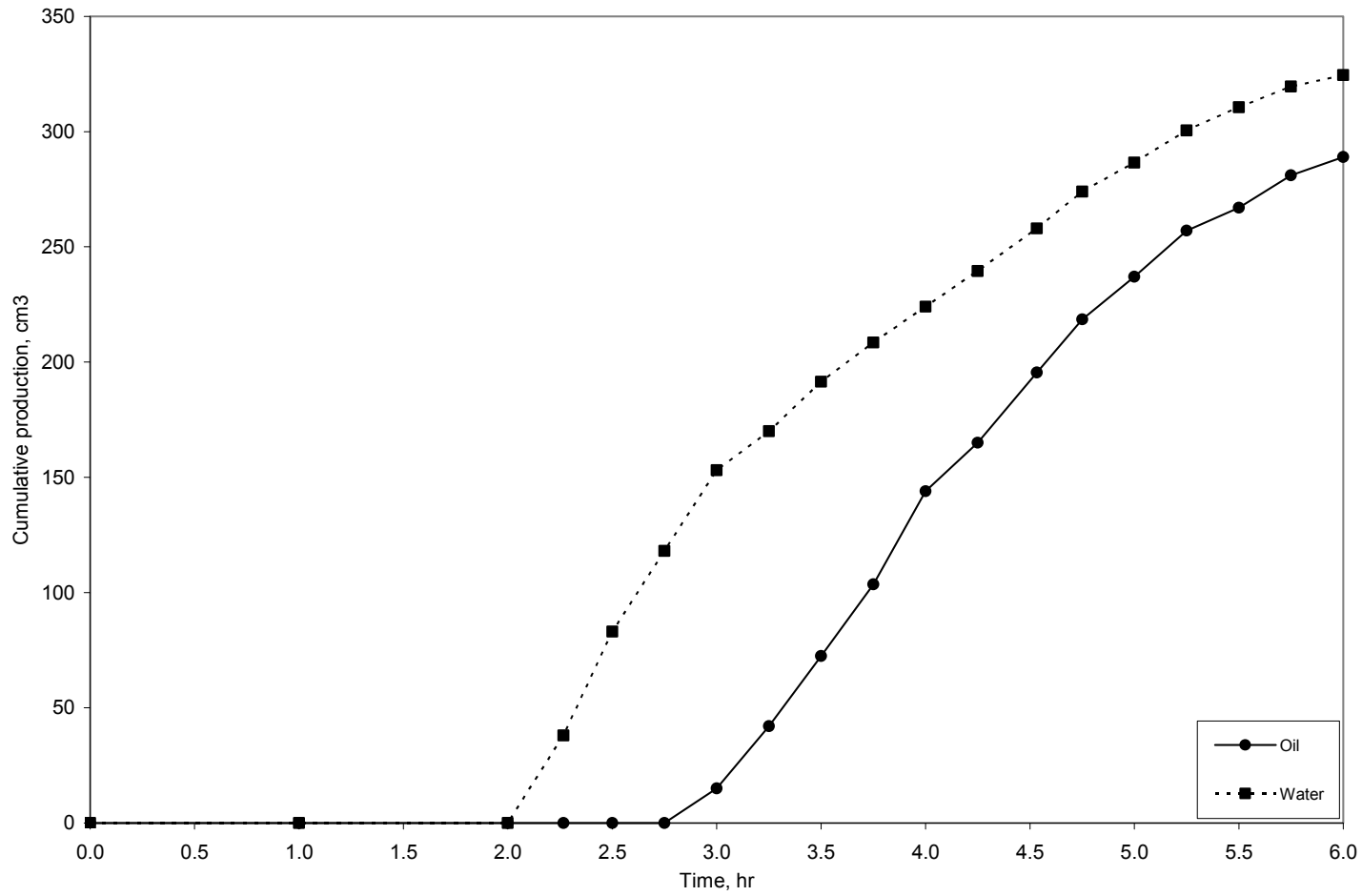


Fig. 4.25—Cumulative oil and water production (run no. 3, 30% oxygen).

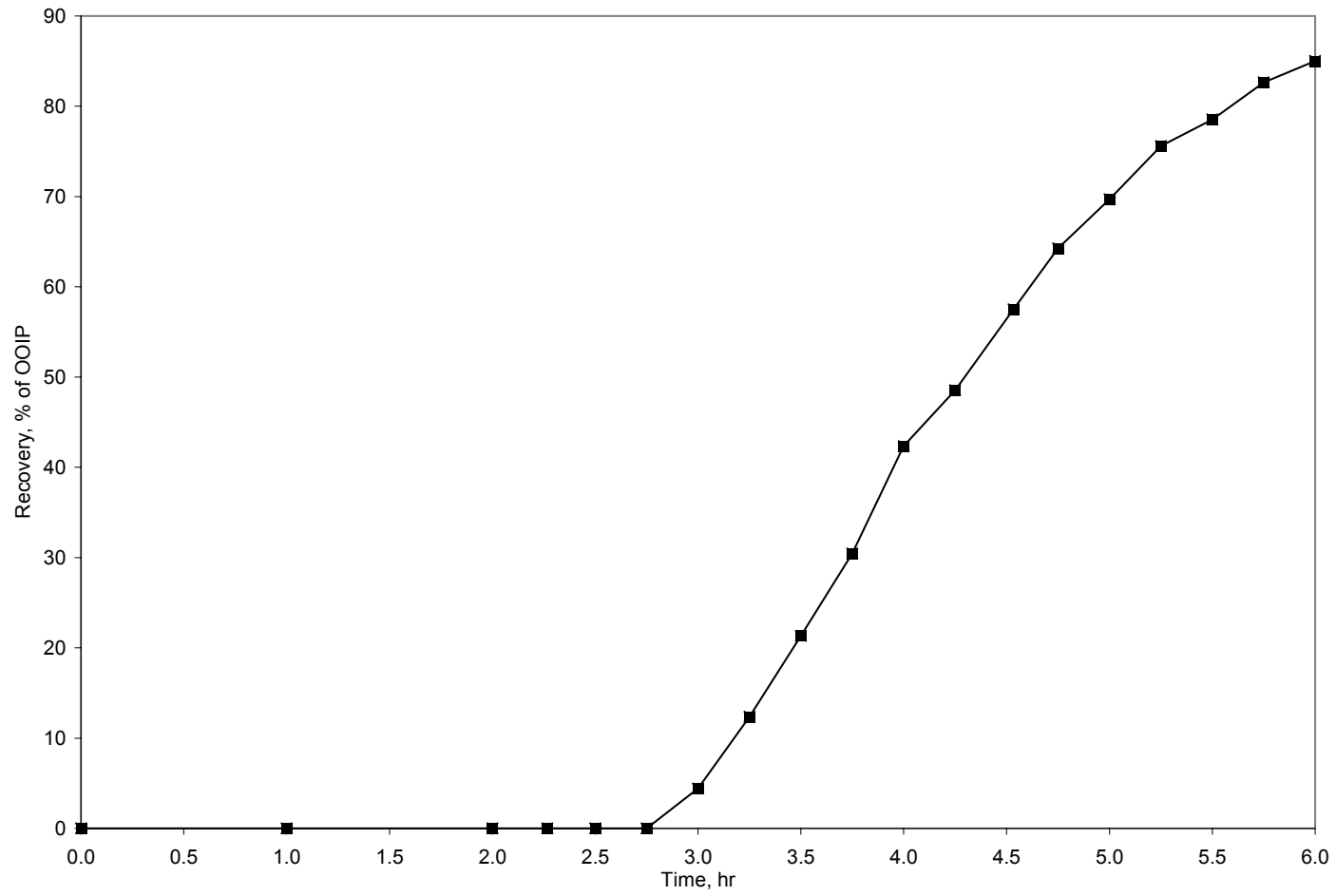


Fig. 4.26—Oil recovery (run no. 3, 30% oxygen).

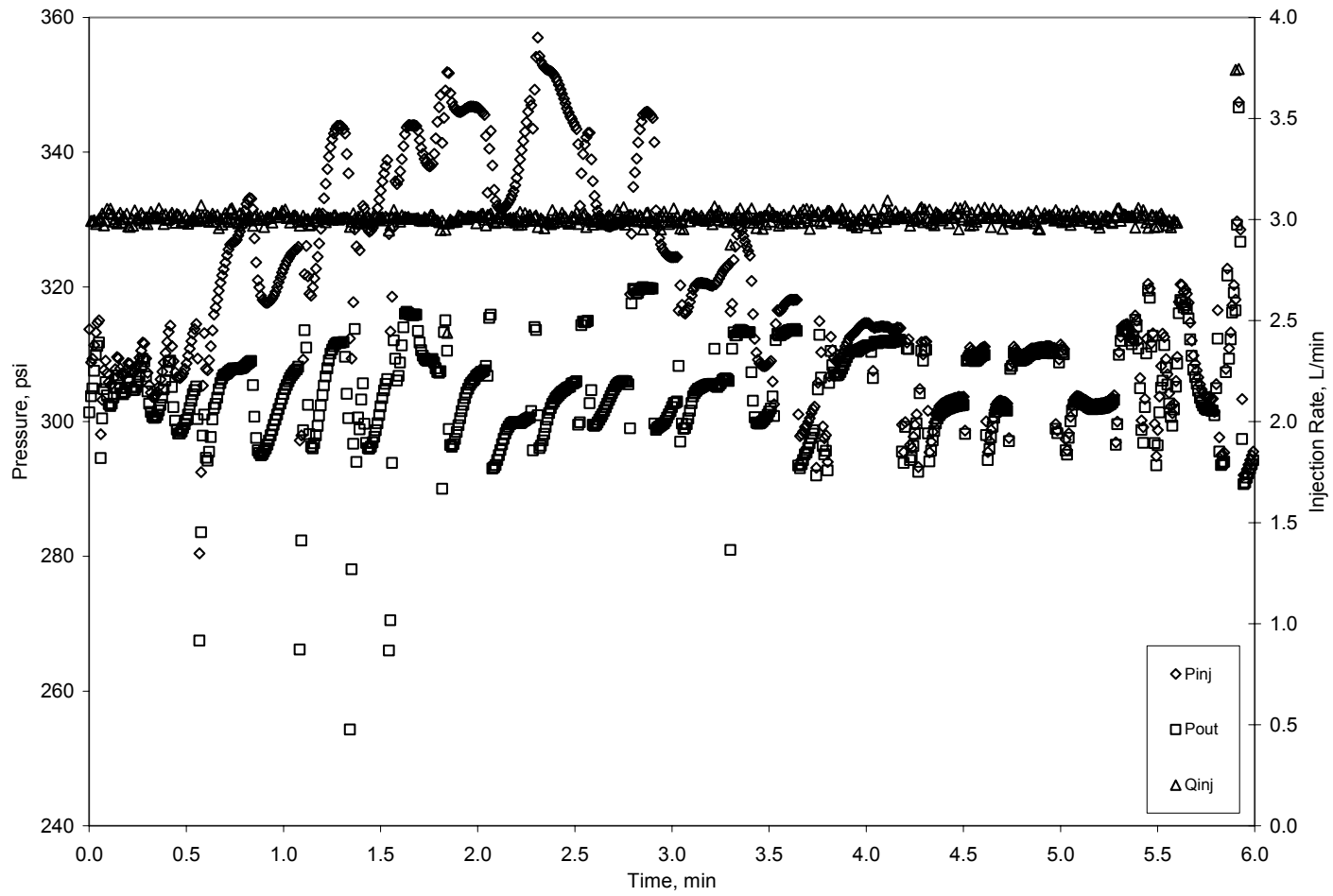


Fig. 4.27—Injection and production pressures, and gas injection rate (run no. 3, 30% oxygen).

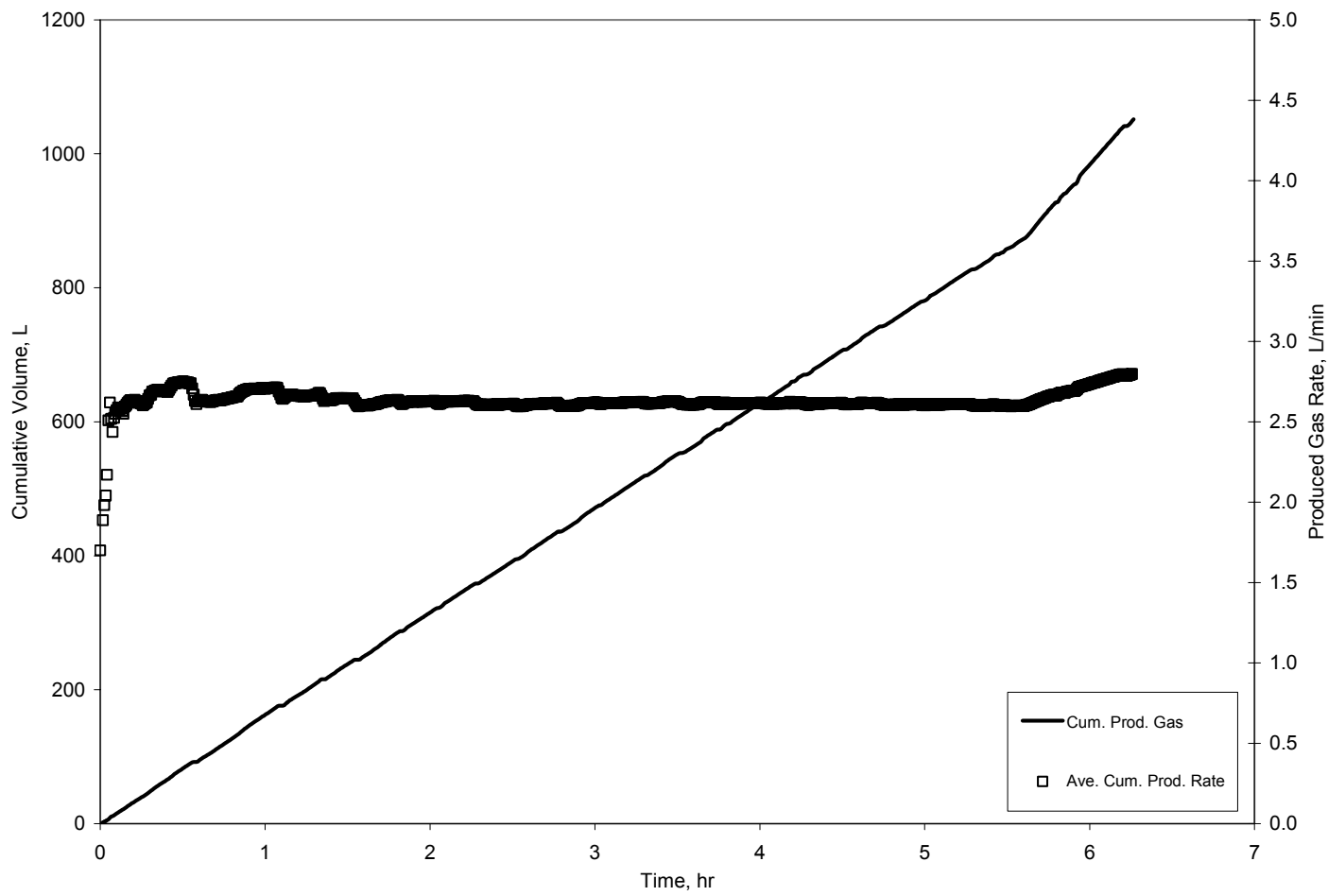


Fig. 4.28—Cumulative volume and produced gas rate (run no. 3, 30% oxygen).

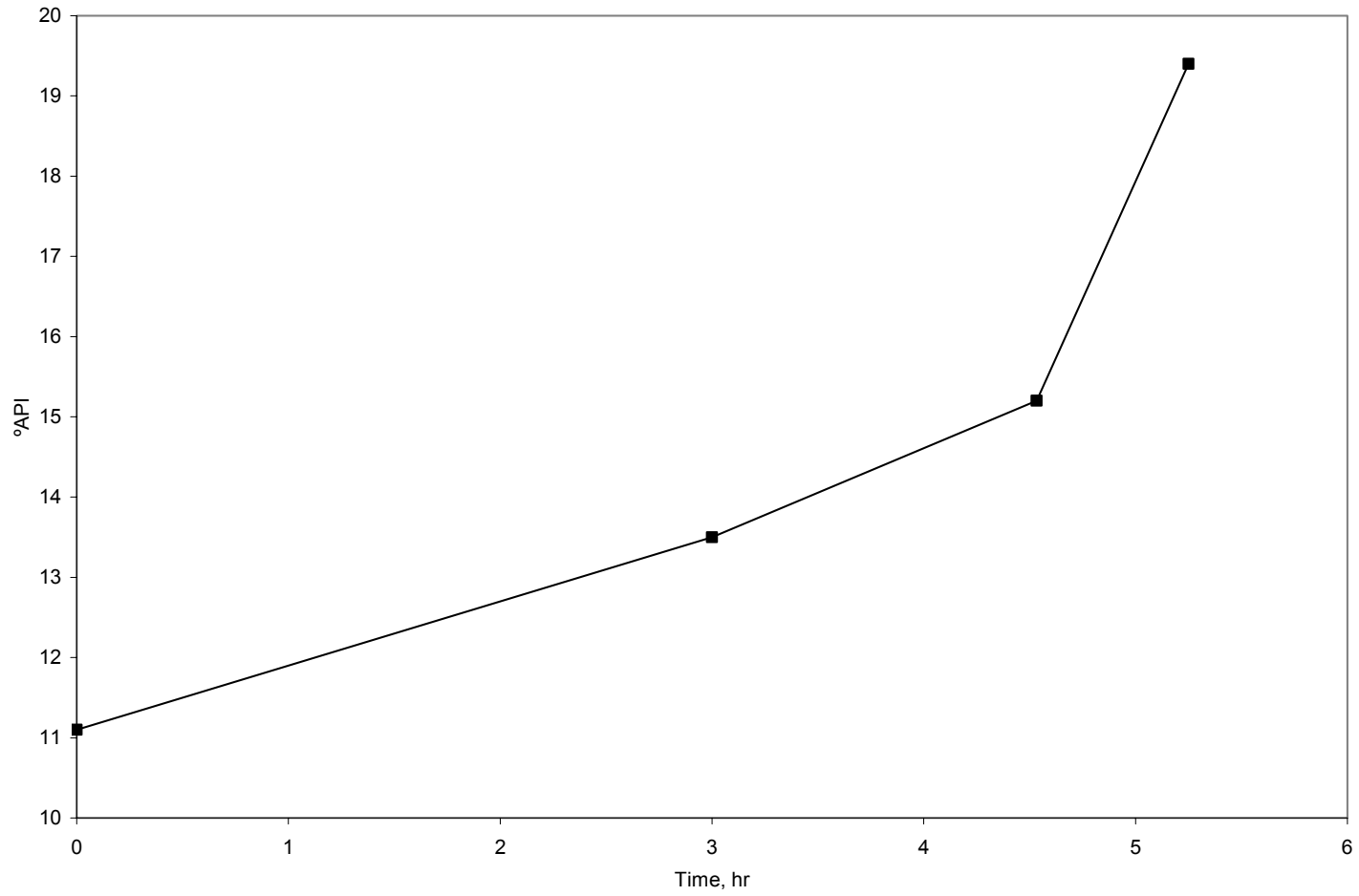


Fig. 4.29—Produced oil gravity (run no. 3, 30% oxygen).

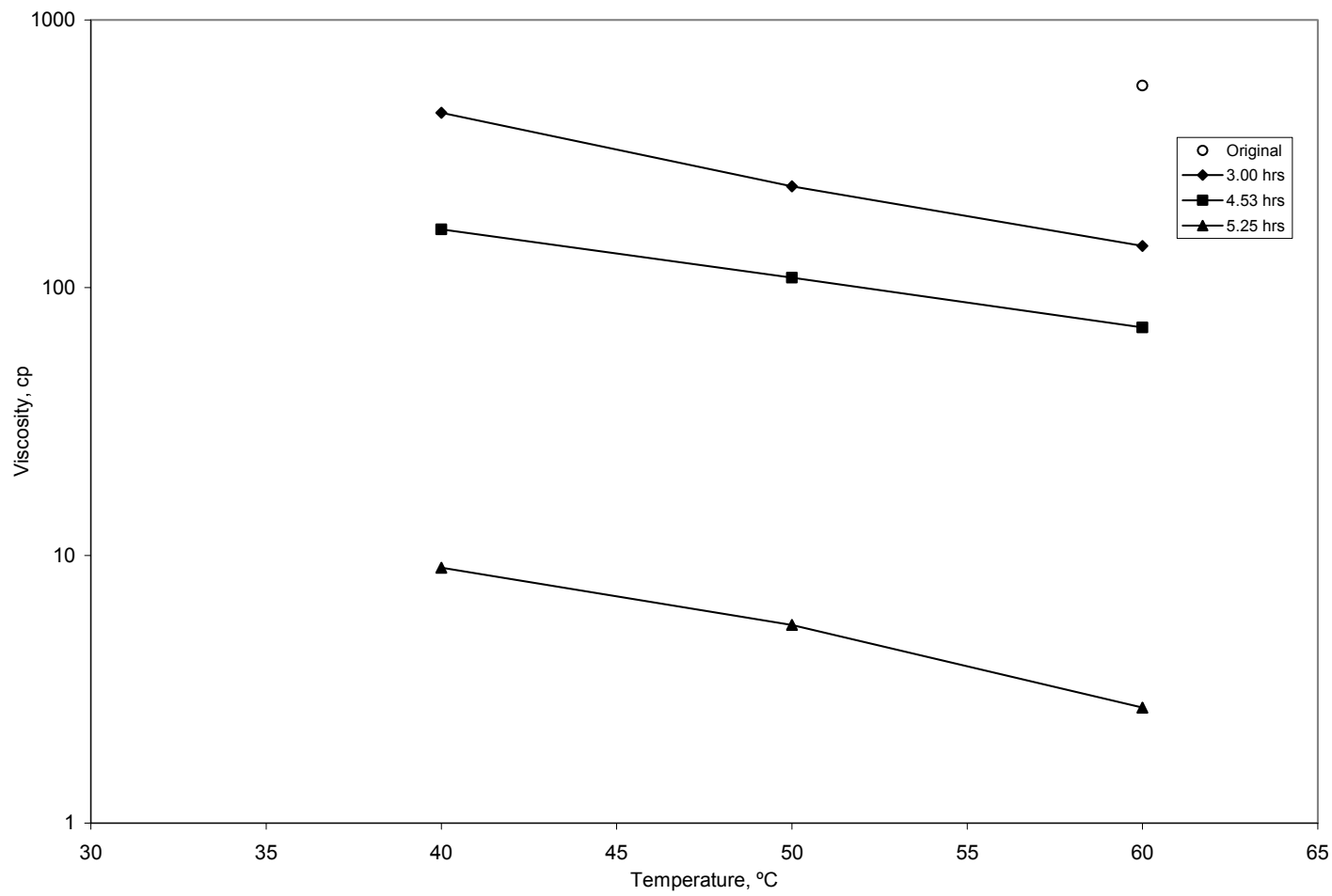


Fig. 4.30—Produced oil viscosity (run no. 3, 30% oxygen).

4.4 Combustion run no. 4 (30% oxygen)

The combustion gas composition in this run was observed to be stable during the period between 2 to 4 hours (**Fig. 4.31**). The average concentrations of the produced gases were: CO_2 , 16.94%; O_2 , 4.42%; N_2 , 72.89% and CO , 5.69%.

Fig. 4.32 shows the apparent hydrogen/carbon ratio, F_{HC} , CO_2/CO , and $CO/(CO+CO_2)$ ratios based of the combustion gas analysis. During the unstable part of this run, F_{HC} falls below one; however it is very uniform in the stable period mentioned above. On average, F_{HC} , CO_2/CO , and, $CO/(CO+CO_2)$ ratios are 1.244, 2.976, and 0.251 respectively corresponding to a high temperature oxidation process.

The average combustion temperature was 455 °C (**Fig. 4.33**) and the combustion front velocity observed in **Fig. 4.34** was 19.29 cm/hr (0.633 ft/hr). **Fig. 4.35** shows the cumulative volumes of produced oil and water, with an initial water production occurring at 1.62 hrs. and initial oil production at 2.6 hrs, values that were expected to be smaller than run No. 2. The final oil recovery (**Fig. 4.36**) is 81.8% of the original oil placed in the combustion cell.

Injected gas rate, approximately 3 L/min, production pressure, about 300 psig, and the injection pressure showing a high of approximately 350 psig are observed in **Fig. 4.37**. Again the spread between the injection and production pressure is attributed to the formation of the oil bank inside the combustion cell. **Fig. 4.38** shows the cumulative gas injected volume, and an average gas production rate of 2.599 L/min.

Produced oil gravity at the end of the combustion run was 7.2°API higher than that of the original crude oil (**Fig. 4.39**). Viscosity of the produced oil dropped to 13 cp at 60°C from its original value of 568 cp (**Fig. 4.40**).

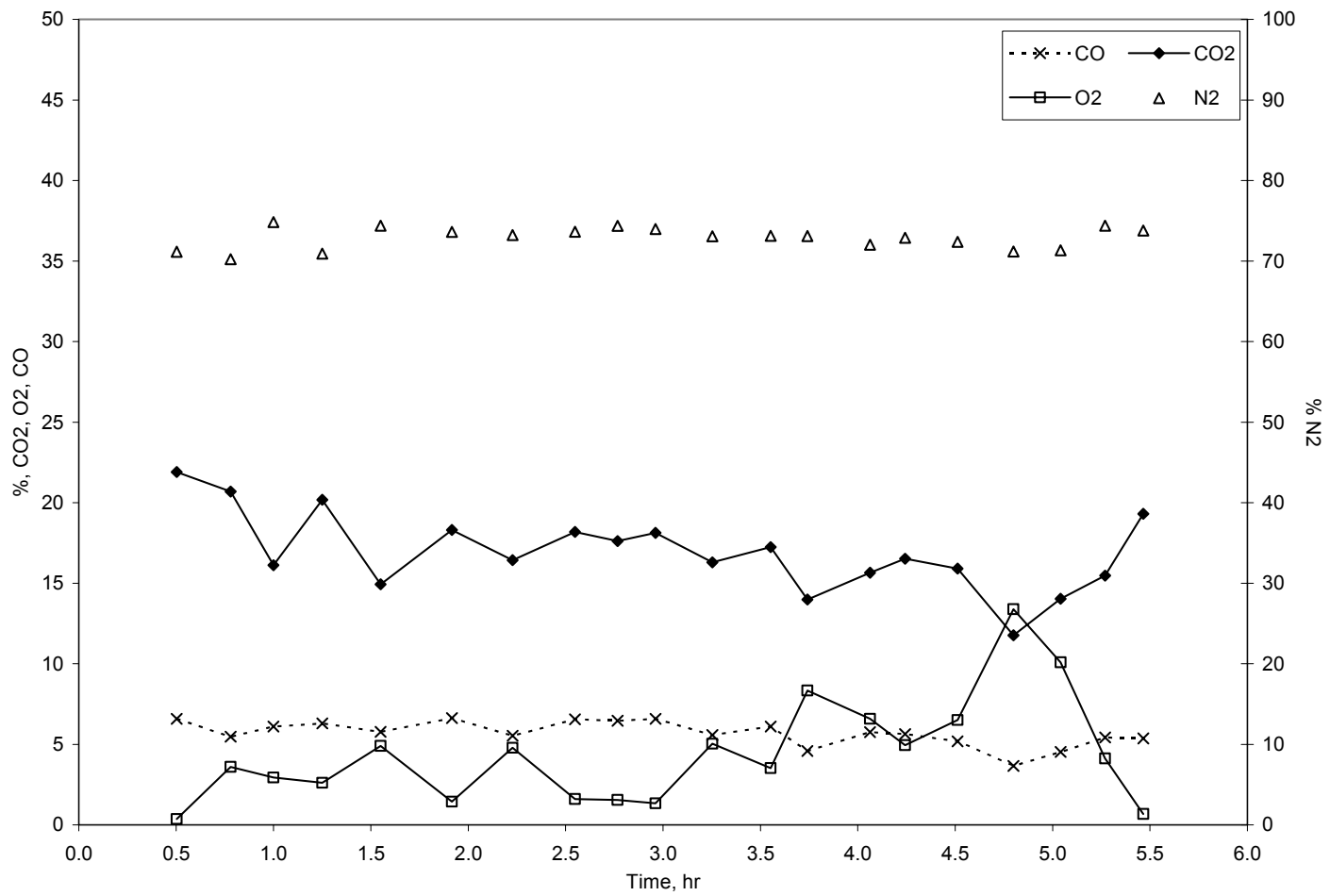


Fig. 4.31—Combustion gas composition (run no. 4, 30% oxygen).

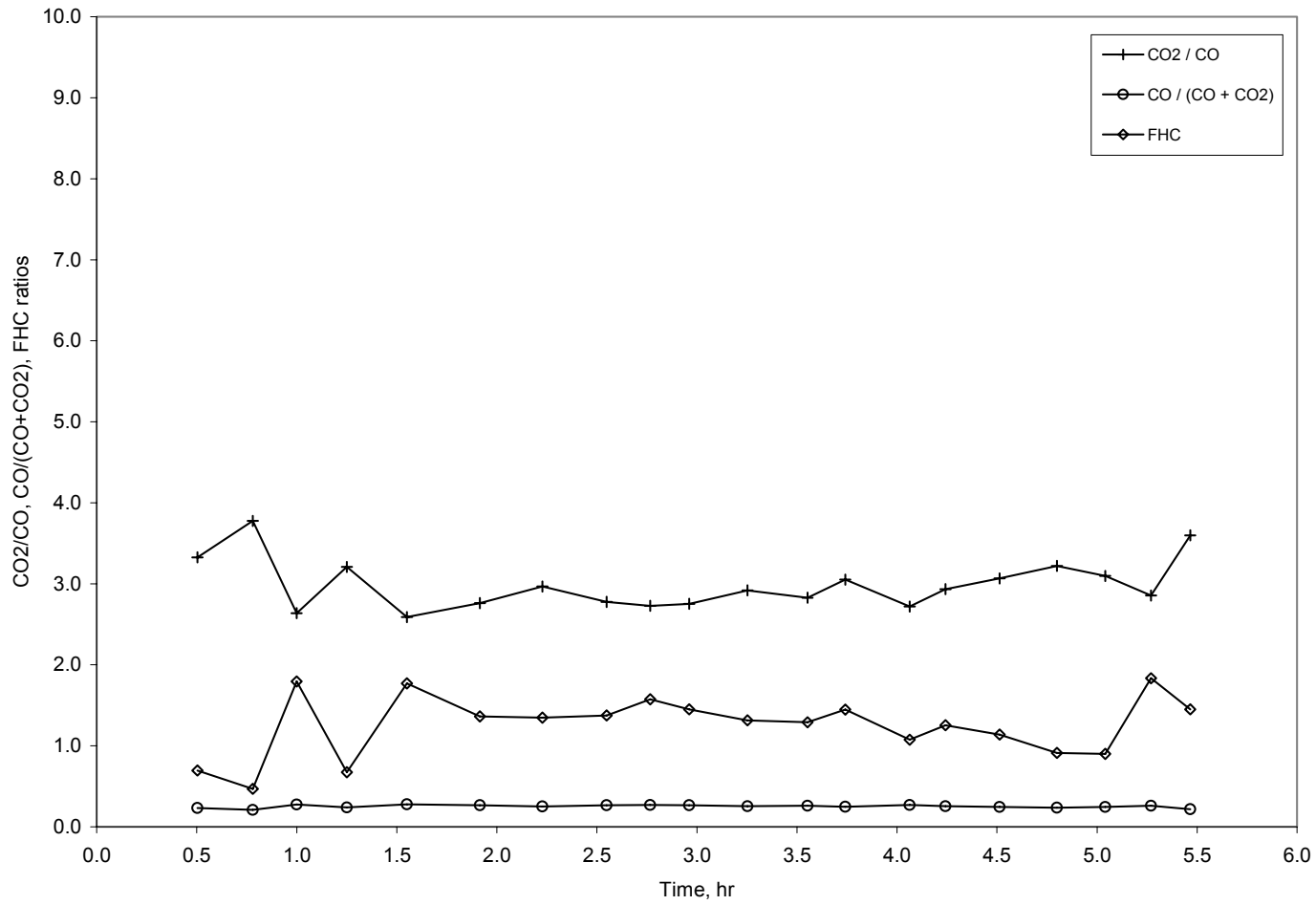


Fig. 4.32— F_{HC} , CO_2/CO , and $CO/(CO+CO_2)$ ratios (run no. 4, 30% oxygen).

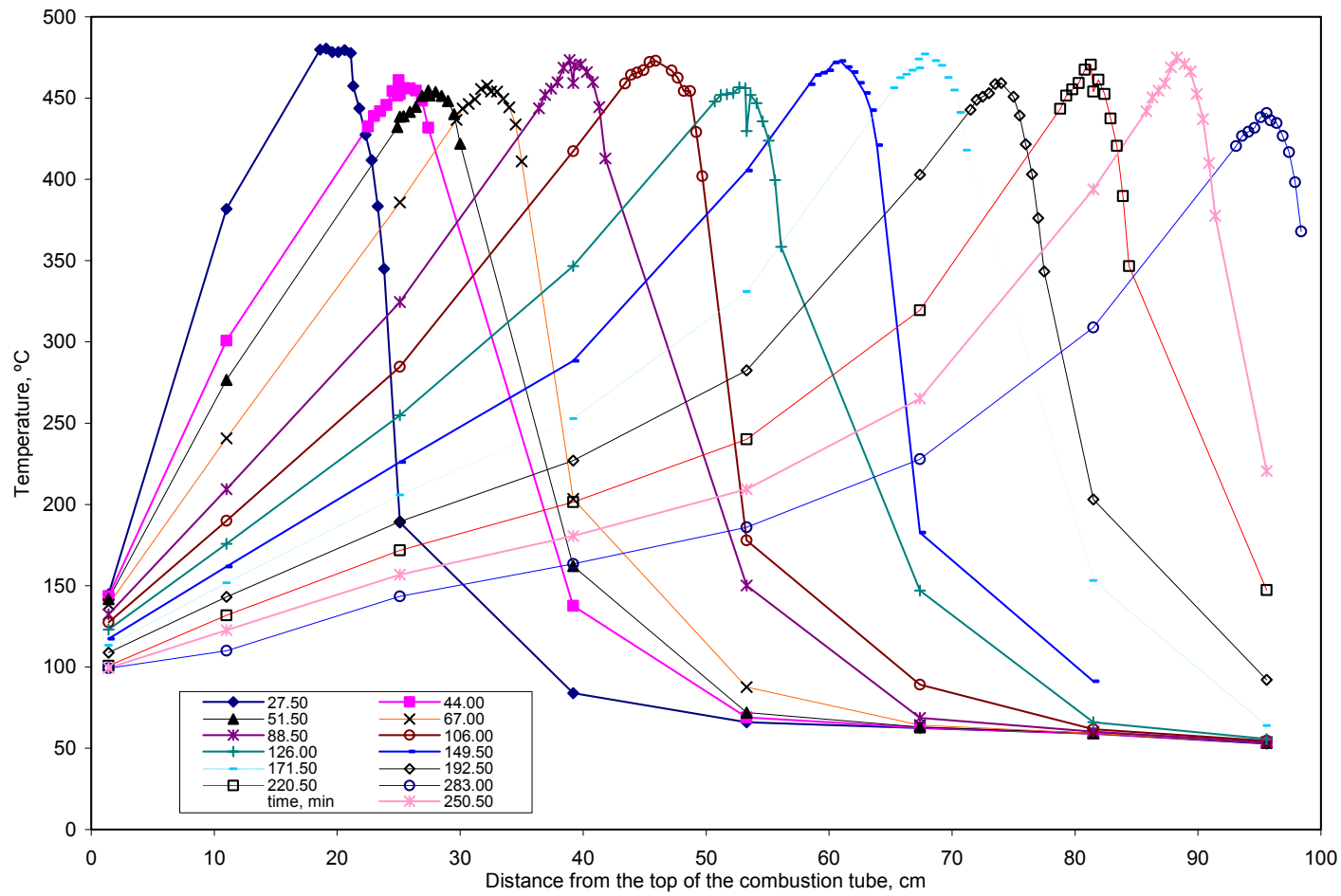


Fig. 4.33—Temperature profiles (run no. 4, 30% oxygen).

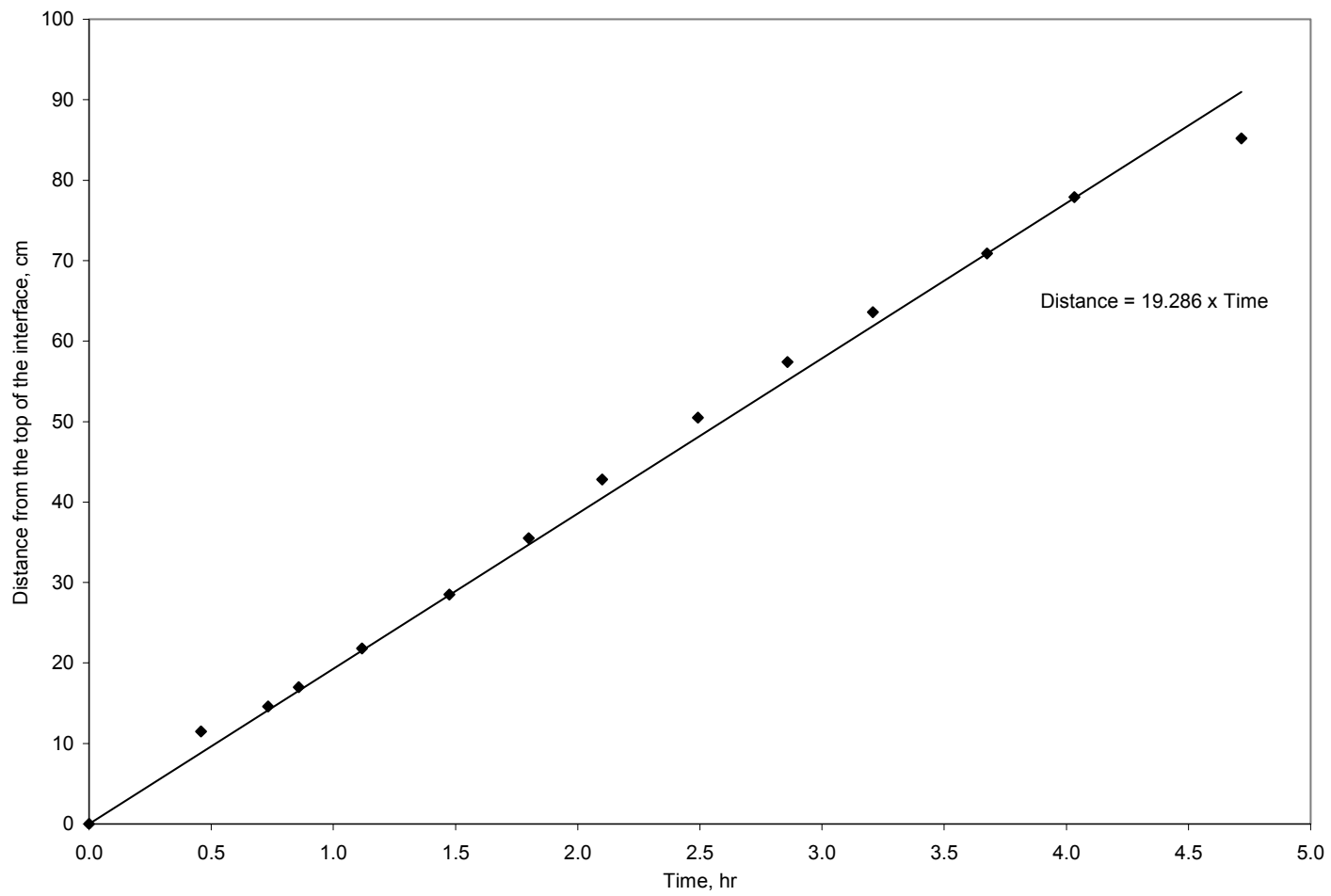


Fig. 4.34—Combustion front velocity (run no. 4, 30% oxygen).

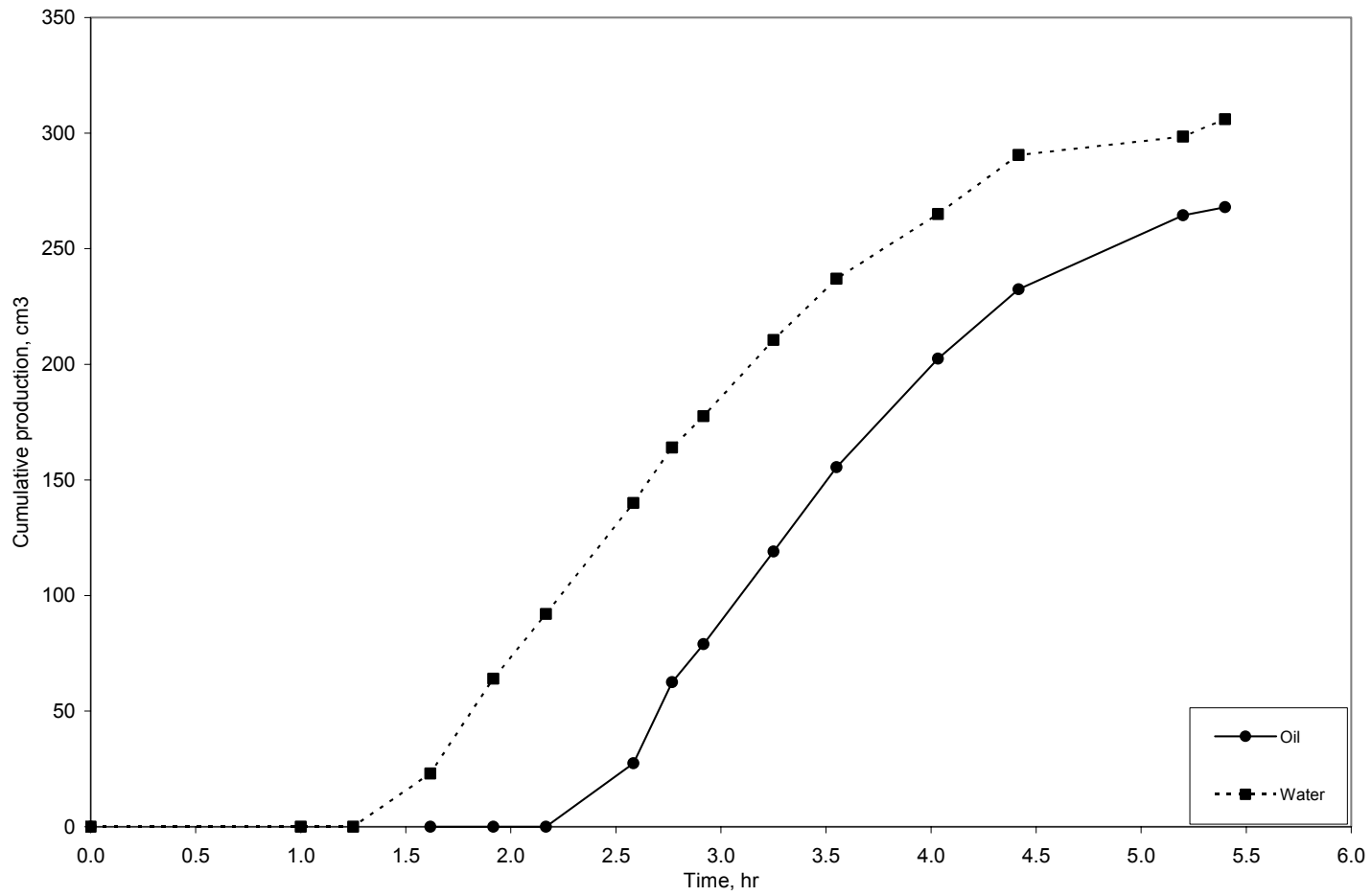


Fig. 4.35—Cumulative oil and water production (run no. 4, 30% oxygen).

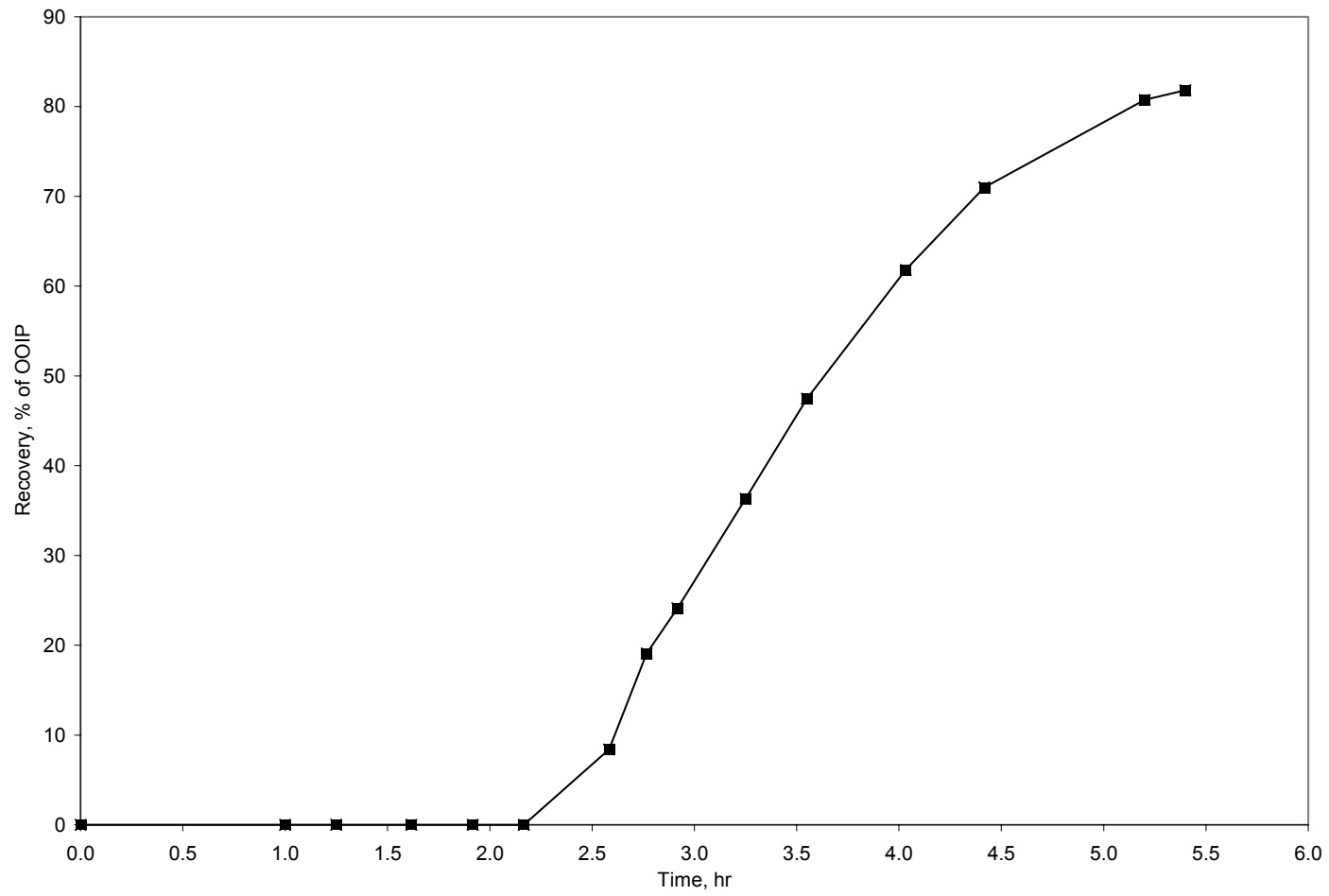


Fig. 4.36—Oil recovery (run no. 4, 30% oxygen).

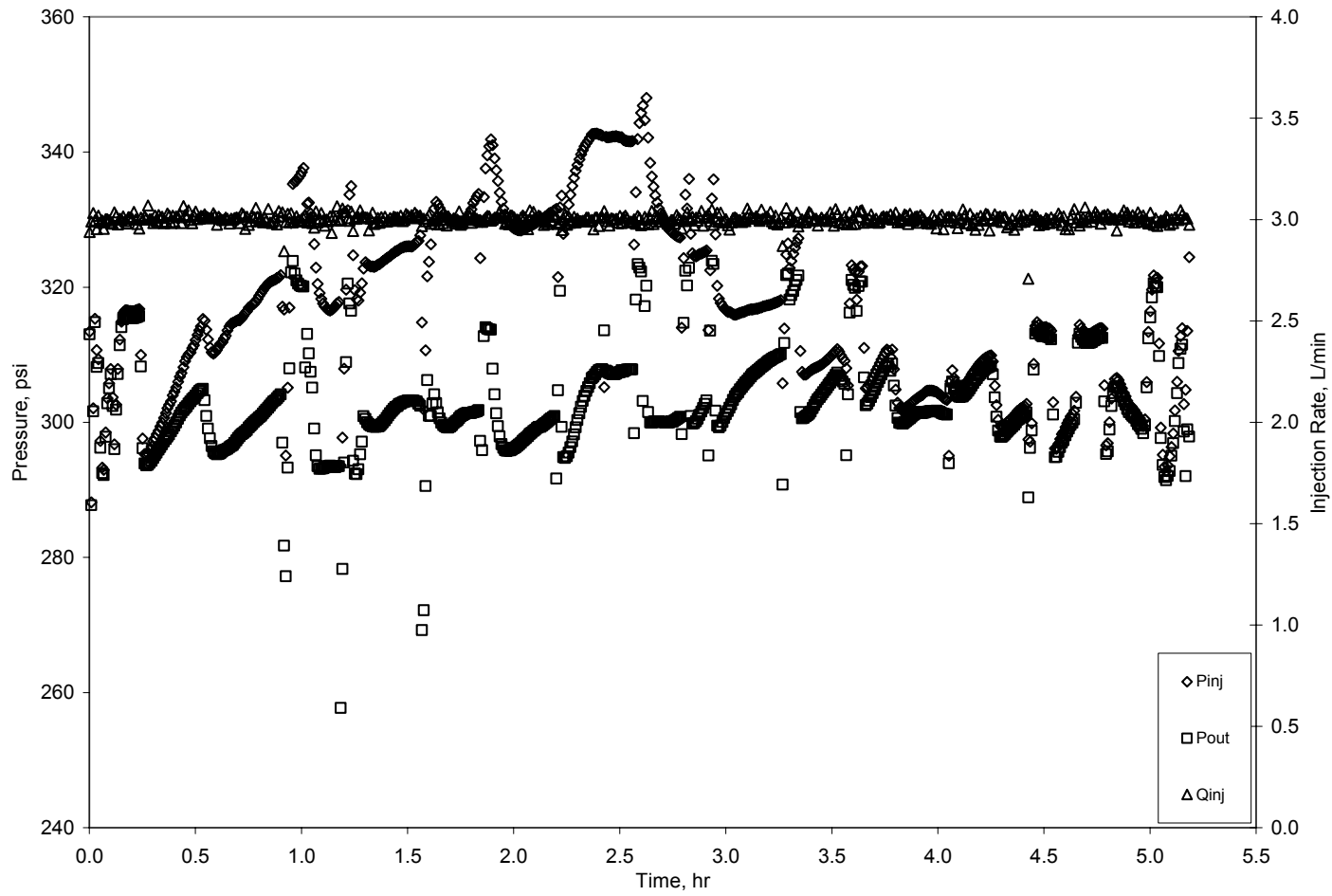


Fig. 4.37—Injection and production pressures, and gas injection rate (run no. 4, 30% oxygen).

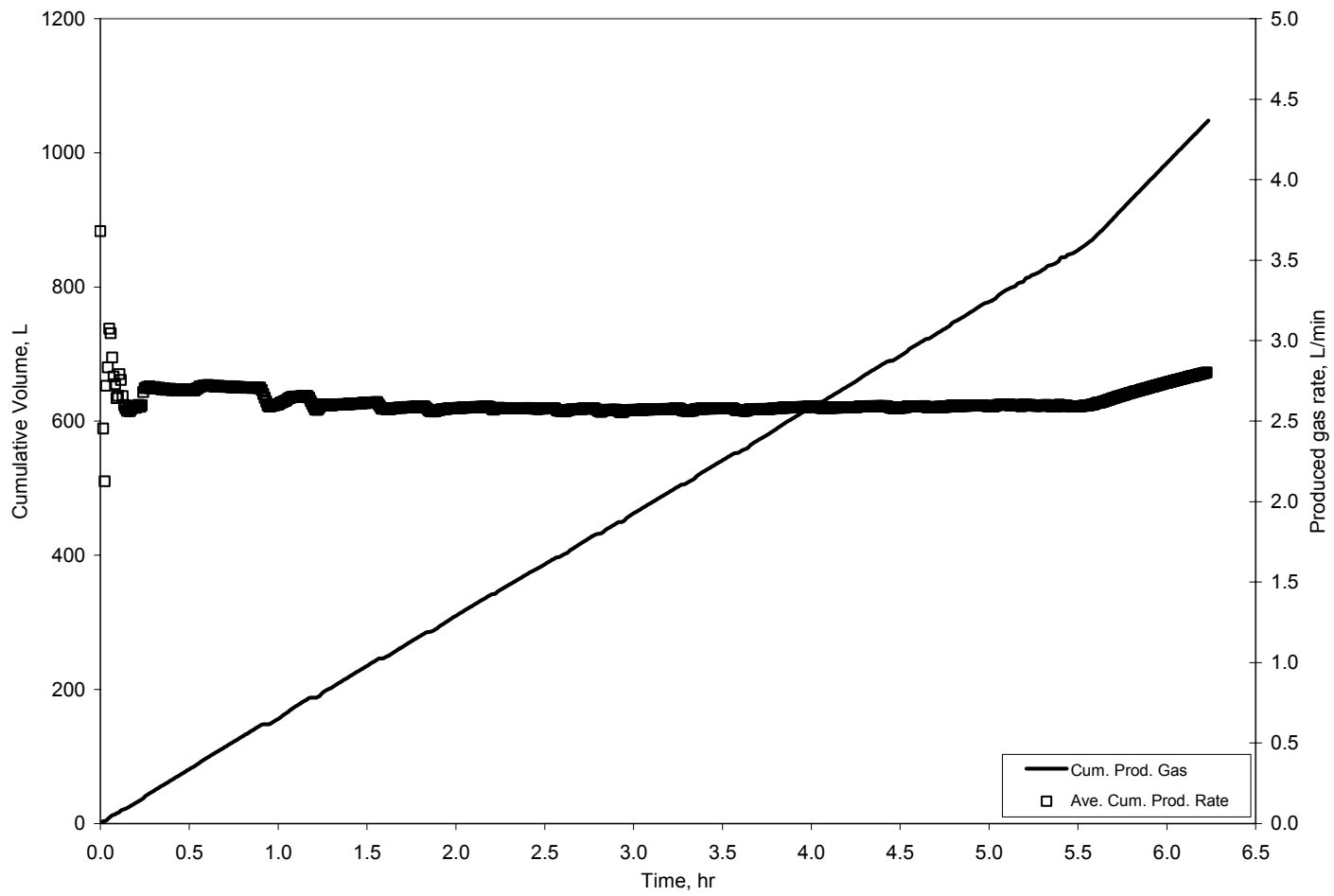


Fig. 4.38—Cumulative volume and produced gas rate (run no. 4, 30% oxygen).

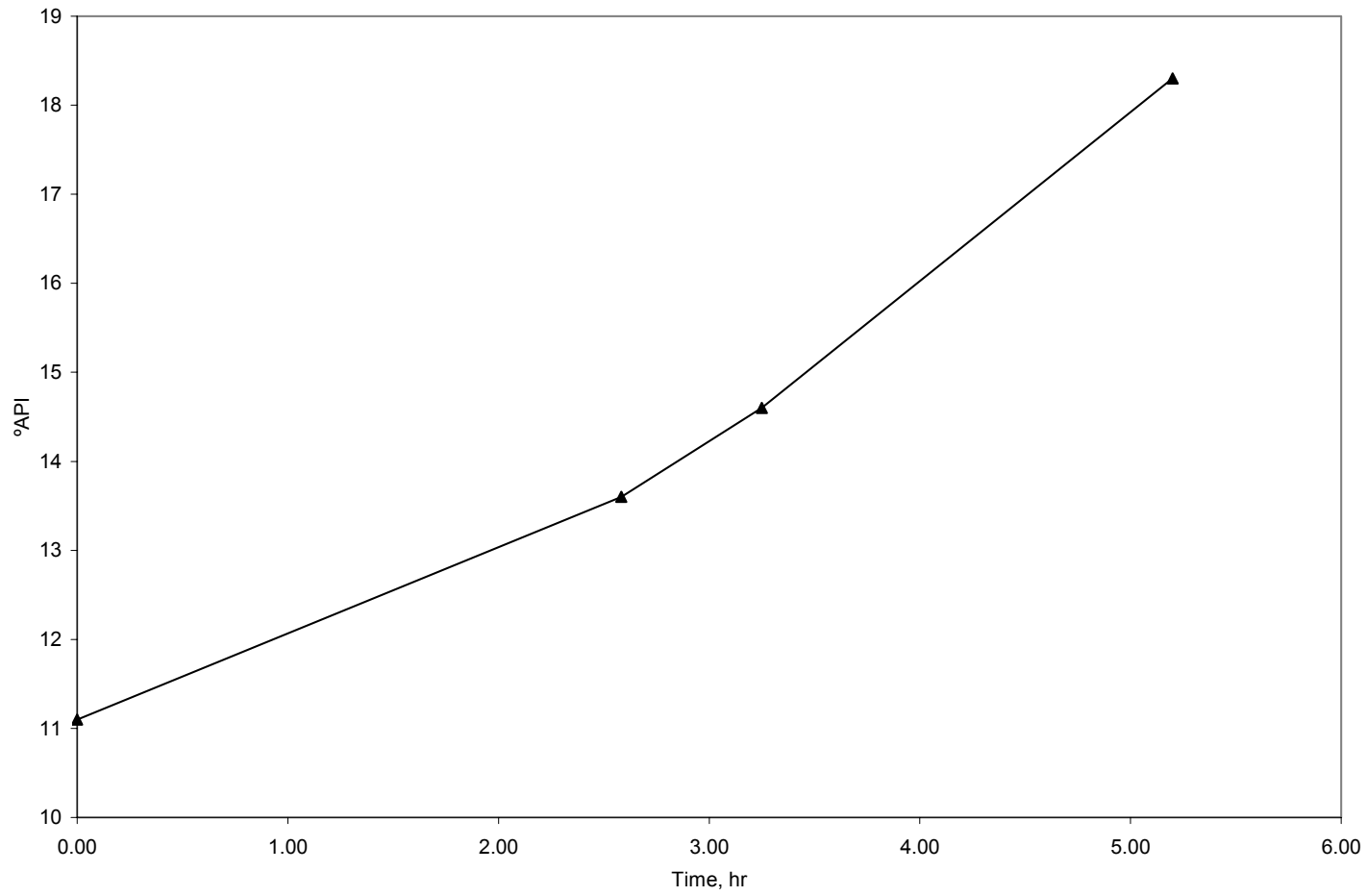


Fig. 4.39—Produced oil gravity (run no. 4, 30% oxygen).

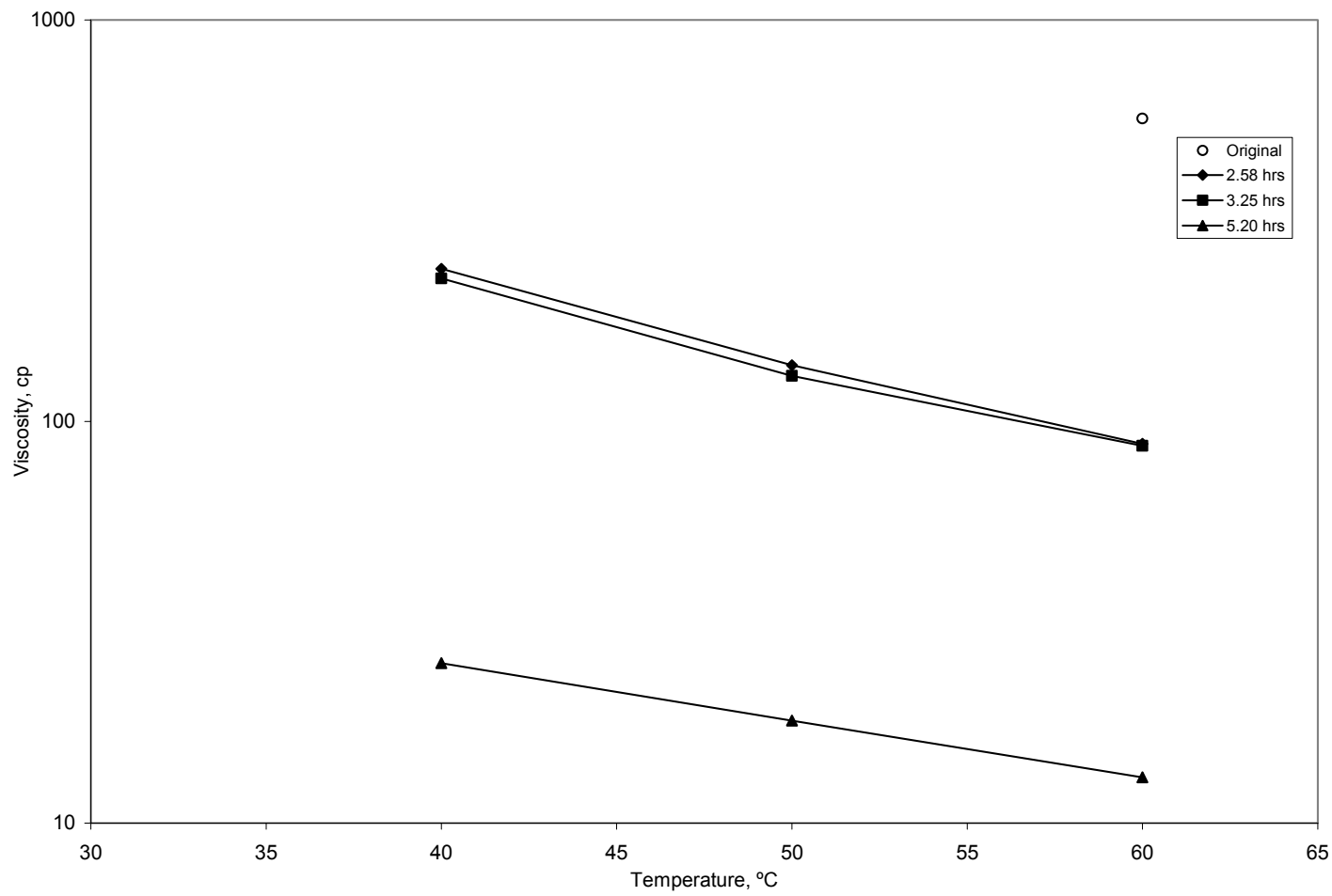


Fig. 4.40—Produced oil viscosity (run no. 4, 30% oxygen).

4.5 Combustion run no. 5 (40% oxygen)

The combustion gas composition during this run was not observed to have a defined trend, with important variability of the concentration of the produced CO_2 and O_2 (**Fig. 4.41**). During the run the average concentrations of the produced gases were: CO_2 , 20.50%; O_2 , 8.12%; N_2 , 63.98% and CO , 7.17%.

Apparent hydrogen/carbon ratio, F_{HC} , CO_2/CO , and, $CO/(CO+CO_2)$ ratios based on the combustion gas analysis are presented in **Fig. 4.42**. With the exception of one reading the F_{HC} ratio is well above one, which is a clear indication of high temperature oxidation. Averages values of F_{HC} , CO_2/CO , and, $CO/(CO+CO_2)$ ratios, 1.511, 2.858, and 0.259 respectively, also confirm this assumption.

The average combustion temperature was 475 °C (**Fig. 4.43**). The combustion front velocity was 22.09 cm/hr (0.73 ft/hr) as observed in **Fig. 4.44**.

Fig. 4.45 shows the cumulative volumes of produced oil and water, with an initial water and oil production registered at 1.28 and 2.02 hrs respectively. Oil recovery was 82.1 % of the original oil placed in the combustion cell **Fig. 4.46**.

Fig. 4.47 shows a maximum pressure of approximately 350 psig during the combustion run. As before, the gas injection rate is constant at 3 L/min, and the production pressure is maintained at about 300 psig. The cumulative injected gas volume and an average production gas rate of 2.674 L/min are shown in **Fig. 4.48**.

Produced oil gravity at the end of the combustion run was 5.0°API higher than that of the original crude oil (**Fig. 4.49**). Viscosity of the produced oil dropped to 75 cp at 60°C from its original value of 568 cp (**Fig. 4.50**).

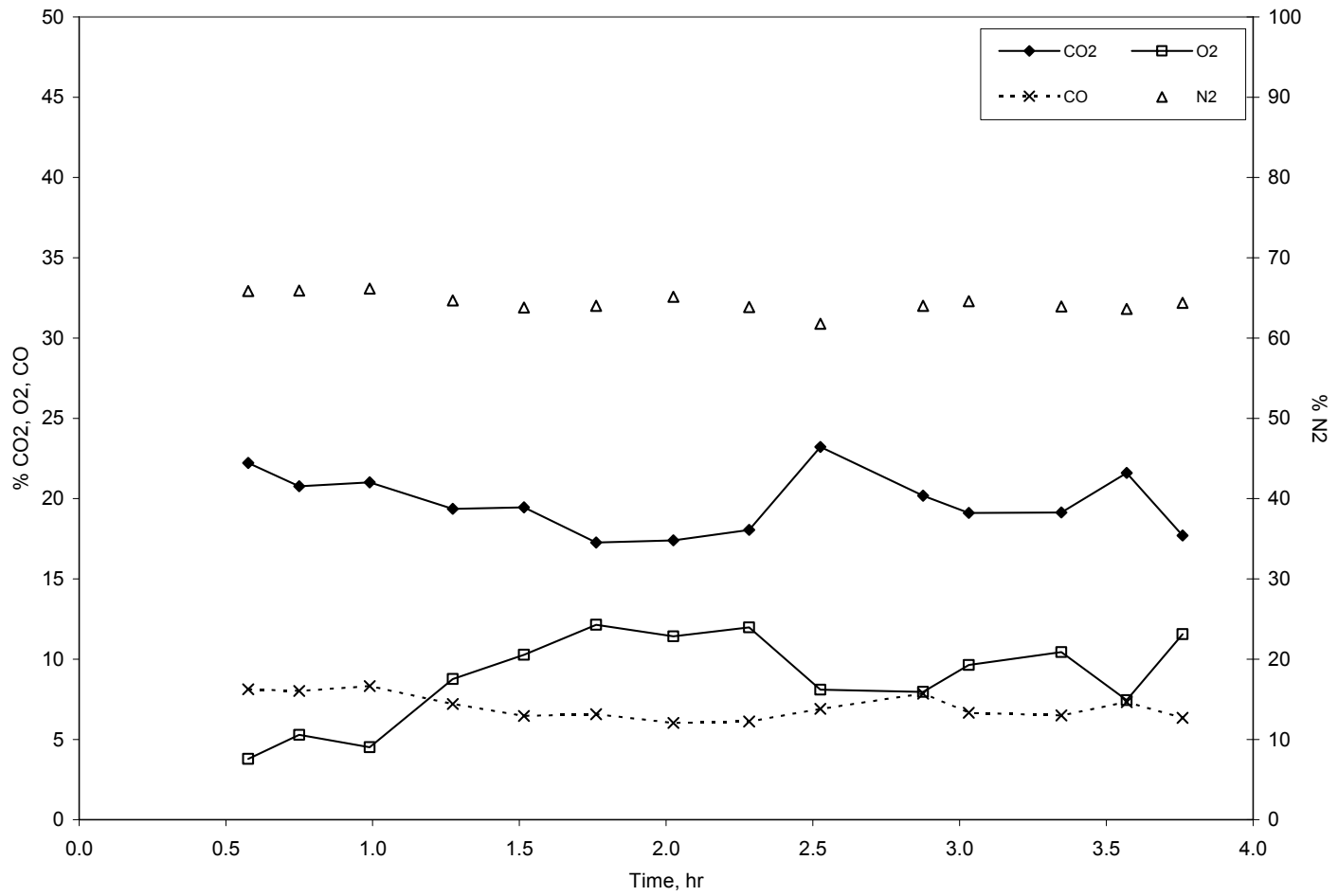


Fig. 4.41—Combustion gas composition run (run no. 5, 40% oxygen).

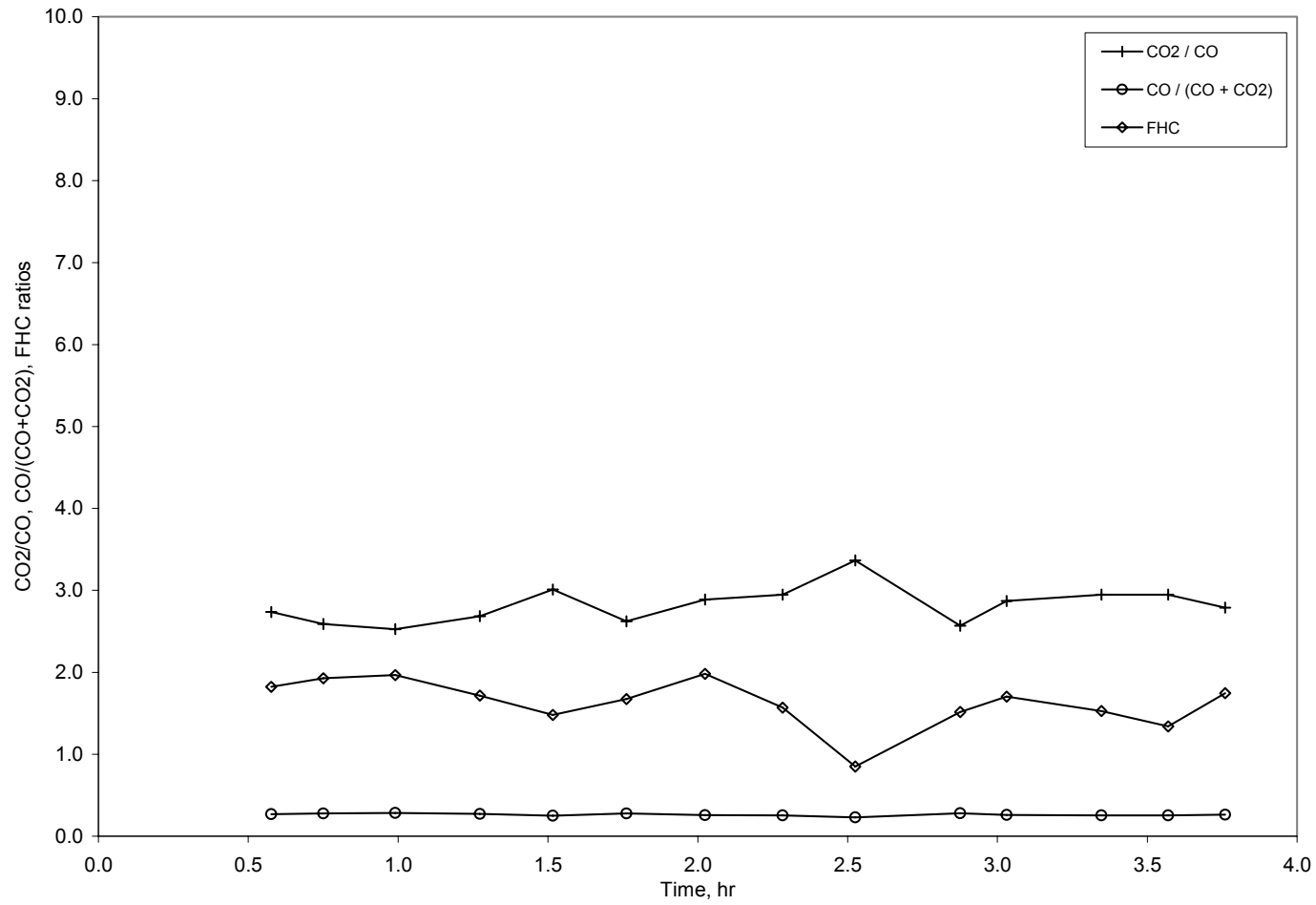


Fig. 4.42— F_{HC} , CO_2/CO , and $CO/(CO+CO_2)$ ratios (run no. 5, 40% oxygen).

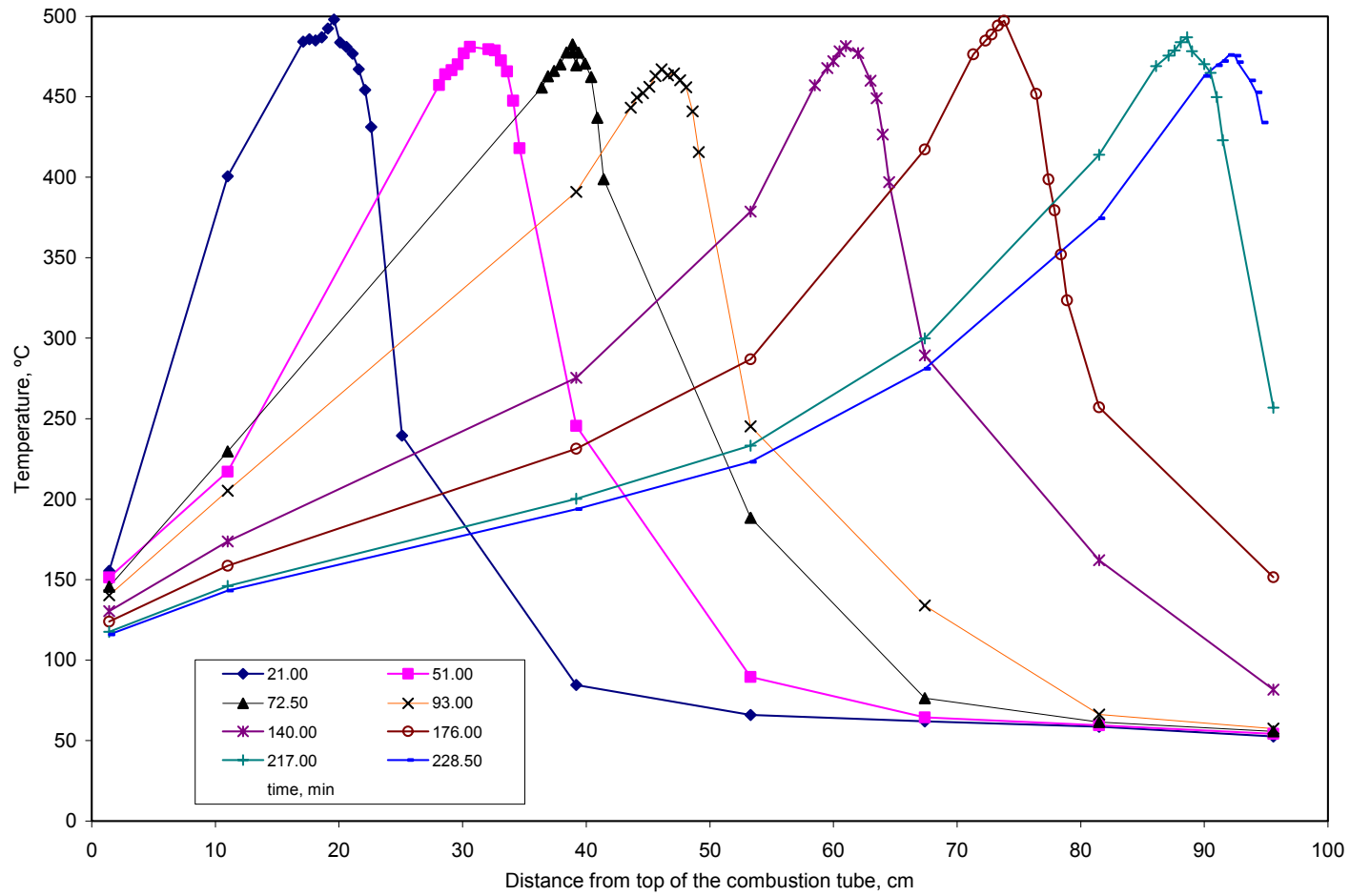


Fig. 4.43—Temperature profiles (run no. 5, 40% oxygen).

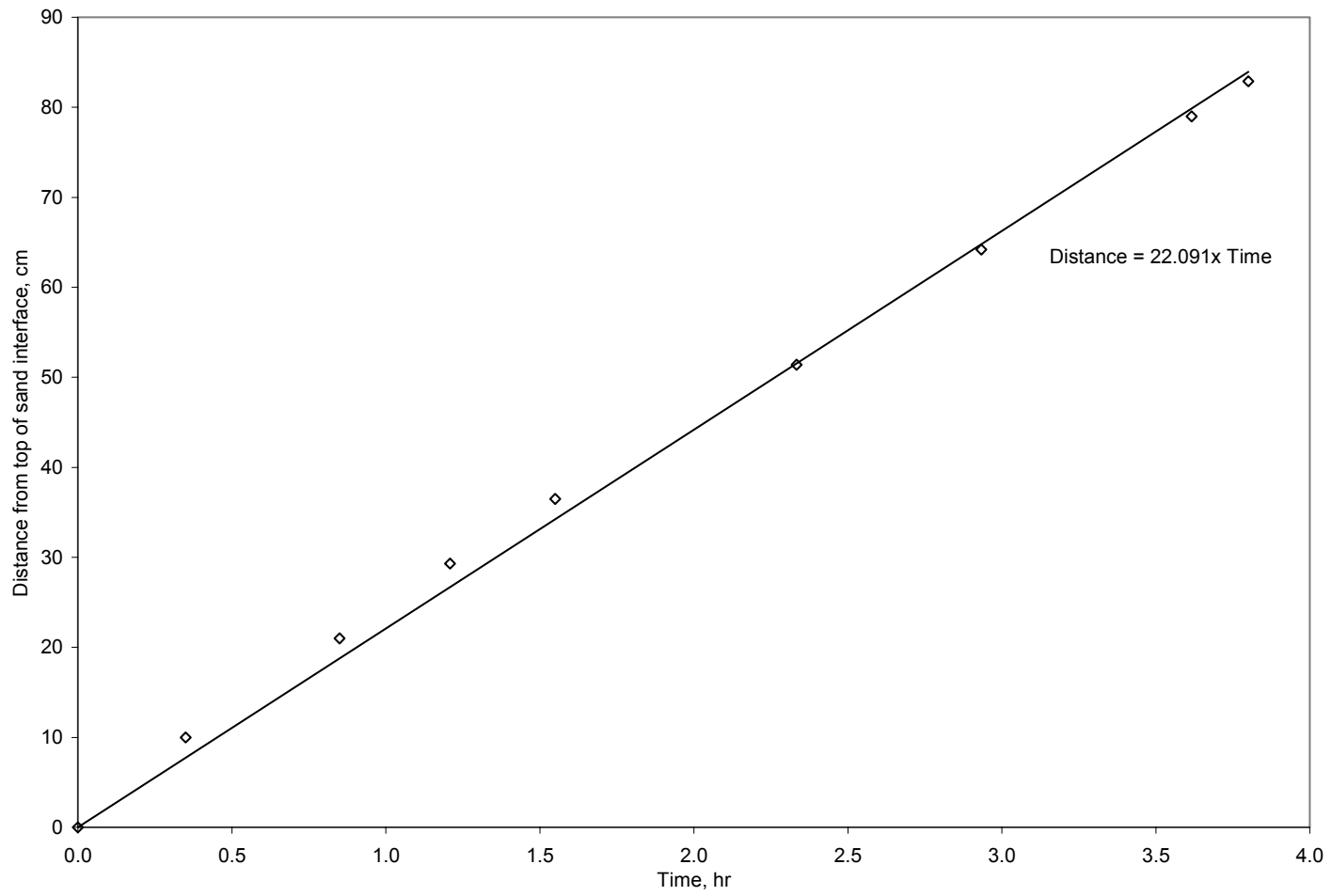


Fig. 4.44—Combustion front velocity (run no. 5, 40% oxygen).

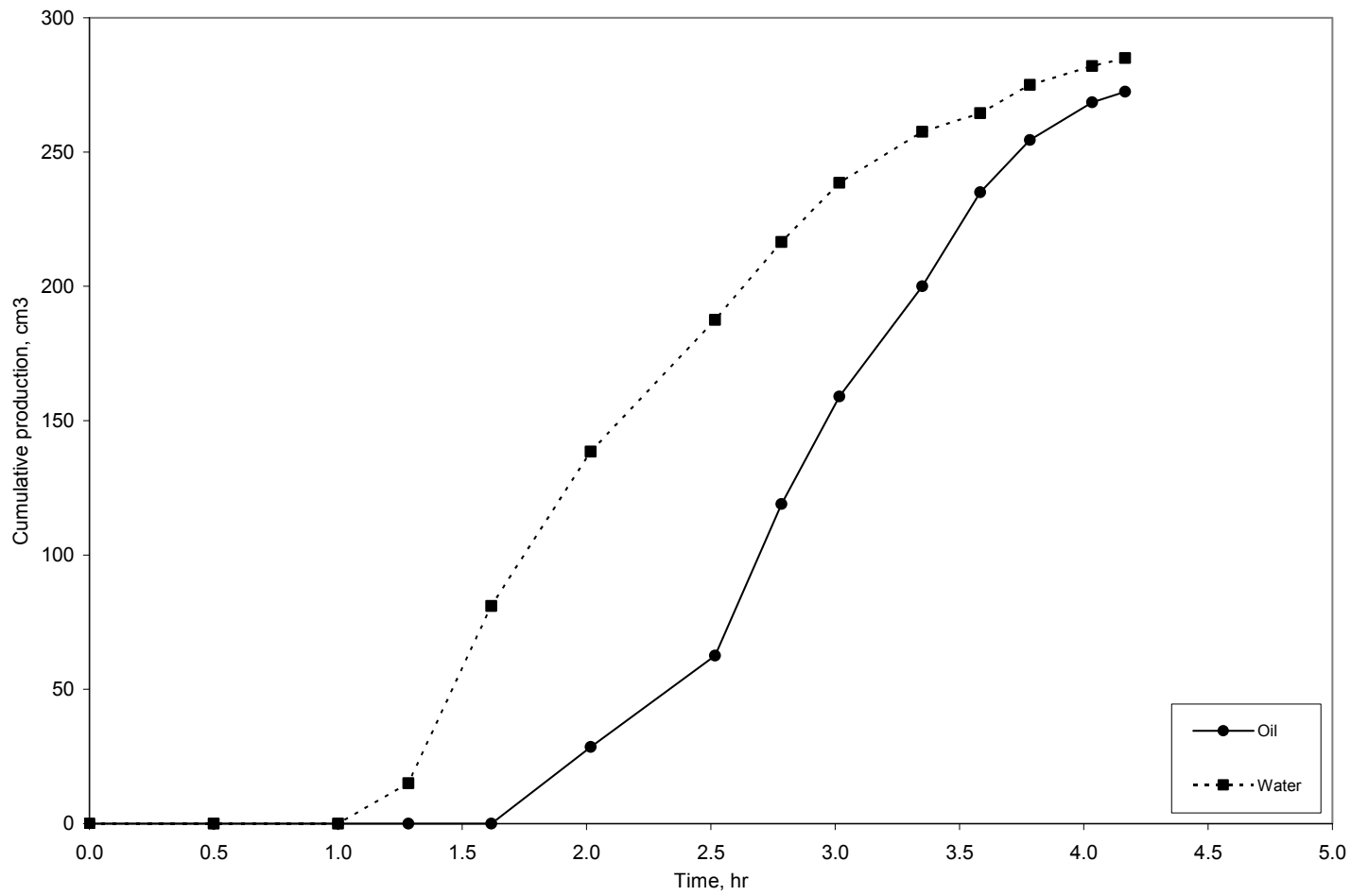


Fig. 4.45—Cumulative oil and water production (run no. 5, 40% oxygen).

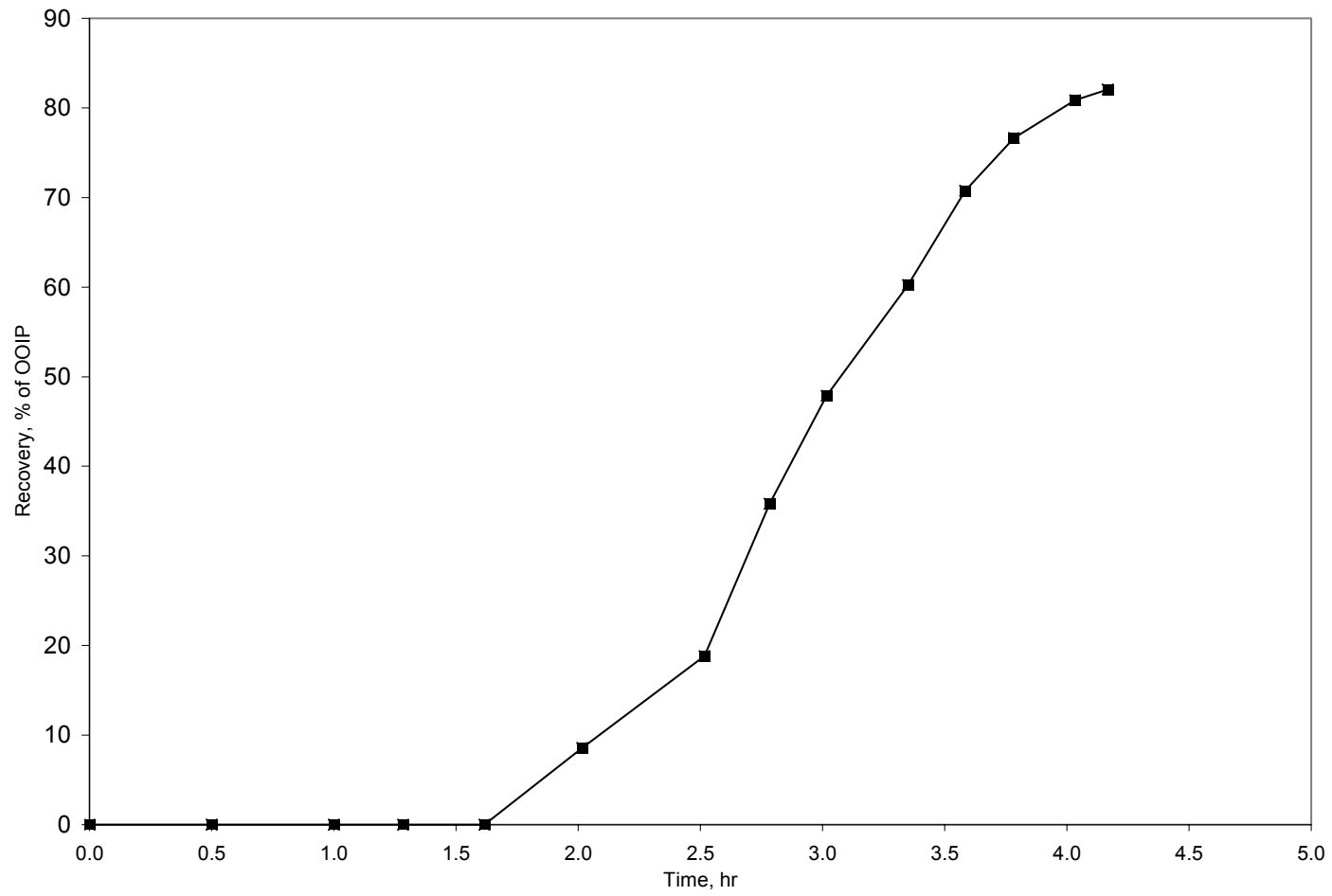


Fig. 4.46—Oil recovery (run no. 5, 40% oxygen).

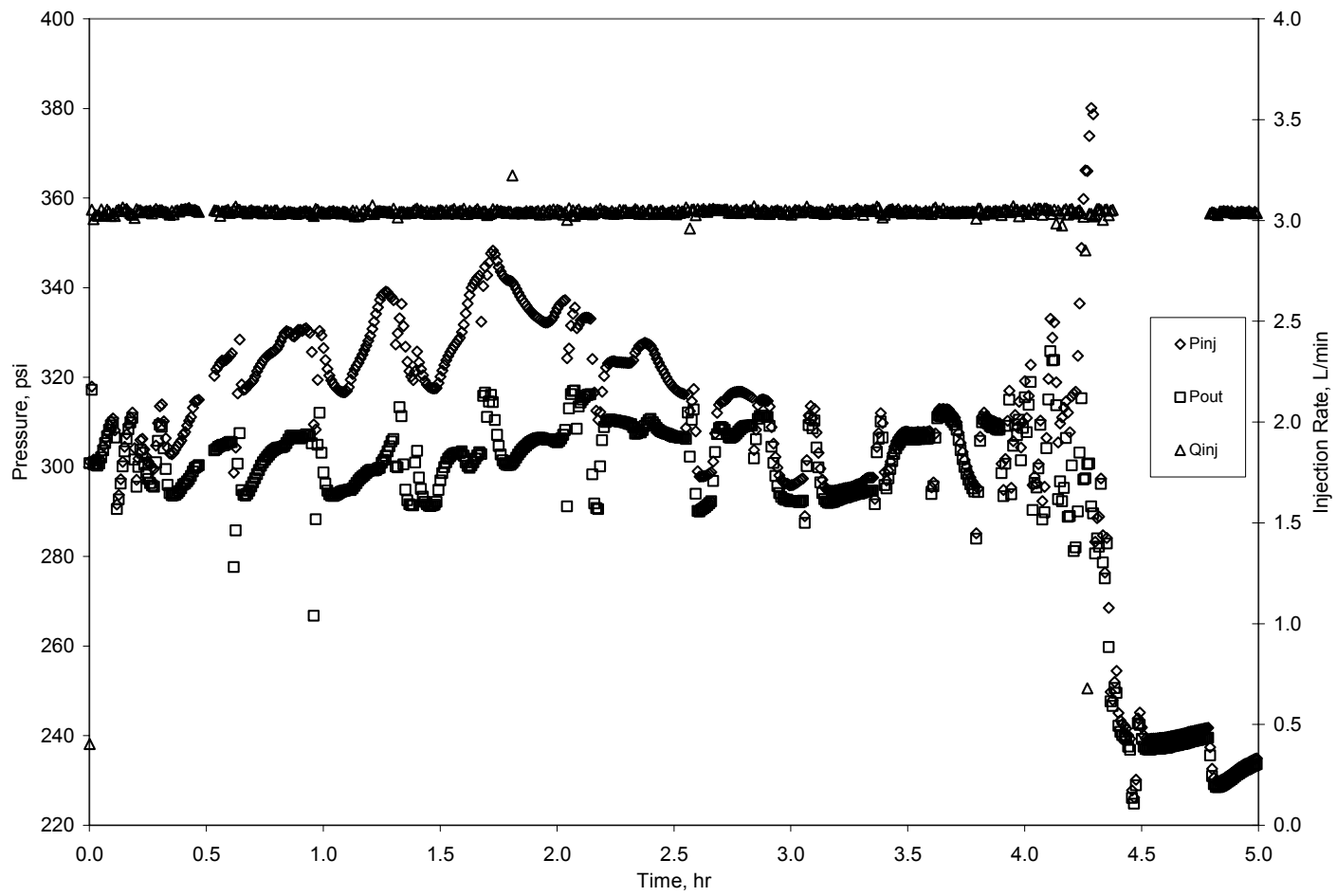


Fig. 4.47—Injection and production pressures, and gas injection rate (run no. 5, 40% oxygen).

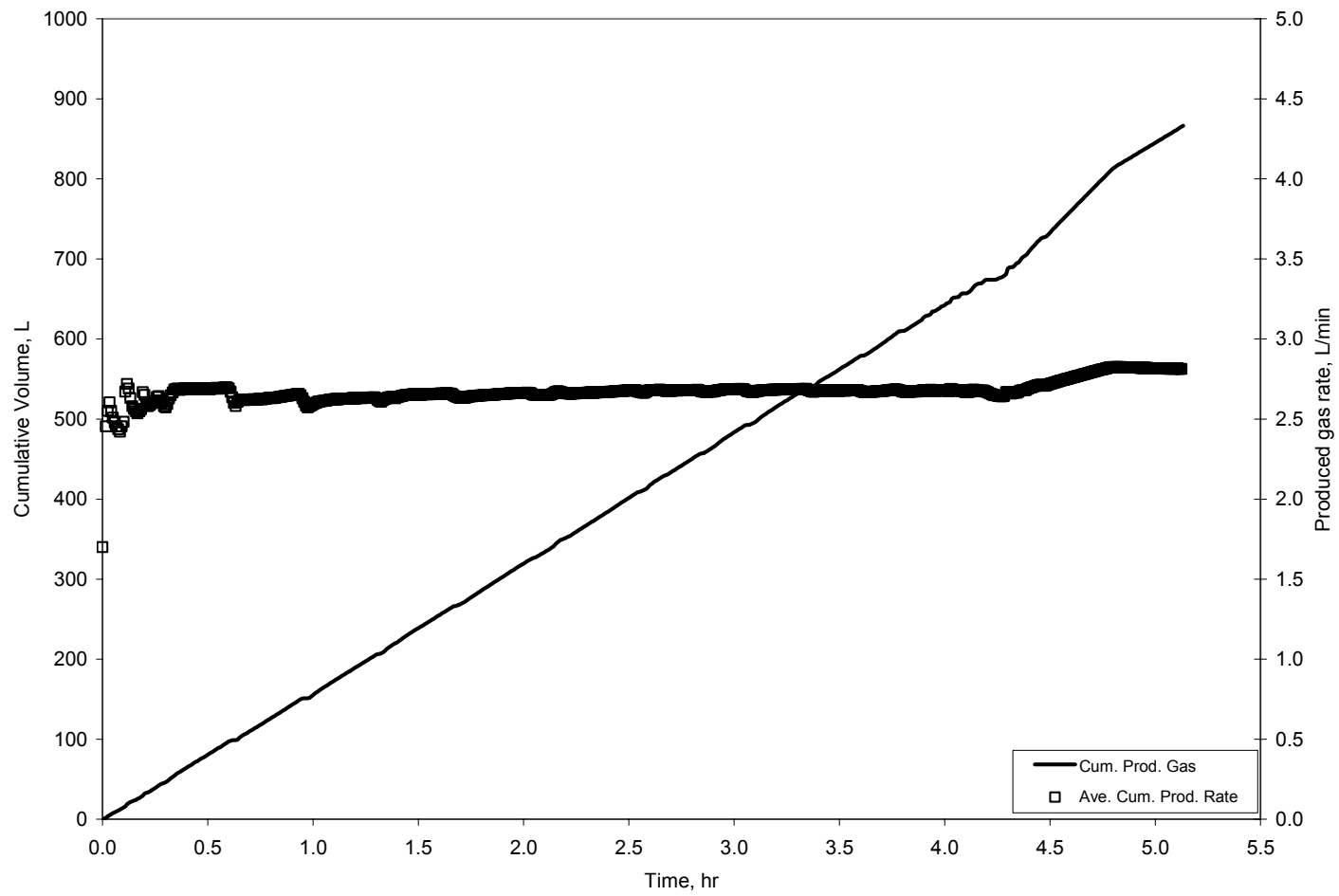


Fig. 4.48—Cumulative volume and produced gas rate (run no. 5, 40% oxygen).

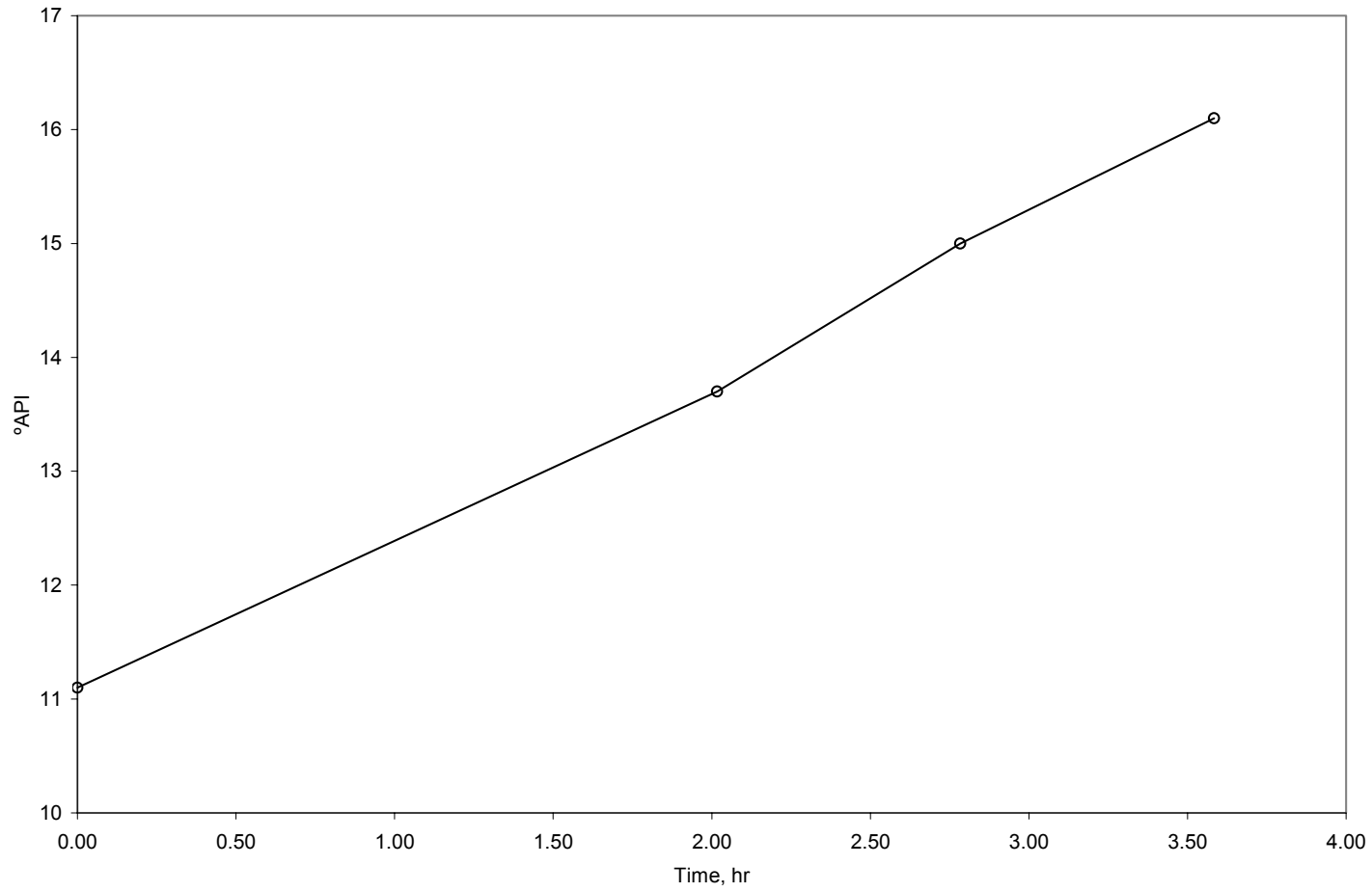


Fig. 4.49—Produced oil gravity (run no. 5, 40% oxygen).

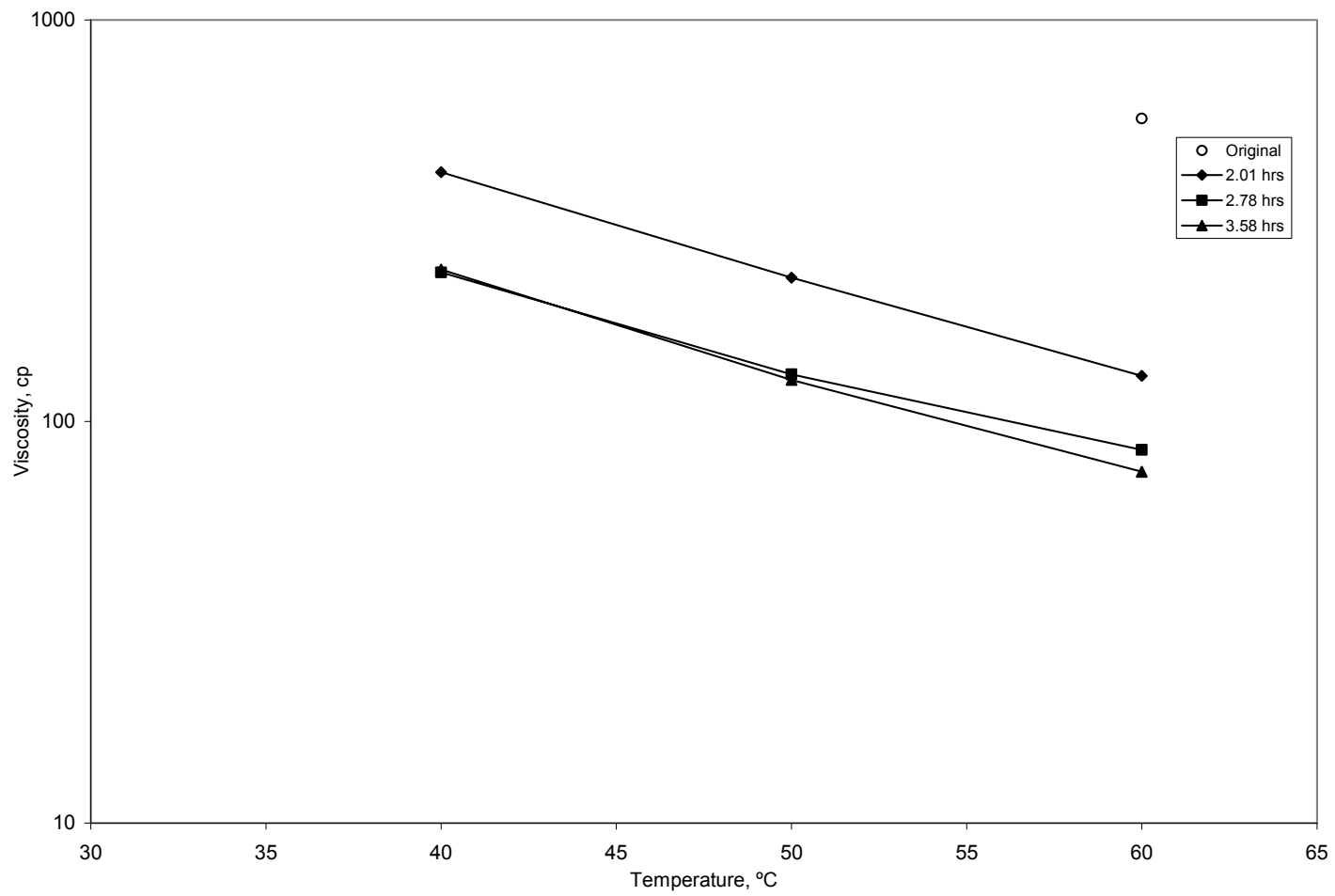


Fig. 4.50—Produced oil viscosity (run no. 5, 40% oxygen).

4.6 Combustion run no. 6 (40% oxygen)

Combustion gas composition in this run was observed to be stable during the first two hours, with relevant variations on the CO_2 and O_2 concentrations for the last two hours (**Fig. 4.51**). The average concentrations of the produced gases were: CO_2 , 20.00%; O_2 , 7.83%; N_2 , 64.84% and CO , 7.40% which are very similar to those of the previous run.

Averages values of F_{HC} , CO_2/CO , and, $CO/(CO+CO_2)$ ratios, 1.709, 2.701, and 0.270 respectively, imply a high temperature oxidation process, which is supported by F_{HC} ratios above one (**Fig. 4.52**).

The average combustion temperature was 465 °C (**Fig. 4.53**) and the combustion front velocity was 24.70 cm/hr (0.81 ft/hr) as observed in **Fig. 4.54**. Initial water and oil production were registered at 1.2 and 1.75 hrs (**Fig. 4.55**) and oil recovery represented 83.6 % of the oil placed in the combustion cell (**Fig. 4.56**).

A maximum high pressure of about 350 psig was observed during this experiment, and, as in other runs, a clear differential between the injected and production pressure reveal the formation of an oil bank (**Fig. 4.57**). The cumulative injected gas volume and the average gas production rate are represented in **Fig. 4.58**.

Produced oil gravity at the end of the combustion run was 7.9°API higher than that of the original crude oil (**Fig. 4.59**). Viscosity of the produced oil dropped to 18 cp at 60°C from its original value of 568 cp (**Fig. 4.60**).

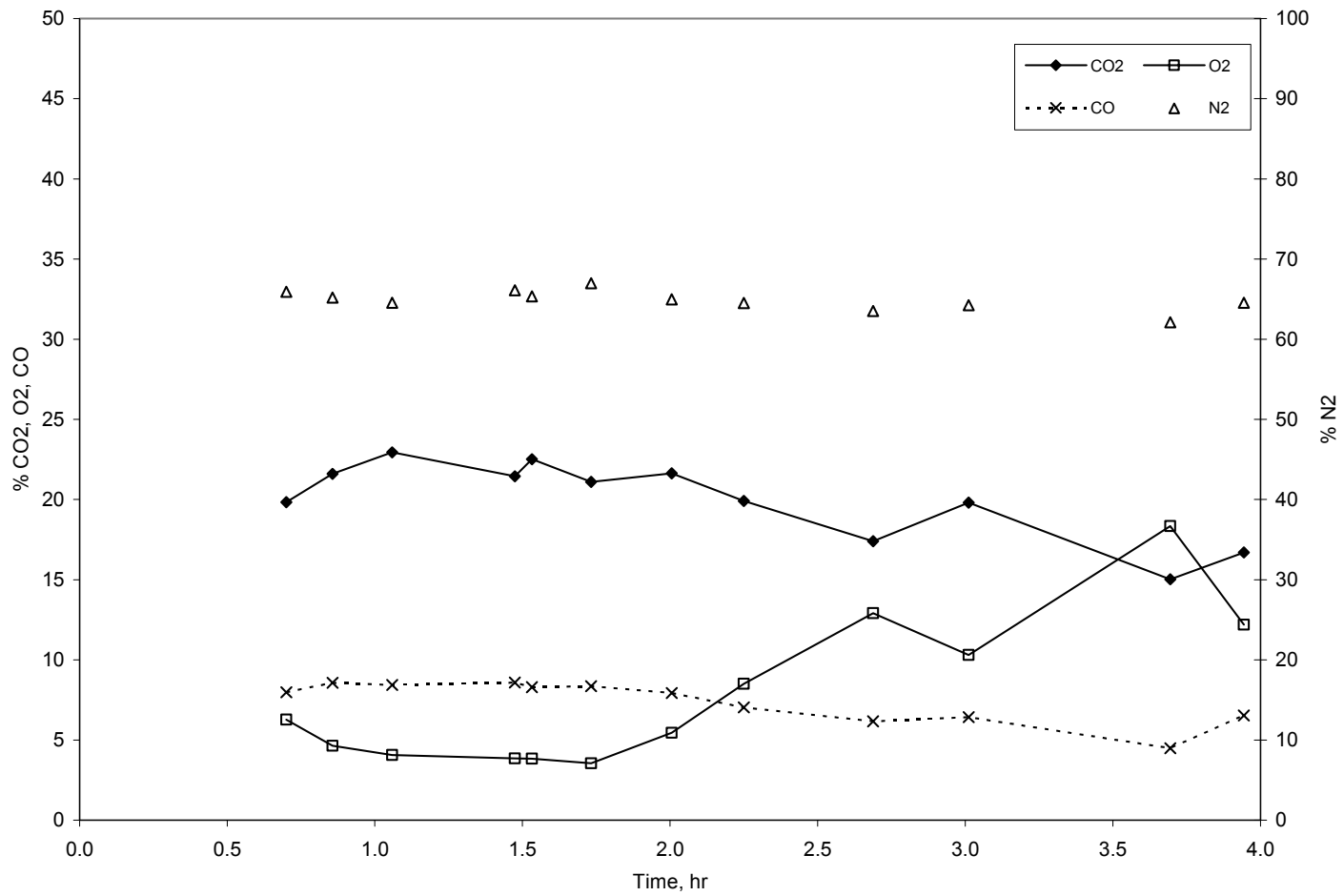


Fig. 4.51—Combustion gas composition (run no. 6, 40% oxygen).

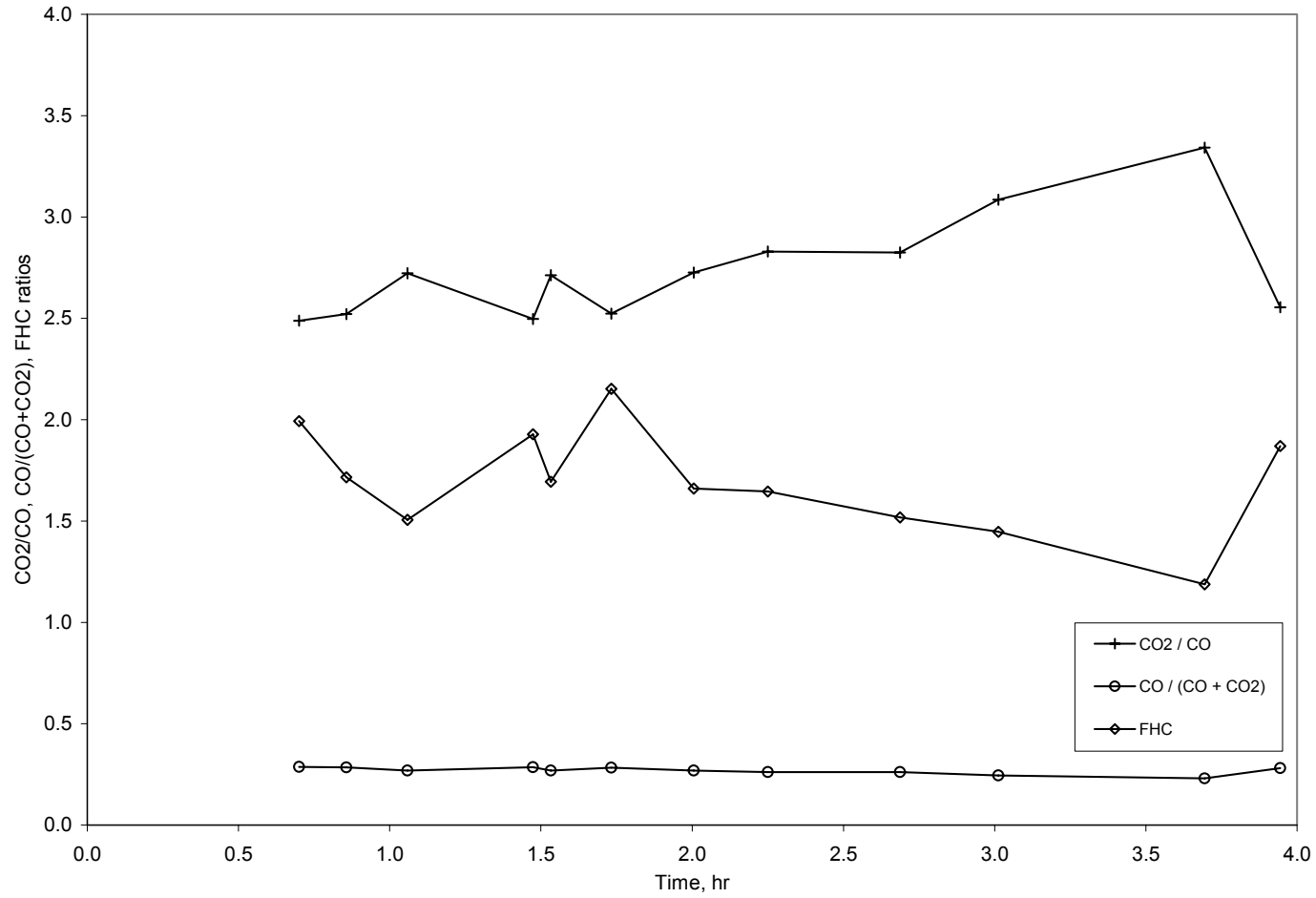


Fig. 4.52— F_{HC} , CO_2/CO , and $CO/(CO+CO_2)$ ratios (run no. 6, 40% oxygen).

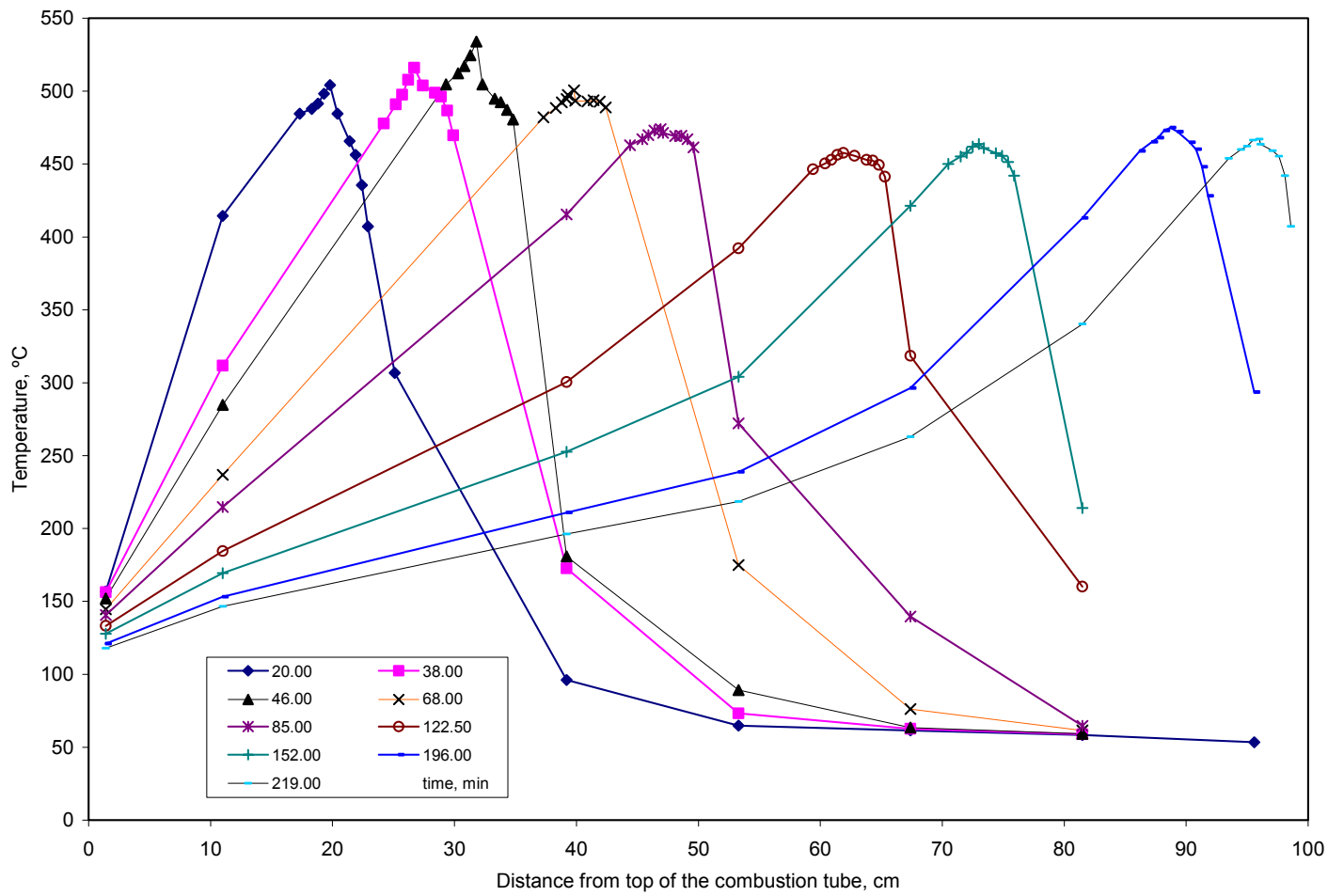


Fig. 4.53—Temperature profiles (run no. 6, 40% oxygen).

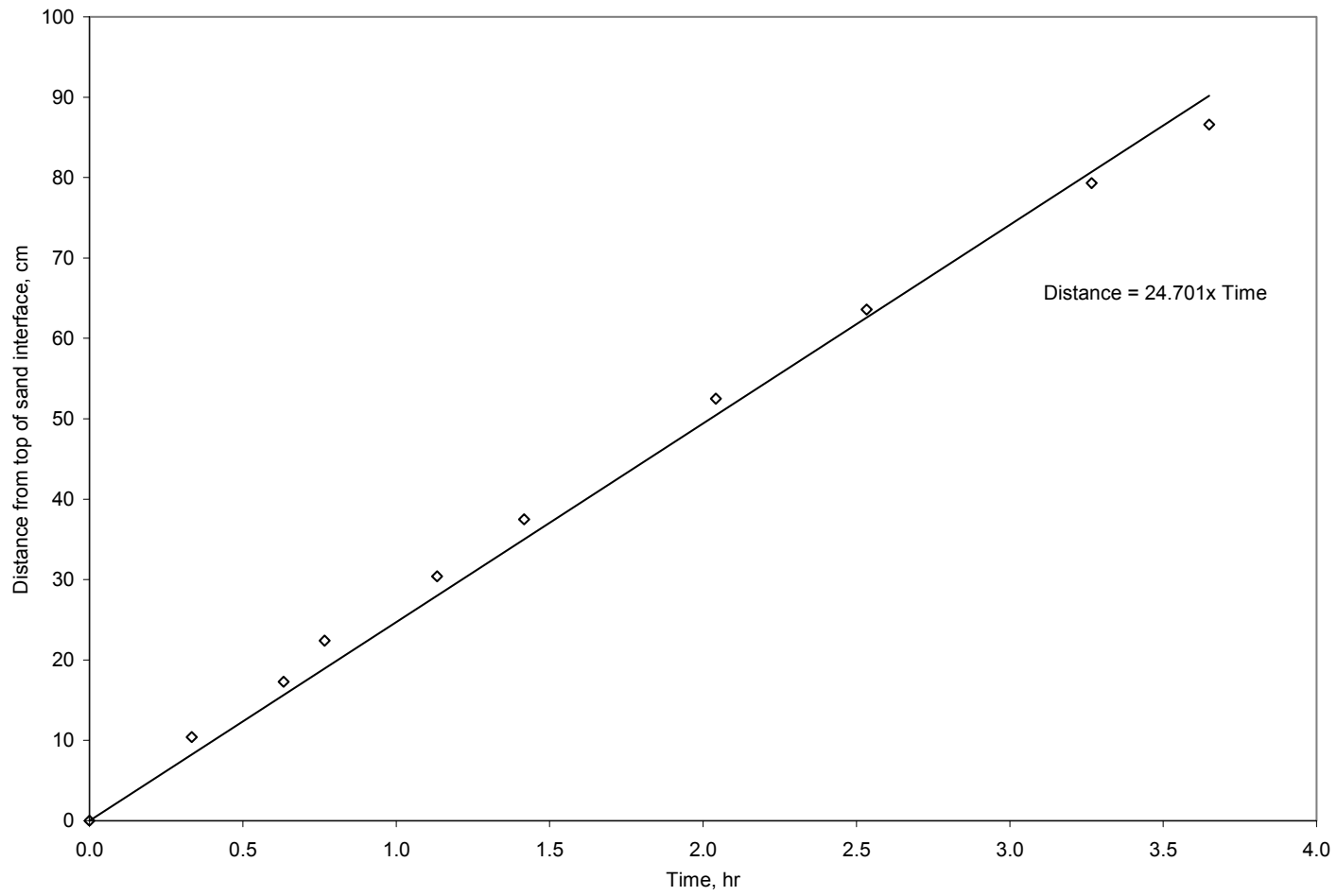


Fig. 4.54—Combustion front velocity (run no. 6, 40% oxygen).

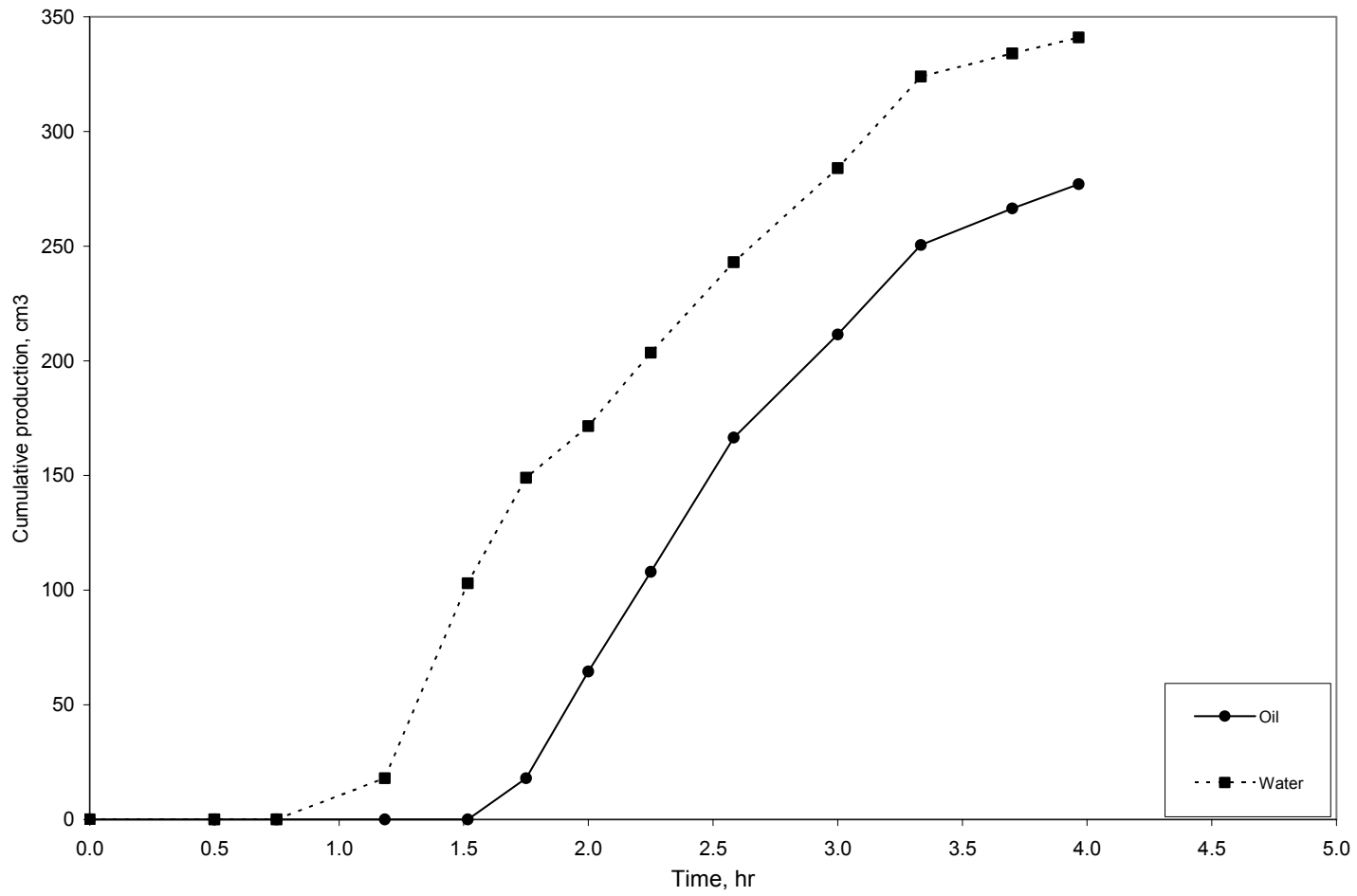


Fig. 4.55—Cumulative oil and water production (run no. 6, 40% oxygen).

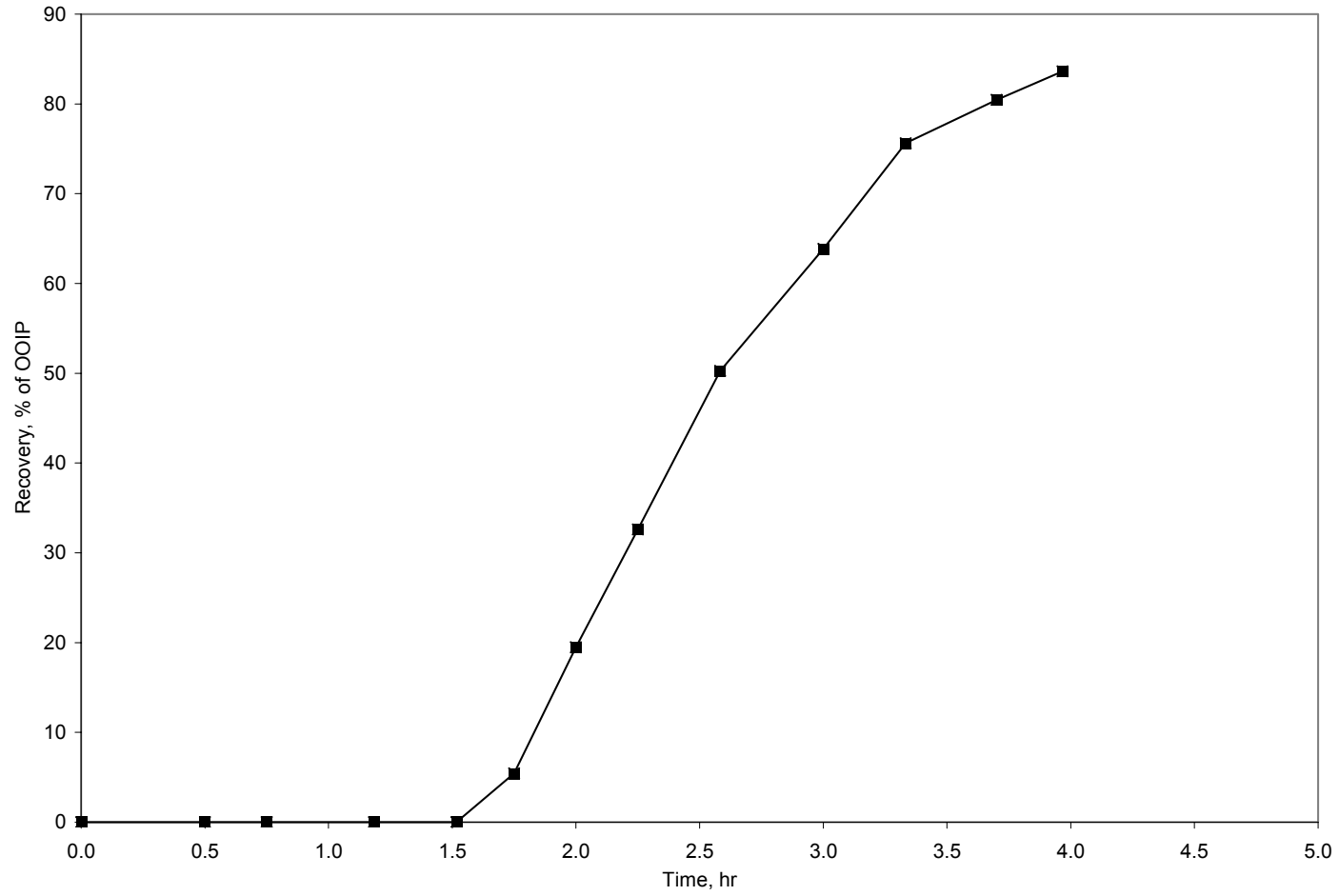


Fig. 4.56—Oil recovery (run no. 6, 40% oxygen).

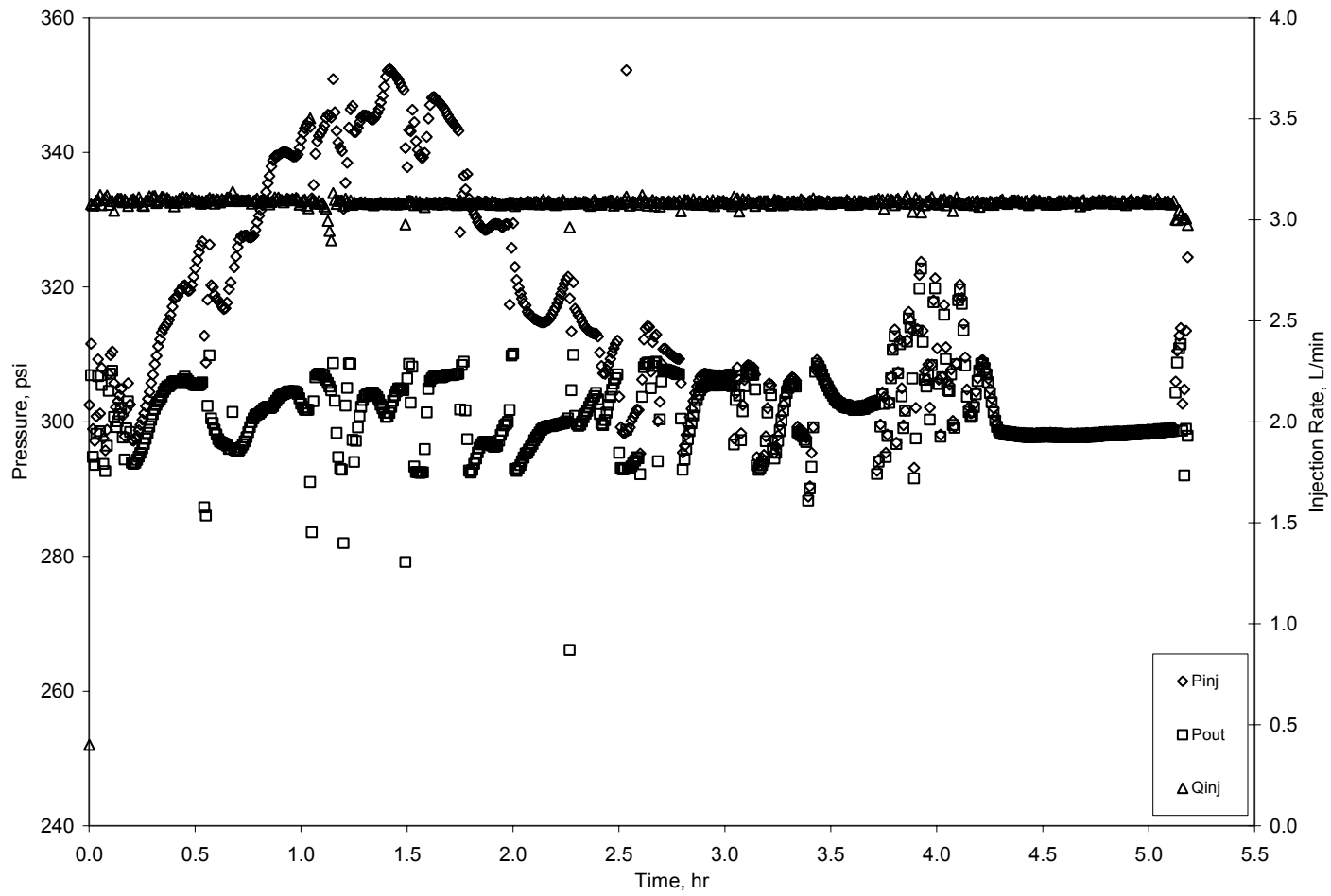


Fig. 4.57—Injection and production pressures, and gas injection rate (run no. 6, 40% oxygen).

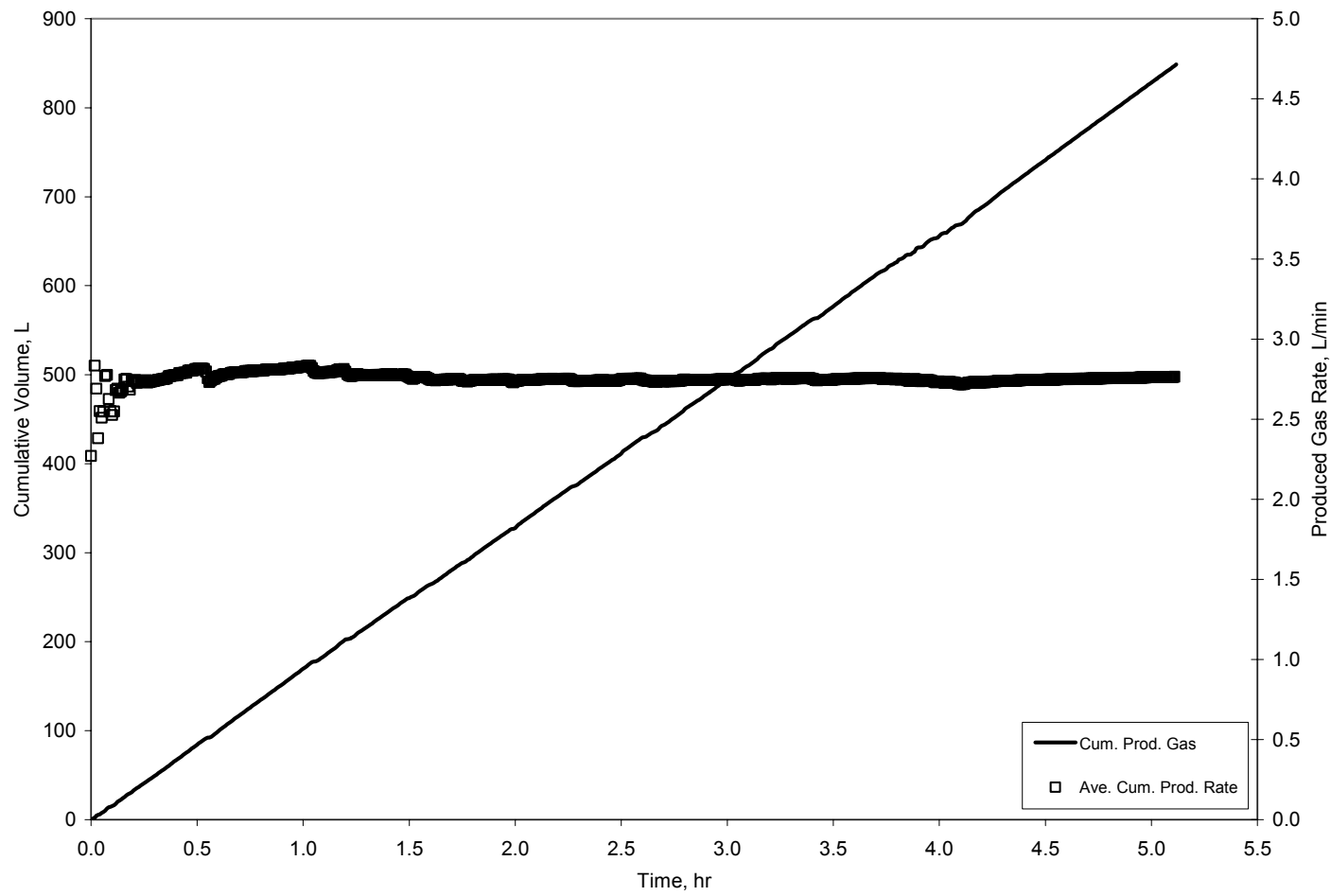


Fig. 4.58—Cumulative volume and produced gas rate (run no. 6, 40% oxygen).

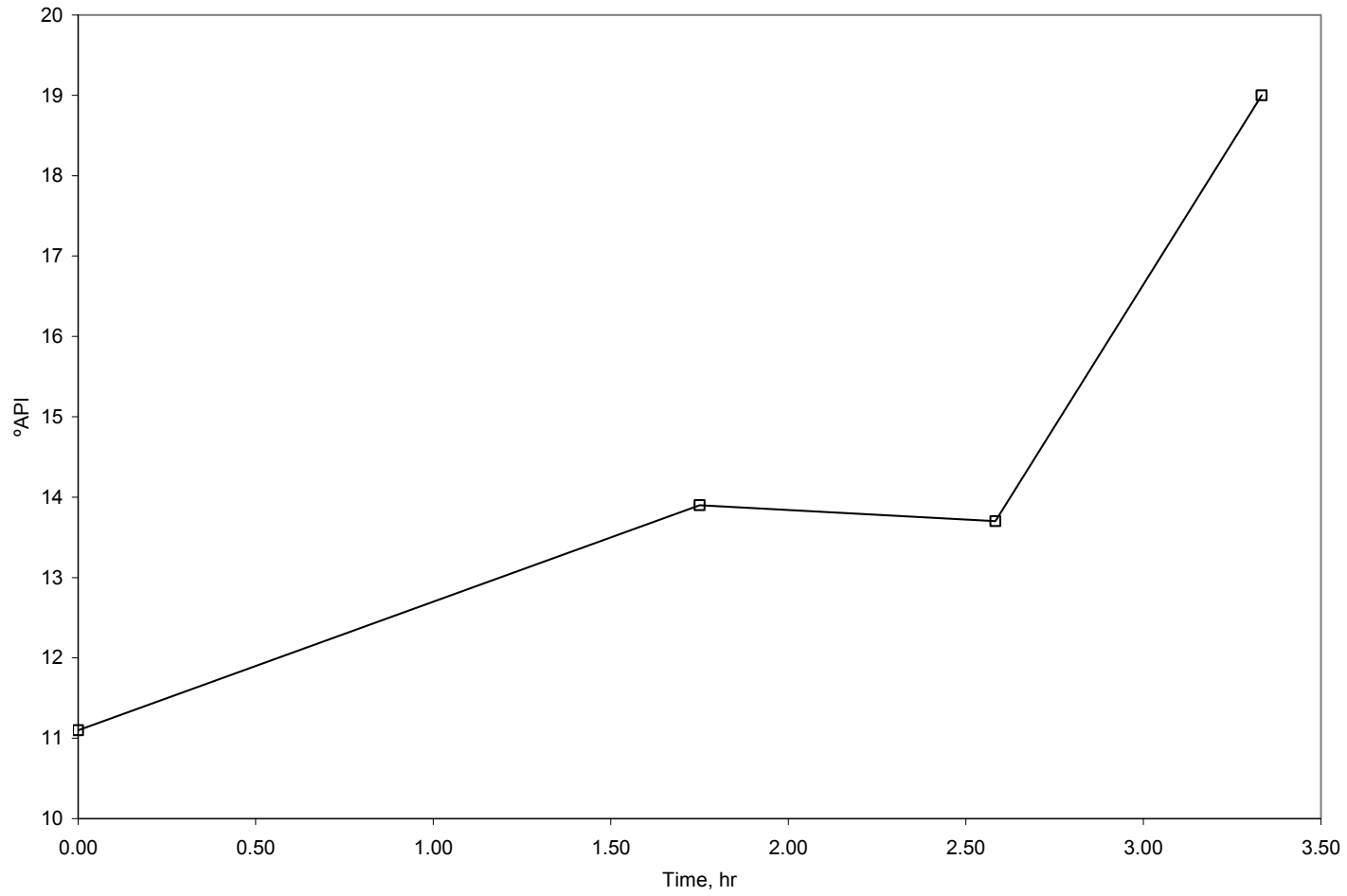


Fig. 4.59—Produced oil gravity (run no. 6, 40% oxygen).

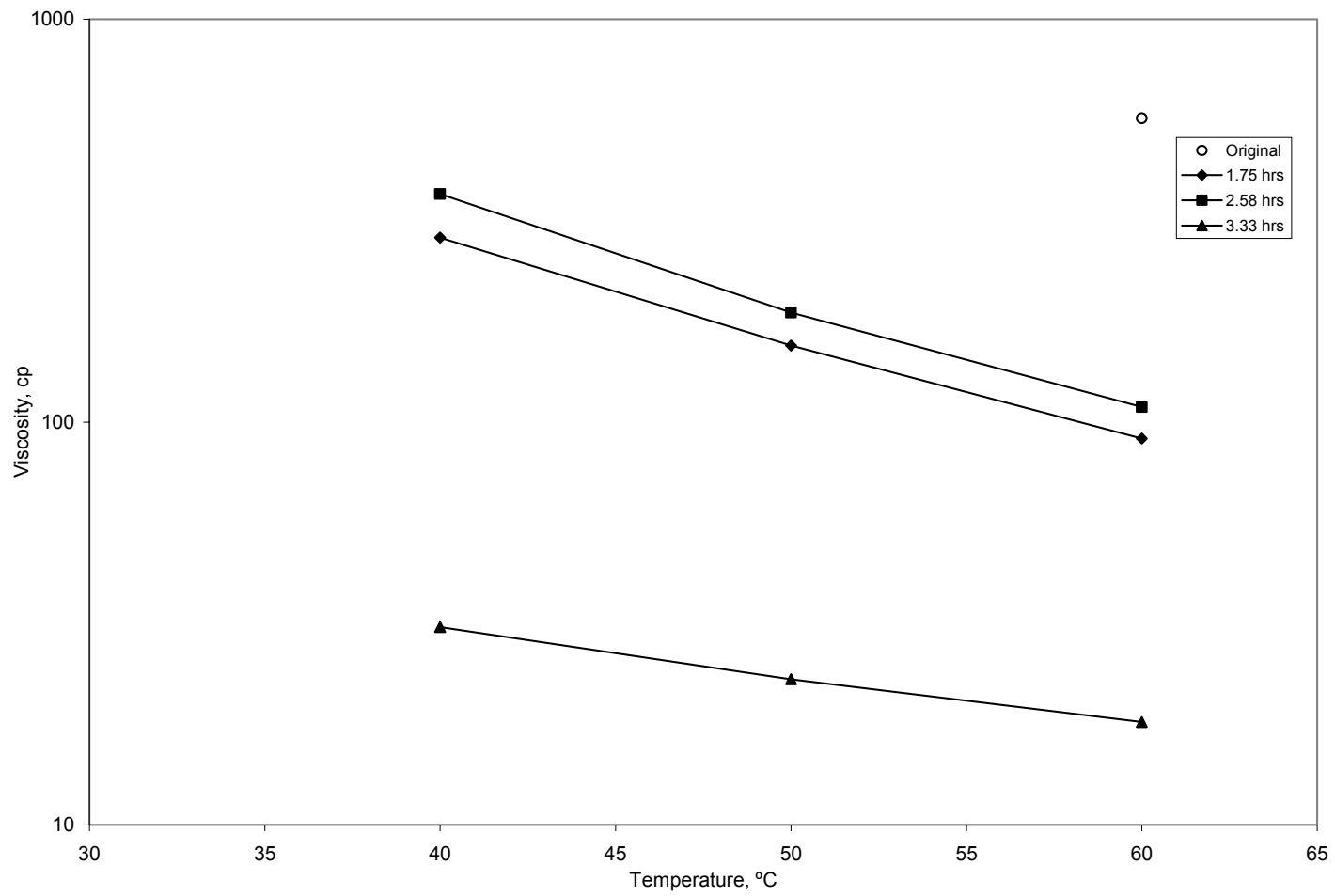


Fig. 4.60—Produced oil viscosity (run no. 6, 40% oxygen).

CHAPTER V

NEW COMBUSTION ZONE ANALYTICAL MODEL

A new combustion zone analytical model has been developed. The model describes the temperature profiles behind and ahead of the combustion zone; the combustion zone thickness; and produced gas composition and fuel concentration in the combustion zone.

5.1 Temperature profiles behind and ahead of the combustion zone

Penberthy¹³ solved the following dimensionless partial differential equation for heat conduction in a combustion tube:

$$\frac{\partial^2 T_D}{\partial x_D^2} + \frac{\partial T_D}{\partial x_D} - C T_D = \frac{\partial T_D}{\partial t_D} \quad (5.1)$$

with initial and boundary conditions:

$$T_D(x_D, 0) = \frac{T_a}{T_a - T_c} \quad (5.2)$$

$$T_D(0, t_D) = 1 \quad (5.3)$$

$$\lim_{x_D \rightarrow \infty} \frac{\partial T_D}{\partial x_D} = 0 \quad (5.4)$$

where T_a is the ambient temperature, and T_c is the combustion front temperature.

Also, the dimensionless temperature, distance, and time are defined as follows:

$$T_D = \frac{T(x, t) - T_a}{T_c - T_a} \quad (5.5)$$

$$x_D = \frac{\beta x}{\alpha} \quad (5.6)$$

$$t_D = \frac{\beta^2 t}{\alpha} \quad (5.7)$$

where, $T(x, t)$ is the temperature as a function of the positive distance x (ahead or behind the combustion front) and time t , and β , and α are expressed as:

$$\beta = V_f - \frac{\rho_g C_g U_a}{\rho_g C_g} \quad (5.8)$$

$$\alpha = \frac{k}{\rho_m C_m} \quad (5.9)$$

Here, V_f is the combustion front velocity, ρ_g and ρ_m are the gas and matrix densities, C_g and C_m are the gas and formation specific heats, U_a is the injected air flux, and k is the thermal conductivity.

The solution for the dimensionless temperature for the region ahead of the combustion front is:

$$\begin{aligned} T_D(x_D, t_D) = & \frac{T_a}{T_a - T_c} e^{-Ct_D} \\ & + \frac{T_a}{2(T_a - T_c)} e^{-Ct_D} \left\{ e^{-x_D} \operatorname{erfc} \left[\frac{x_D}{2\sqrt{t_D}} - \frac{1}{2}\sqrt{t_D} \right] + \operatorname{erfc} \left[\frac{x_D}{2\sqrt{t_D}} + \frac{1}{2}\sqrt{t_D} \right] \right\} \\ & + \frac{1}{2} \left\{ e^{\frac{-x_D(1+\sqrt{1+4C})}{2}} \operatorname{erfc} \left[\frac{x_D}{2\sqrt{t_D}} - \frac{1}{2}\sqrt{(1+4C)t_D} \right] + e^{\frac{-x_D(1-\sqrt{1+4C})}{2}} \operatorname{erfc} \left[\frac{x_D}{2\sqrt{t_D}} + \frac{1}{2}\sqrt{(1+4C)t_D} \right] \right\} \end{aligned} \quad (5.10)$$

and the dimensionless temperature solution behind the combustion front is:

$$\begin{aligned} T_D(x_D, t_D) = & \frac{T_a}{T_a - T_c} e^{-Ct_D} \\ & + \frac{T_a}{2(T_a - T_c)} e^{-Ct_D} \left\{ \operatorname{erfc} \left[\frac{x_D}{2\sqrt{t_D}} - \frac{1}{2}\sqrt{t_D} \right] + e^{x_D} \operatorname{erfc} \left[\frac{x_D}{2\sqrt{t_D}} + \frac{1}{2}\sqrt{t_D} \right] \right\} \\ & + \frac{1}{2} \left\{ e^{\frac{-x_D(-1+\sqrt{1+4C})}{2}} \operatorname{erfc} \left[\frac{x_D}{2\sqrt{t_D}} - \frac{1}{2}\sqrt{(1+4C)t_D} \right] + e^{\frac{x_D(1+\sqrt{1+4C})}{2}} \operatorname{erfc} \left[\frac{x_D}{2\sqrt{t_D}} + \frac{1}{2}\sqrt{(1+4C)t_D} \right] \right\} \end{aligned} \quad (5.11)$$

Penberthy's^{13,14} approach to determine the temperature profile ahead and behind the combustion front was to estimate the heat loss constant, C , and the velocity of the combustion front, V_f , where;

$$C = \frac{\alpha \gamma}{\beta^2} \quad (5.12)$$

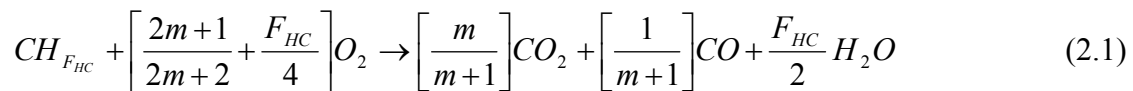
where:

$$\gamma = \frac{2U}{\rho_m C_m r_t} \quad (5.13)$$

Here, U is the overall heat transfer coefficient through the annular insulation based on the radius of the combustion tube, r_t .

5.2 Combustion zone thickness model

Benham and Poettmann³³ described fuel combustion in terms of the following stoichiometric equation (recall Eq. 2.1):



where F_{HC} is atomic hydrogen-to-carbon ratio, m is the ratio of moles of CO_2 to CO produced, and $CH_{F_{HC}}$ is the hydrocarbon fuel. They also derived an expression for the combustion front velocity as a function of the air flux, fuel concentration, oxygen utilization efficiency, hydrogen to carbon ratio, and the ratio of CO_2 to CO produced, m (Eq. 2.2);

$$V_f = \frac{E_{O_2} O_{2i} U_a}{379 F_c} \frac{(12 + F_{HC})}{\left[\frac{2m+1}{2m+2} + \frac{F_{HC}}{4} \right]} \quad (2.2)$$

where E_{O_2} is the oxygen utilization efficiency, U_a is the injected air flux, O_{2i} is the injected oxygen concentration, and F_c is the fuel concentration. The atomic hydrogen-

to-carbon ratio, F_{HC} , the oxygen utilization efficiency, E_{O_2} , and the fuel concentration, F_C , are defined as follows:

$$F_{HC} = \frac{4 \left[\left(\frac{O_{2i}}{1 - O_{2i}} \right) N_2 - (CO_2 + 0.5 CO + O_2) \right]}{(CO_2 + CO)} \quad (5.14)$$

$$E_{O_2} = 1 - \left[\frac{(1 - O_{2i})}{O_{2i}} \right] \left[\frac{O_2}{N_2} \right] \quad (5.15)$$

$$F_C = \frac{\text{Mass of fuel burned}}{\text{Total volume burned}} \quad (5.16)$$

where O_{2i} , O_2 , N_2 , CO_2 , and CO , are mole percentage of injected oxygen, produced oxygen, nitrogen carbon dioxide, and carbon monoxide respectively.

The main objective of the new combustion zone thickness model is the estimation of the mass of fuel consumed in the combustion zone. An iterative procedure is used to calculate the fuel concentration. **Fig. 5.1** is a graphical representation of the combustion zone divided into n elements of length dx .

The goal of this method is to arrive at an oxygen concentration at the end of the combustion zone, which in turn will match with the estimated fuel concentration. The approach is summarized as follows:

- Step 1 Guess the initial fuel mass dm_1 that will be burned in the first element.
- Step 2 Estimate the injected and consumed oxygen during the time period.

$$O_{2i} = \frac{Q_{inj}}{379} \frac{\%O_{2i}}{100} \frac{dx}{V_f} \quad (5.17)$$

where Q_{inj} is the rate of air injected.

$$O_{2c} = \frac{dm_1}{(12 + F_{HC})} \left[\frac{(2m + 1)}{(2m + 2)} + \frac{F_{HC}}{4} \right] \quad (5.18)$$

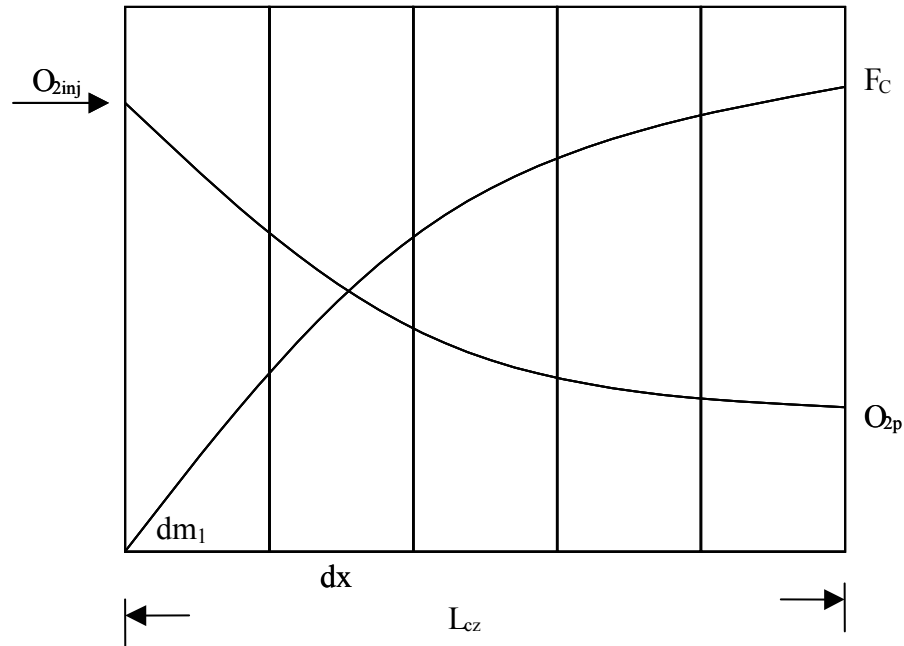


Fig. 5.1—Schematic diagram of the combustion zone model.

Step 3 Estimate the fuel mass burned in the next element (recall Eq. 2.9)

$$O_2 \propto m_f \quad (5.19)$$

At time dt , the mass of fuel burned can be written:

$$dm_{n+1} = dm_n \frac{O_{2n+1}}{O_{2n}} \quad (5.20)$$

where dm_{n+1} and O_{2n+1} are the fuel mass burned and oxygen concentration in the element $n+1$, and dm_n and O_{2n} are the fuel mass and oxygen concentration element n .

Step 4 Check O_{2n} with the experimental oxygen concentration (the fuel concentration will also match).

Step 5 If match is not satisfactory, return to Step 1 with a new guess of dm_1 .

As noted, the combustion front thickness must also be estimated in order to proceed to the determination of the amount of heat released. After several attempts to do this by analytical means, it was found that the length of the combustion front and the fuel consumed in the first element are dependent on one another. Thus, it is not possible to estimate a unique solution of the combustion zone thickness. It was decided that a combustion zone thickness of about 0.50 to 0.90 inches would be assumed, based on Penberthy^{13,14} and results obtained in this study.

5.3 Heat generated and lost in the combustion zone

Burger and Sahuquet²¹ expressed the heat of combustion as:

$$\Delta H_c = \frac{1800}{12 + F_{HC}} (94.0 - 67.9m' + 31.2F_{HC}) \quad (2.15)$$

where:

$$m' = \frac{CO}{CO + CO_2} \quad (5.21)$$

A heat balance is performed for the combustion zone. Thus, the heat generated at the combustion zone minus heat loss at the combustion zone equals the heat required to raise the temperature of the combustion zone. That is, in a time period, dt , when the combustion zone advances a distance dx :

$$\begin{aligned} & \text{Heat generated at combustion front} - \text{losses at combustion front} = \\ & \text{heat stored at the combustion front} + \text{heat stored just ahead of the combustion front} \end{aligned} \quad (5.22)$$

$$\text{Heat generated at combustion front} = \Delta H_c \Sigma dm \quad (5.23)$$

$$\text{Losses at combustion front} = 2\pi r_i L_{cz} U dt (T_{ci} - T_{ext}) \quad (5.24)$$

$$\text{Heat stored at the combustion front} = (1 - \phi) \rho_m C_m A L_{cz} (T_{ci+1} - T_{ci}) \quad (5.25)$$

$$\text{Heat stored just ahead of the combustion front} = (1 - \phi) \rho_m C_m A dx (T_{ci+1} - T_{ah}) \quad (5.26)$$

where, T_{ah} is the temperature at a distance dx of the combustion front, T_{ci} and T_{ci+1} are the combustion zone temperature at time i and $i+1$, T_{ext} is the exterior temperature, ΔH_c is the heat released when a mass dm of fuel is burned, L_{cz} is the combustion zone thickness, and A is the cross sectional area of the combustion tube.

Thus:

$$\begin{aligned} \Delta H_c \Sigma dm - 2\pi r_i L_{cz} U dt (T_{ci} - T_{ext}) = \\ (1 - \phi) \rho_m C_m A L_{cz} (T_{ci+1} - T_{ci}) + (1 - \phi) \rho_m C_m A dx (T_{ci+1} - T_{ah}) \end{aligned} \quad (5.27)$$

and finally solving for T_{ci+1} ,

$$T_{ci+1} = \frac{\Delta H_c \Sigma dm - 2\pi r_i L_{cz} U \frac{dx}{V_f} (T_{ci} - T_{ext}) + (1 - \phi) \rho_m C_m A (L_{cz} T_{ci} + dx T_{ah})}{(1 - \phi) \rho_m C_m A (L_{cz} + dx)} \quad (5.28)$$

The process to obtain the combustion zone temperature is iterative. It is assumed that the rise in temperature begins at the moment of ignition (about 300°C); that is $T_{ci}=300^\circ\text{C}$. The combustion zone temperature will increase (**Fig. 5.2**) until $T_{ci}=T_{ci+1}$, which is the combustion zone temperature.

In summary, the approach to estimate the combustion front temperature is as follows:

- Select the combustion front thickness
- Evaluate oxygen consumption and fuel concentration (section 5.2).
- Estimate the amount of heat released from Eq. 2.15.
- Calculate the combustion zone temperature iteratively using Eq. 5.28.
- Compare the calculated and experimental combustion front temperature.
- Adjust the combustion zone thickness and/or the heat loss constant, C , if necessary.

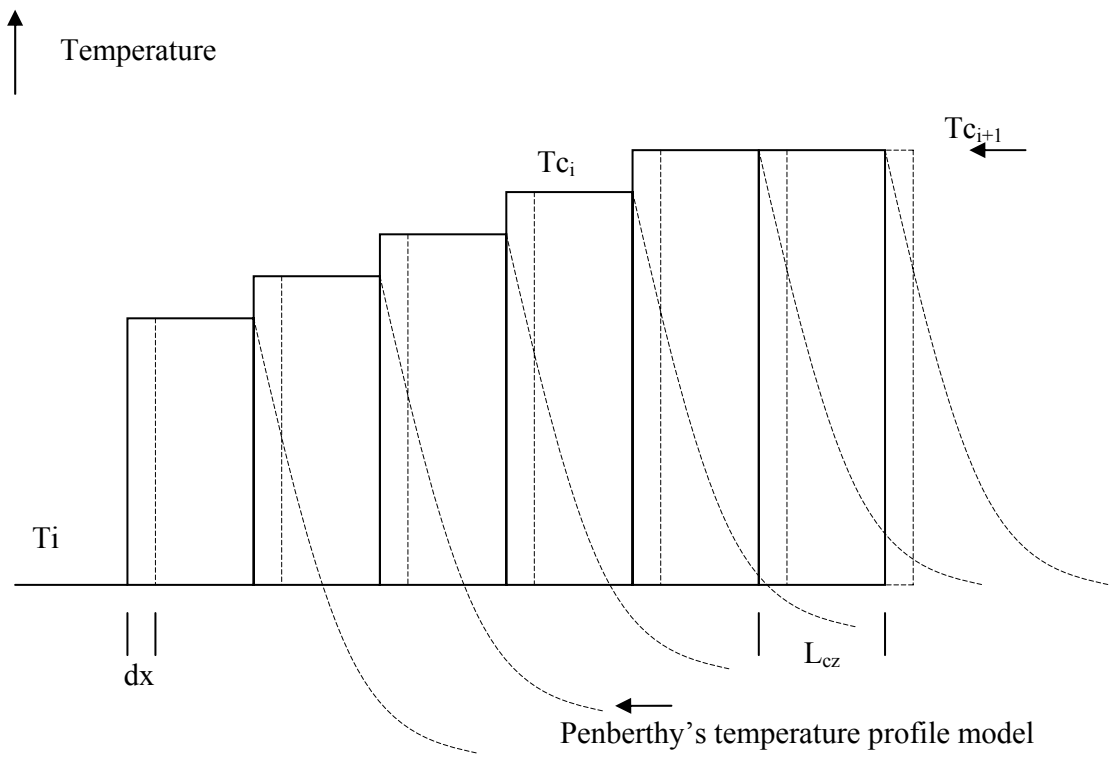


Fig. 5.2—Schematic diagram of the combustion front temperature model.

5.4 Verification of model

The mathematical models described in the previous sections were programmed in Microsoft Excel Visual Basic (**Appendix**). Program input include data from the combustion tube experiment, such as average produced gas composition, run time, injected oxygen concentration, and combustion front thickness.

The following sections describe the results of verification of the new model, tested:

5.4.1 Run no. 2 (21% oxygen)

Fig. 5.3 is the representation of the increase of fuel concentration in the combustion zone, estimated for this run to be 0.85 in. Note that the produced gas composition matches the average data from section 4.1. The model and observed combustion zone temperatures and temperature profiles are presented in **Fig. 5.4**. The calculated temperature profiles agree with the observed temperature profiles very closely. The estimated combustion zone thickness is in good agreement with the observed profiles.

5.4.2 Run no. 7 (21% oxygen)

The combustion zone thickness was estimated to be 0.75 in. **Fig. 5.5** shows the good agreement between the calculated and observed average gas composition (section 4.2) in this region and the increase of fuel concentration in the combustion zone. The average combustion zone temperature of 440°C is presented in the temperature profiles of **Fig. 5.6**. The estimated and calculated temperature profiles are very similar near the combustion zone.

5.4.3 Run no. 3 (30% oxygen)

The combustion zone thickness was estimated to be 0.70 in. **Fig. 5.7** shows the good match of the average gas composition (section 4.3) in this region and the increase of fuel concentration in the combustion zone. The average combustion zone temperature of 460°C is presented in the temperature profiles of **Fig. 5.8**. The estimated and calculated temperature profiles are very similar near the combustion zone.

5.4.4 Run no. 4 (30% oxygen)

Calculated gas composition agreed with observed values (section 4.4) in this combustion zone of 0.55 in. **Fig. 5.9**. Again, good agreement is observed between the estimated and observed temperature profiles near the combustion zone, where an average temperature of 455°C is estimated (**Fig. 5.10**).

5.4.5 Run no. 5 (40% oxygen)

The combustion zone thickness for this run was estimated at 0.70 in. (**Fig. 5.11**). The fuel concentration increases in this region and the calculated produced gas composition agree with averaged observed values as given in section 4.5. The estimated combustion zone temperature for this experiment was 475°C. However some instability is observed with the front velocity resulting in the estimated temperature profiles to be in some disagreement with the data (**Fig. 5.12**).

5.4.6 Run no. 6 (40% oxygen)

Average produced gas composition in section 4.6 is matched in this run with a combustion zone thickness of 0.56 in. (**Fig. 5.13**). As in run no. 5, the estimated temperature profiles differ somewhat from the recorded data where the estimated combustion zone temperature was 465°C (**Fig. 5.14**).

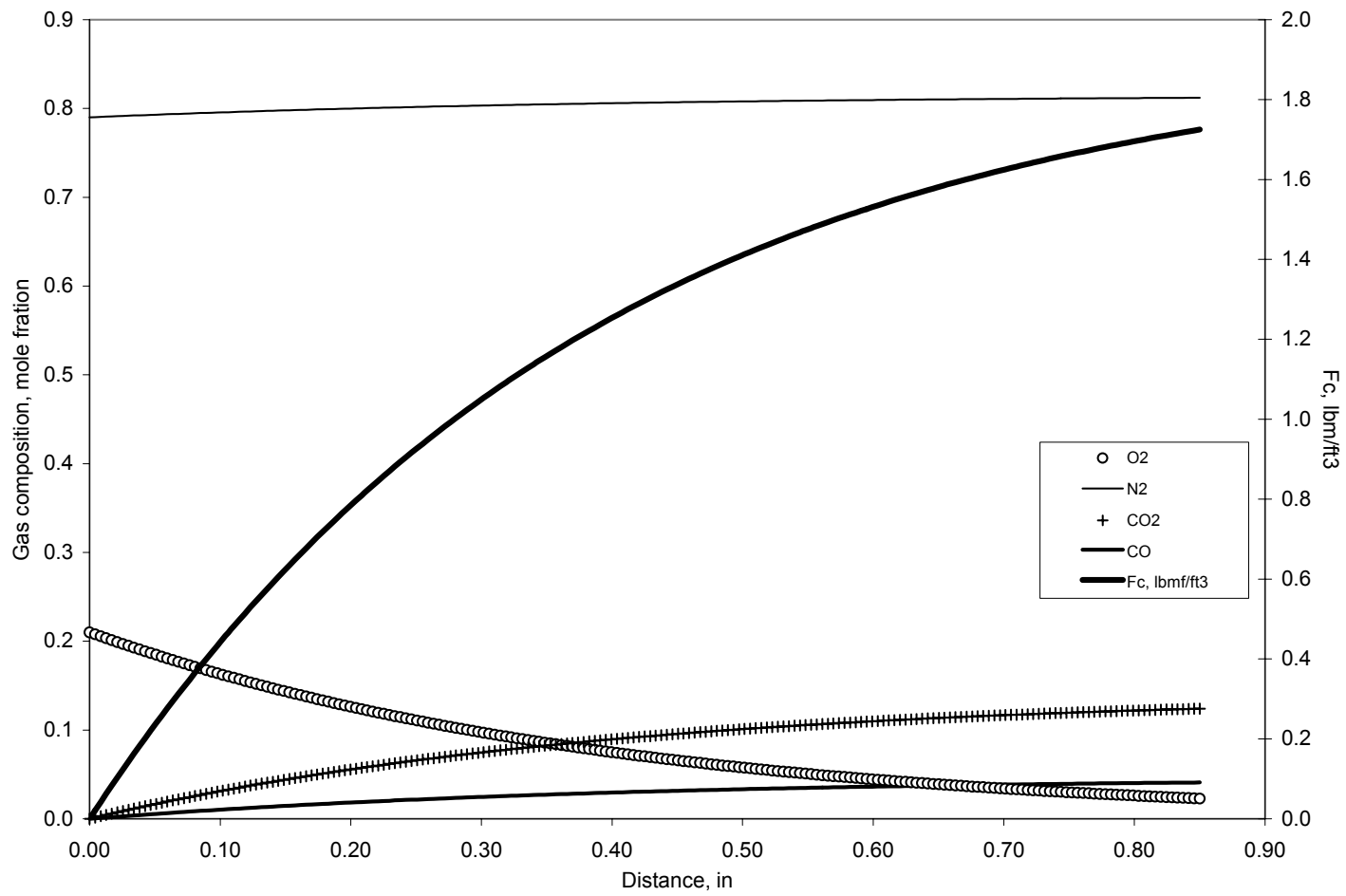


Fig. 5.3—Verification of the combustion zone model (run no. 2, 21% oxygen).

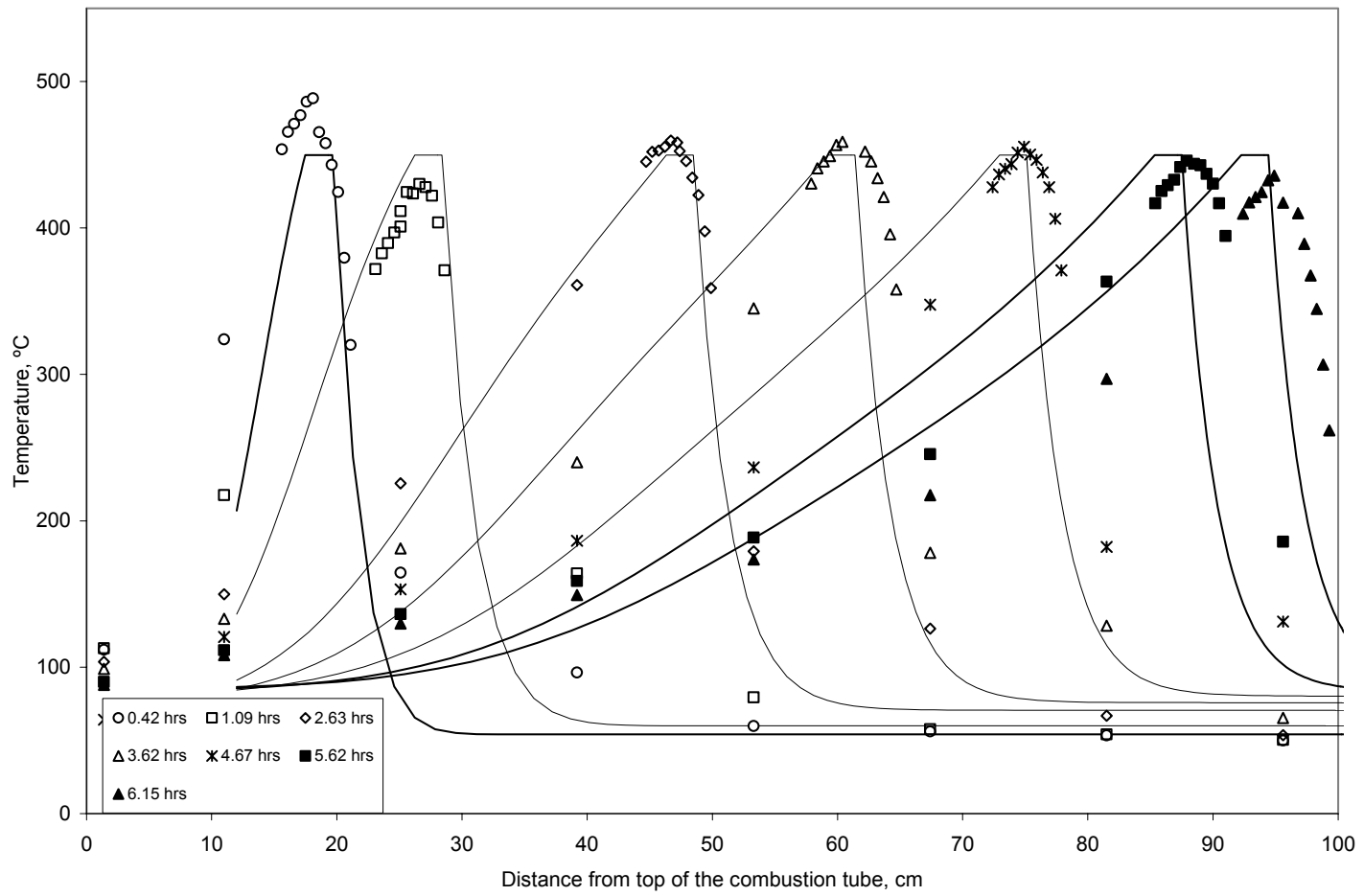


Fig. 5.4—Observed and estimated temperature profiles (run no. 2, 21% oxygen).

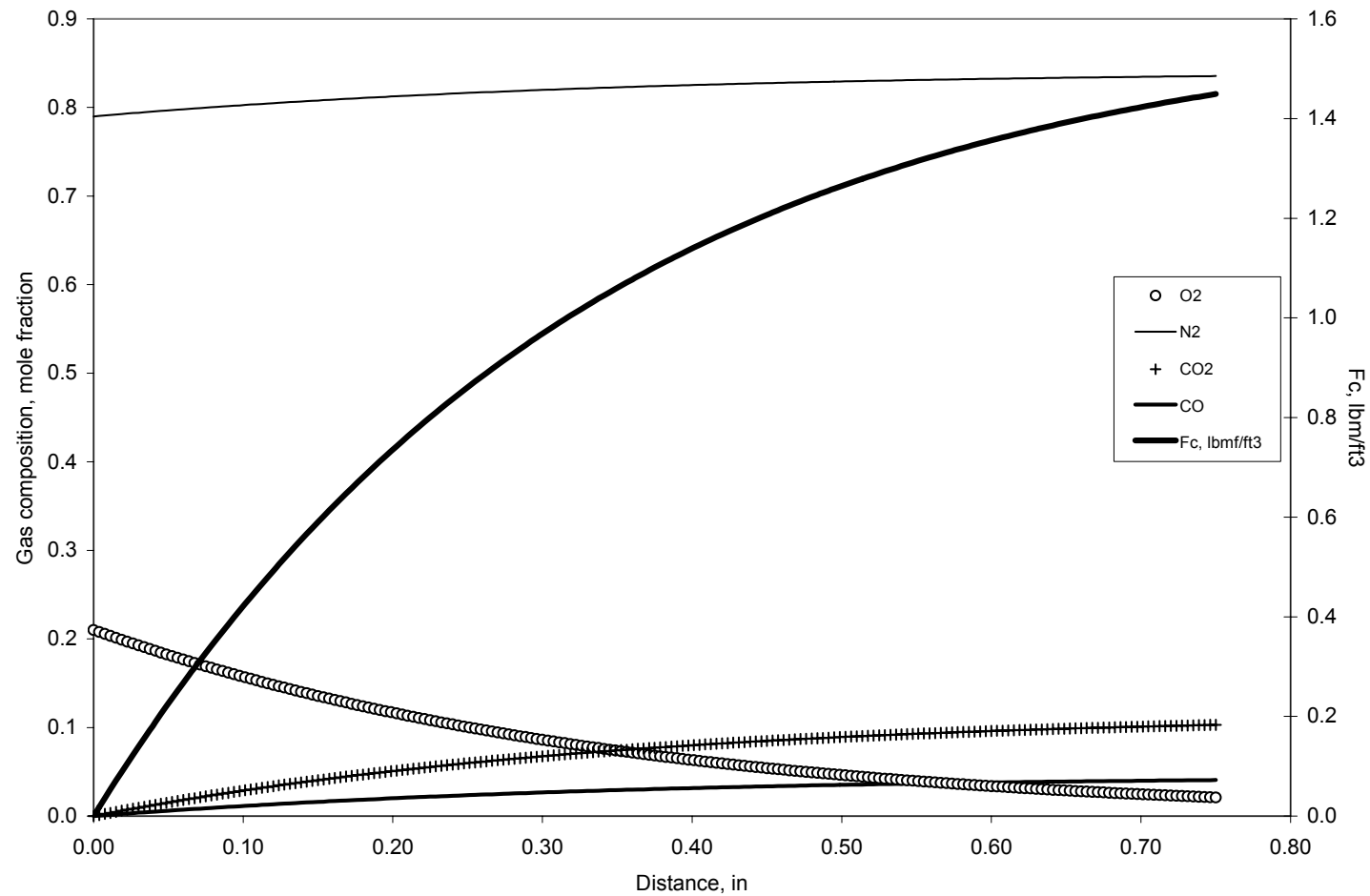


Fig. 5.5—Verification of the combustion zone model (run no. 7, 21% oxygen).

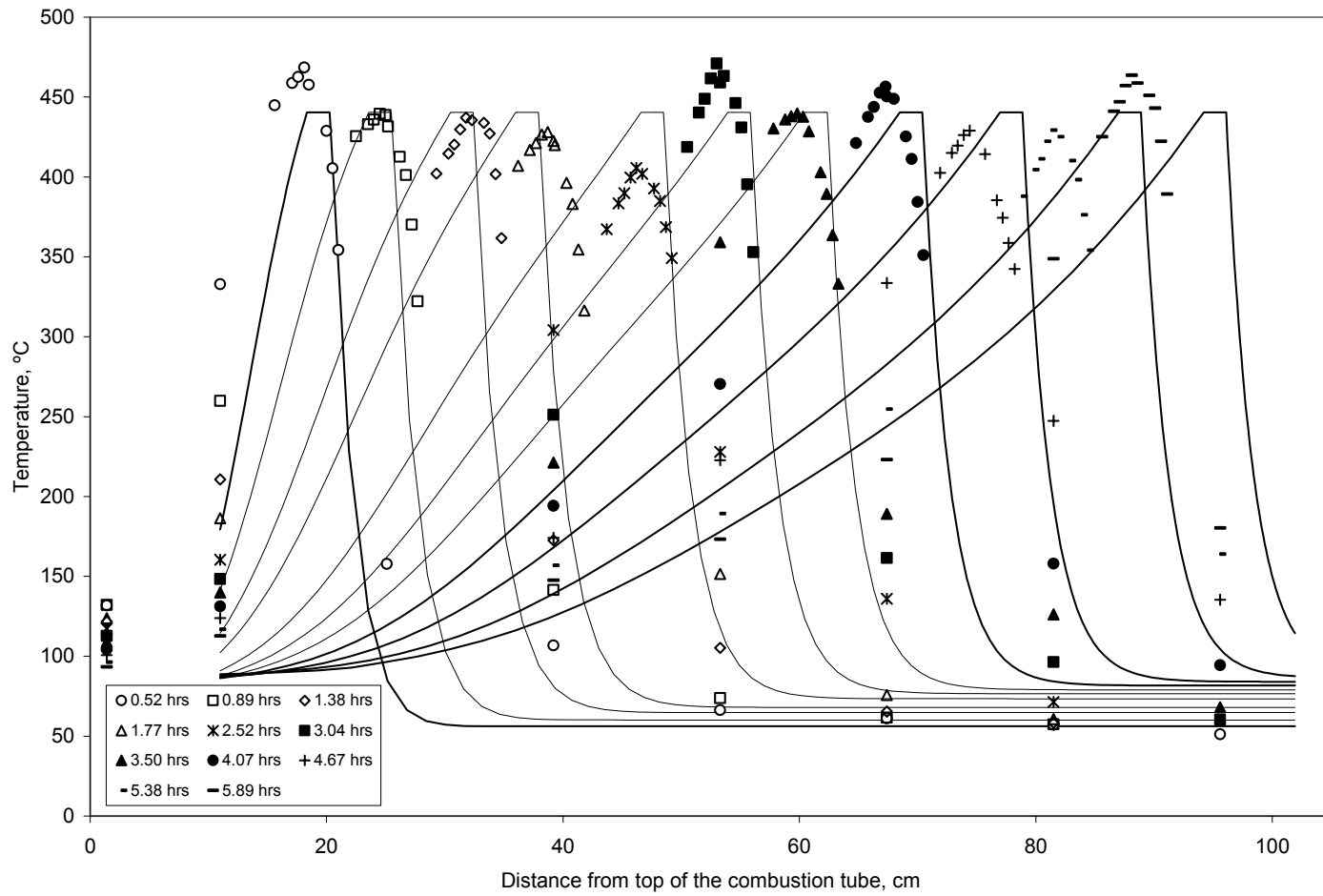


Fig. 5.6—Observed and estimated temperature profiles (run no. 7, 21% oxygen).

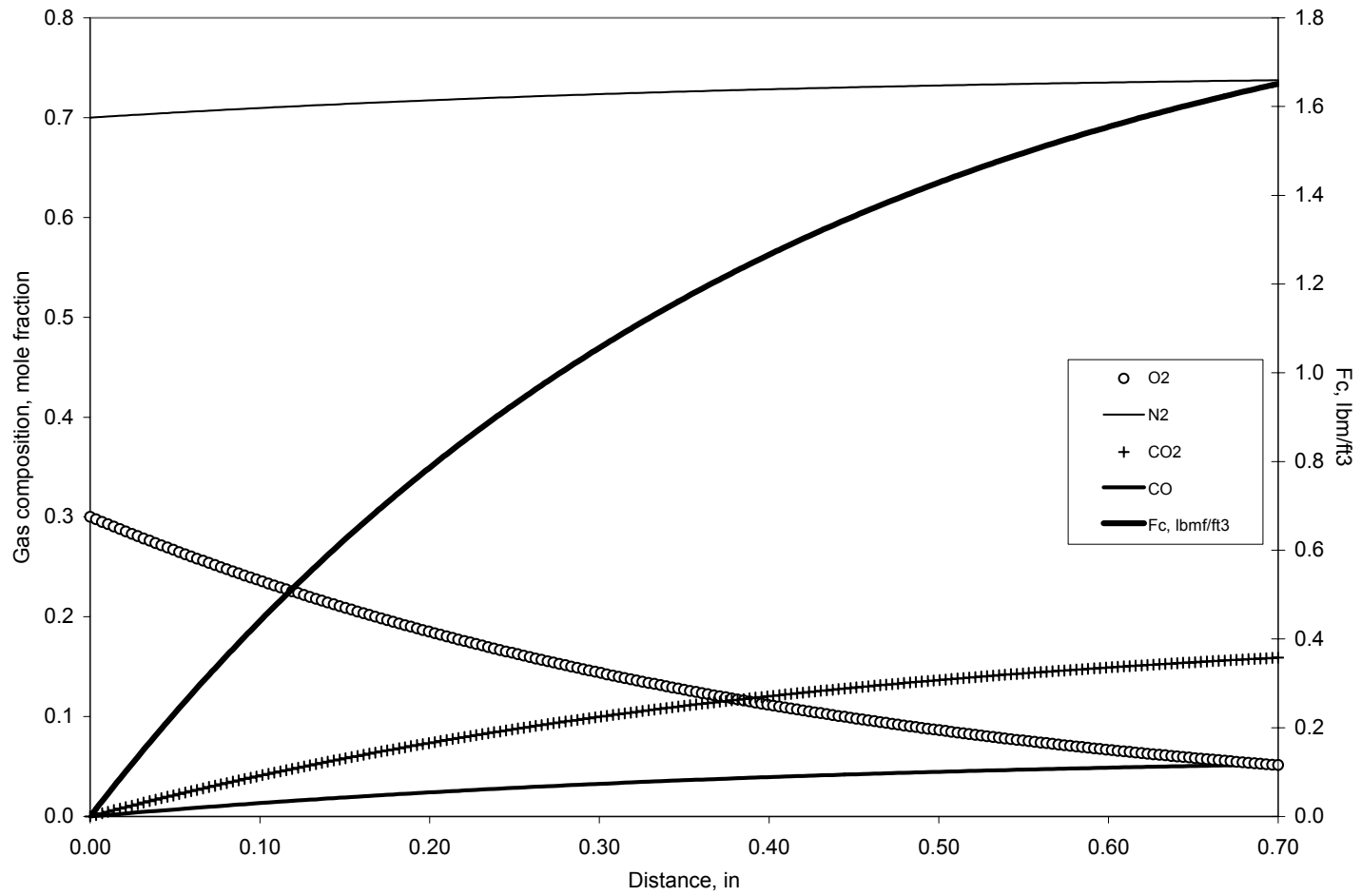


Fig. 5.7—Verification of the combustion zone model (run no. 3, 30% oxygen).

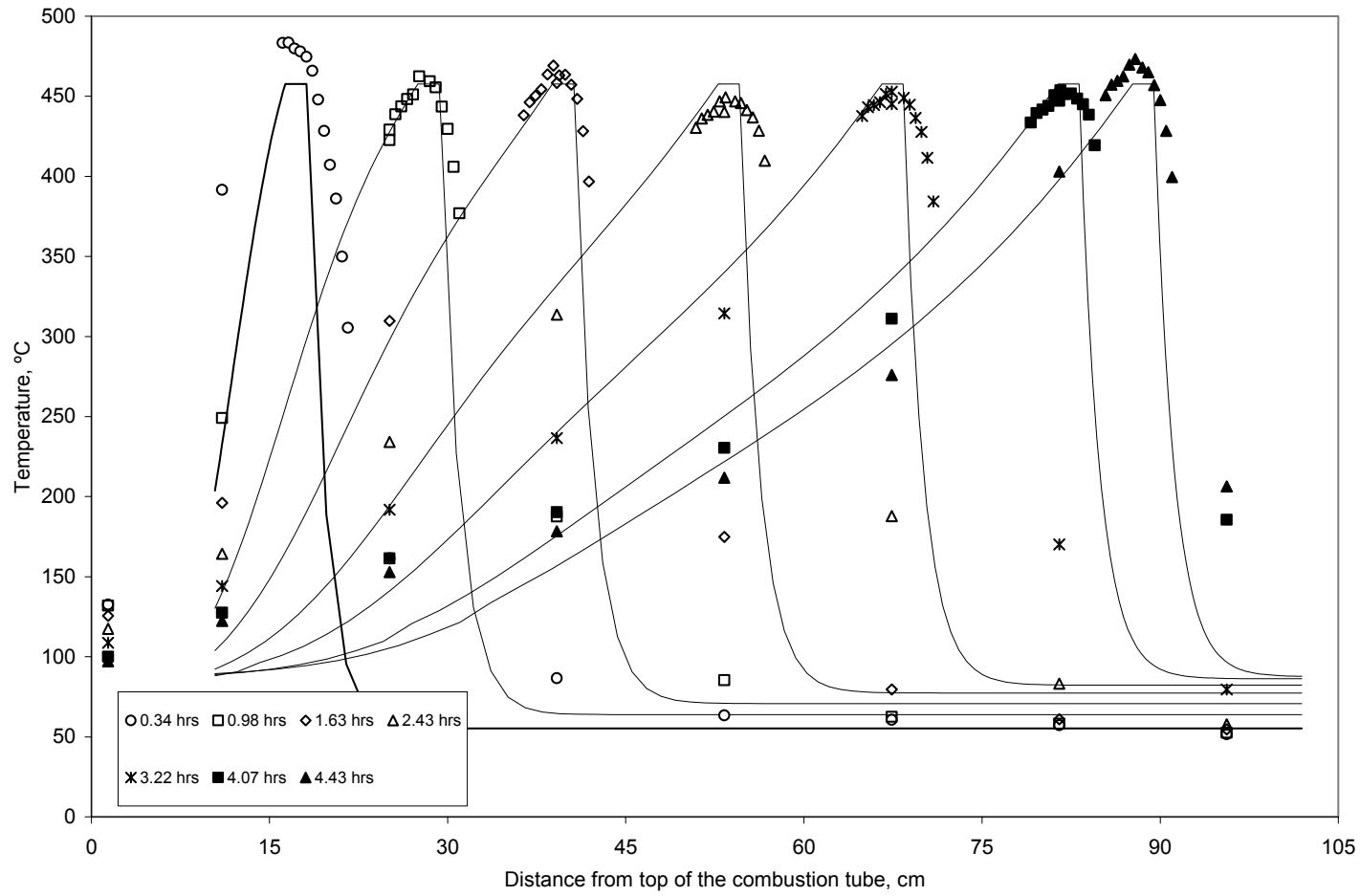


Fig. 5.8—Observed and estimated temperature profiles (run no. 3, 30% oxygen).

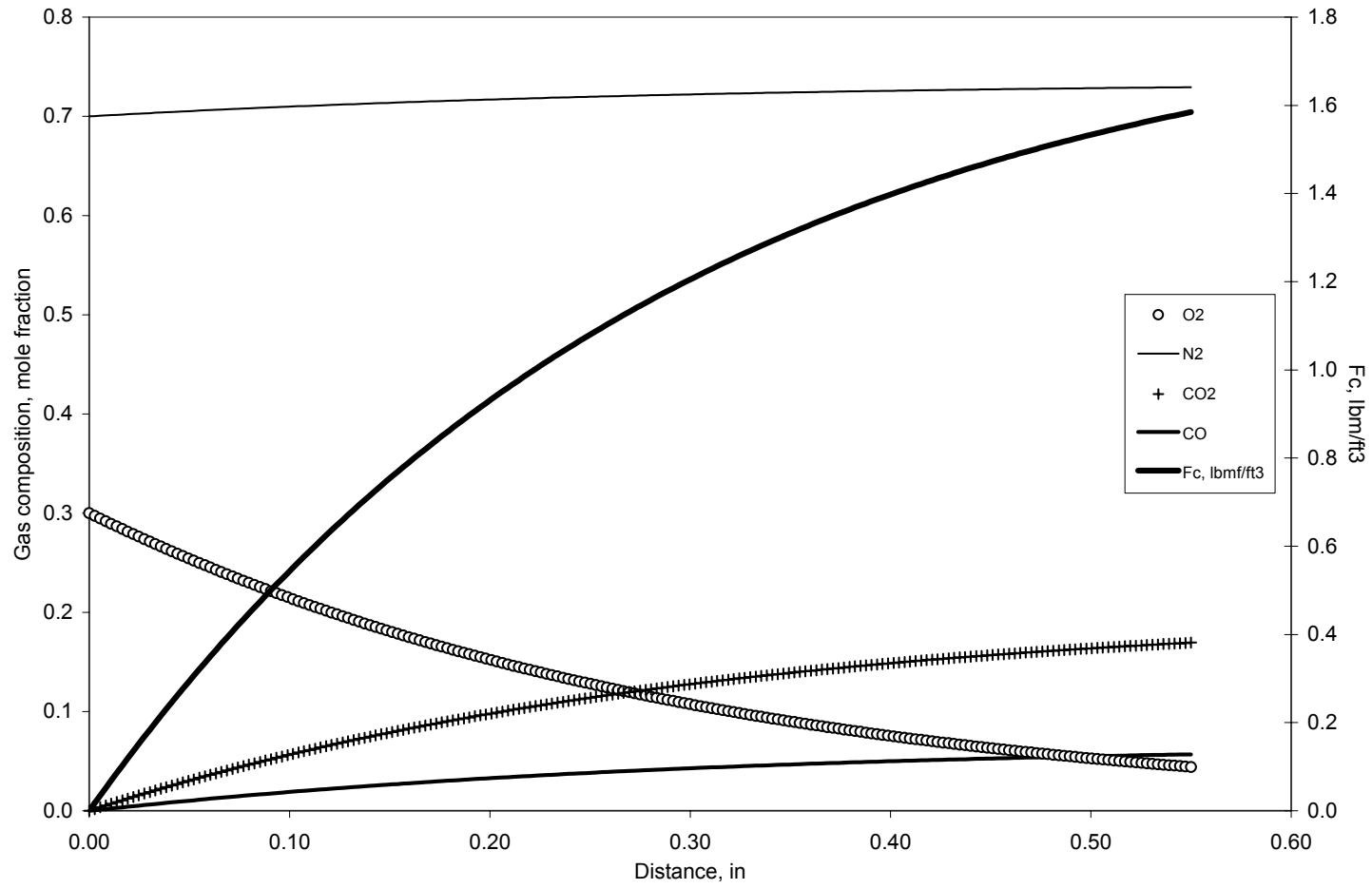


Fig. 5.9—Verification of the combustion zone model (run no. 4, 30% oxygen).

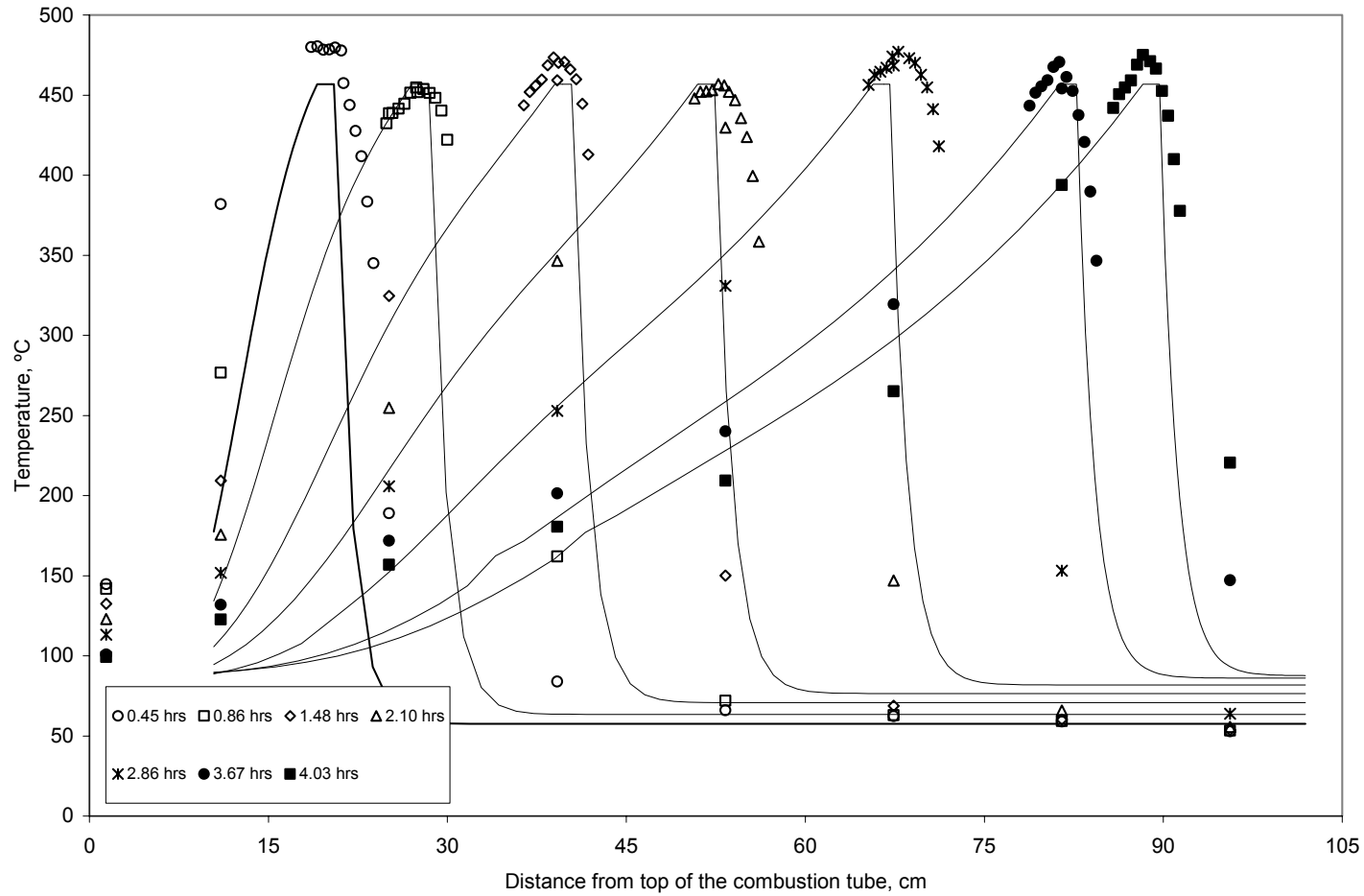


Fig. 5.10—Observed and estimated temperature profiles (run no. 4, 30% oxygen).

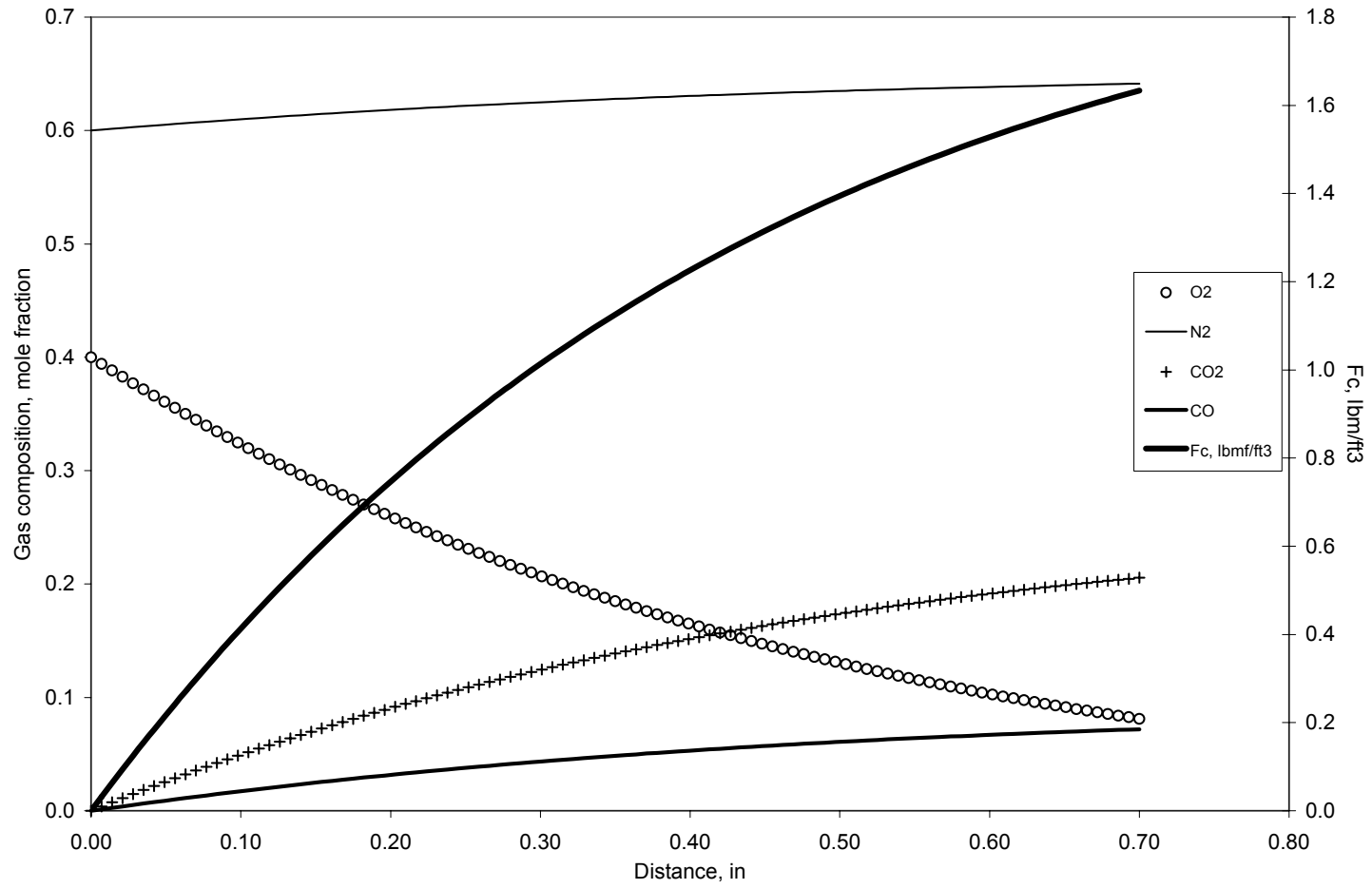


Fig. 5.11—Verification of the combustion zone model (run no. 5, 40% oxygen).

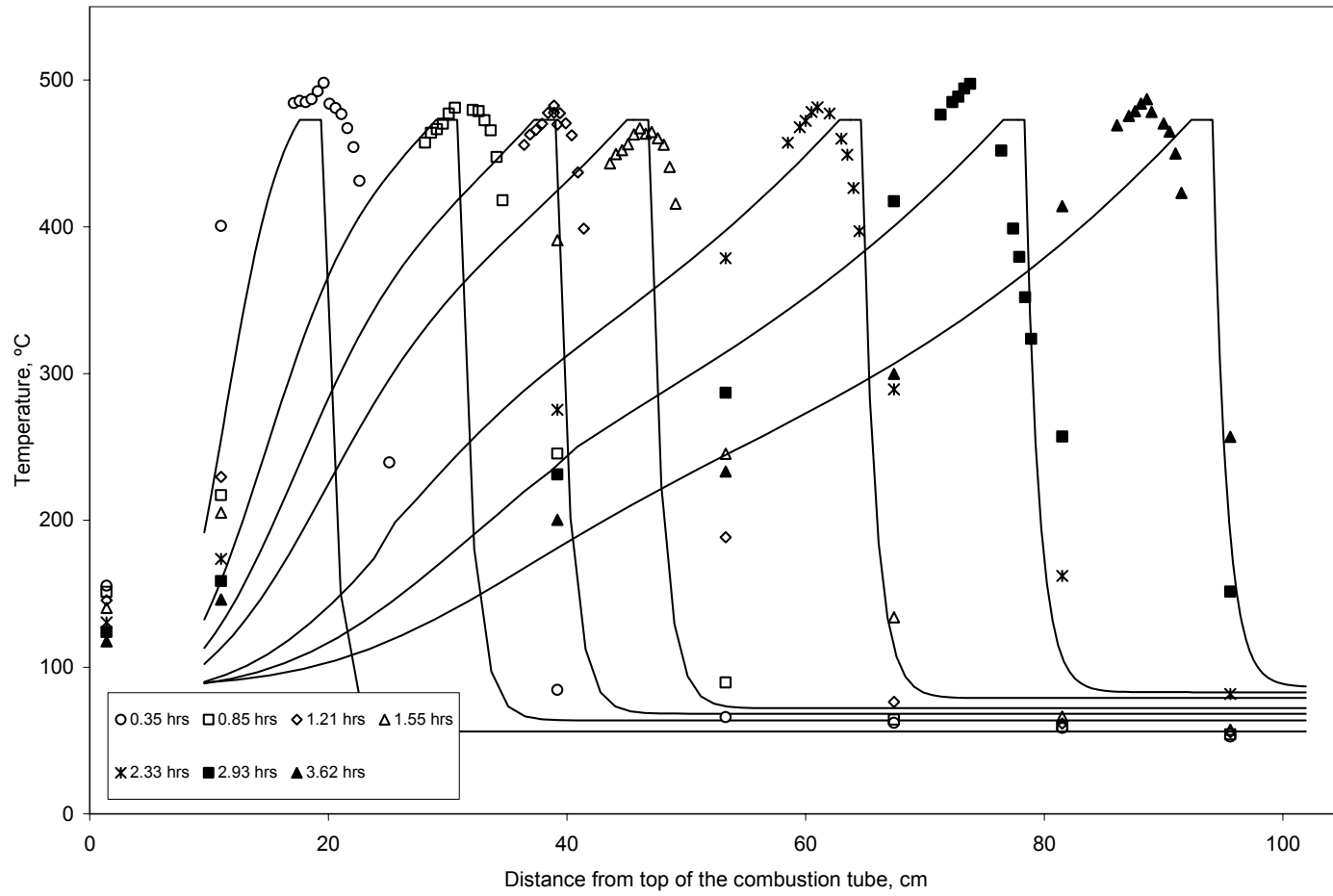


Fig. 5.12—Observed and estimated temperature profiles (run no. 5, 40% oxygen).

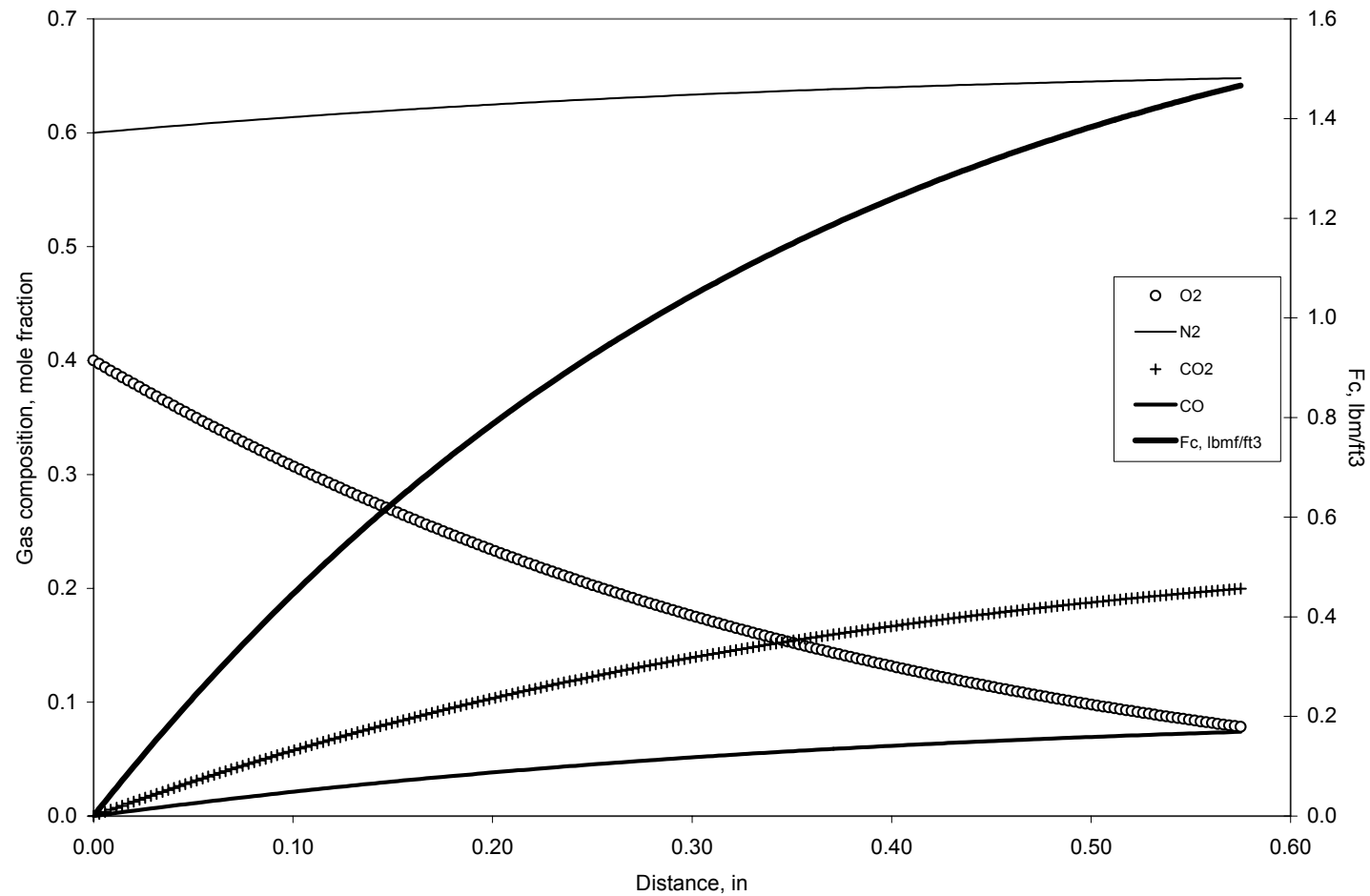


Fig. 5.13—Verification of the combustion zone model (run no. 6, 40% oxygen).

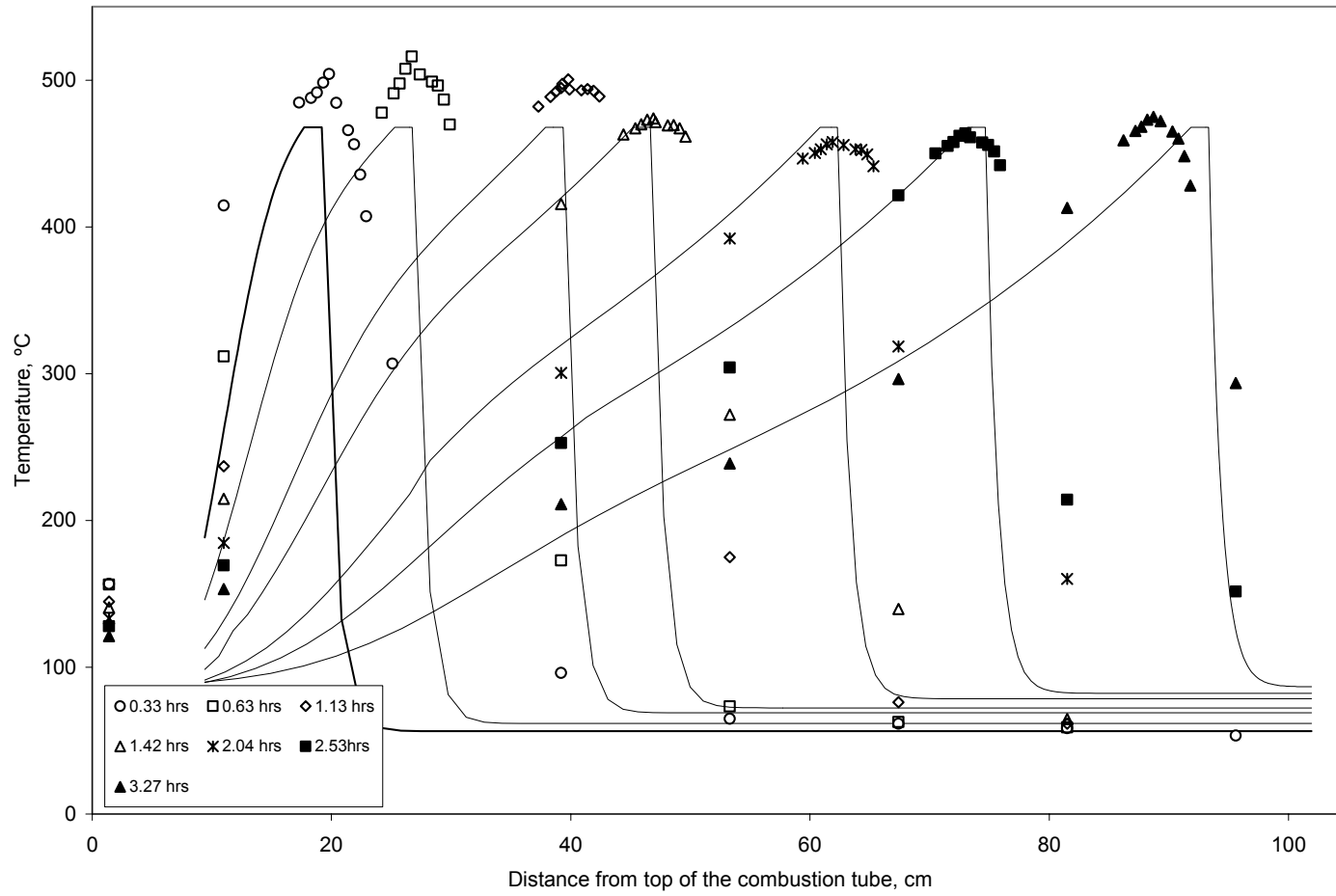


Fig. 5.14—Observed and estimated temperature profiles (run no. 6, 40% oxygen).

5.5 Summary of experimental results

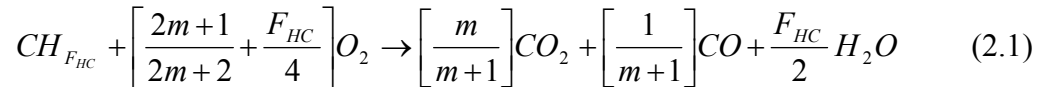
Table 5.1 is a summary of the most important parameters observed and estimated for the different experimental runs.

TABLE 5.1—SUMMARY OF EXPERIMENTAL RESULTS						
	Run 2	Run 7	Run 3	Run 4	Run 5	Run 6
O_2 inj., mole %	21	21	30	30	40	40
CO_2 prod. , mole %	12.41	10.30	15.90	16.94	20.50	20.00
O_2 prod. , mole %	2.29	2.09	5.14	4.42	8.12	7.83
N_2 prod. , mole %	81.22	83.55	73.73	72.89	63.98	64.84
CO prod. , mole %	4.10	4.07	5.21	5.69	7.17	7.40
F_C , lbmfuel/ft ³	1.725	1.449	1.651	1.585	1.632	1.467
ΔH_c , Btu/lbm fuel	15544	18100	16566	15731	16458	16934
F_{HC}	1.174	2.230	1.509	1.244	1.511	1.709
$CO / (CO + CO_2)$	0.248	0.283	0.247	0.251	0.259	0.270
CO_2 / CO	3.029	2.537	3.054	2.976	2.858	2.701
CO / CO_2	0.330	0.394	0.327	0.336	0.350	0.370
Comb. front. vel., cm/hr	13.42	13.46	17.55	19.29	22.09	24.70
O_2 efficiency	0.894	0.906	0.837	0.859	0.810	0.819
Start oil prod., hrs	3.25	3.08	3.00	2.60	2.02	1.75
Oil recovery, % OIIP	80.56	81.90	85.01	81.82	82.06	83.63
Ave. °API	13.45	16.04	16.21	16.64	15.49	15.48
Ave. viscosity @ 60°C, cp	143.5	66.3	54.7	46.3	80.5	78.5
L_{cz} , in. (model)	0.85	0.75	0.70	0.55	0.70	0.56
T_c , °C (model)	450	440	460	455	475	465

CHAPTER VI

STOICHIOMETRIC ANALYSIS

Stoichiometry of in-situ combustion may be described by Eq. 2.1. The heat of combustion may be estimated from **Fig. 1.1** for a particular hydrogen-carbon ratio and CO/CO_2 ratio of the produced gas.



Stoichiometry analysis is performed to verify any changes that may occur as a result of increasing the oxygen concentration in the injected air during oxygen-enriched in-situ combustion runs.

An observation of Eq. 2.1 leads us to infer, that if the combustion fuel is the same (same F_{HC}), then it is possible that a higher O_2 concentration in the injected air could result in more of the CO gas to react with oxygen to form CO_2 . Thus, with oxygen-enriched in-situ combustion, it is possible that the ratio CO/CO_2 (or the inverse m value in Eq. 2.1) could increase as a result of “cleaner” burning of the fuel.

In **Fig. 1.1**, the coefficient β is the inverse of m ; therefore, an increase in the m value corresponds to a decrease of the coefficient β in **Fig. 1.1**. A smaller β coefficient (cleaner oxidation), for the same combustion fuel will generate more heat per unit mass of burned fuel. However, results of combustion runs (Table 5.1) indicate that the m value does not change with concentration of oxygen in the injected air. Values range 2.5 to 3.0 for oxygen concentration of 21% to 40%. Thus, there is no clear evidence that the combustion stoichiometry changes with oxygen-enriched in situ combustion. The increase in oxygen concentration in the injected air results only in accelerating the combustion of the fuel and thus increasing the combustion front velocity (**Fig. 6.1**). With higher combustion front velocity, heat loss is reduced, resulting in slighter higher combustion zone temperatures. However, oxygen-enriched air injection did not increase the oil recovery (**Fig. 6.2**).

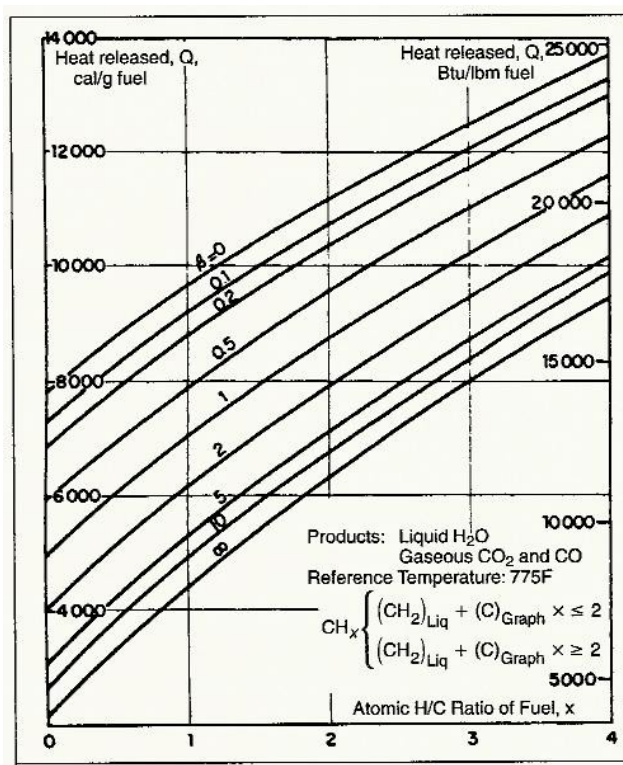


Fig. 1.1—Heat of combustion as a function of the H/C ratio, F_{HC} , of the fuel and the CO/CO_2 ratio in the produced gases.²¹

Increased oil quality (oil upgrading) is seen in **Fig. 6.3**. An increase in the injected oxygen concentration in the air appears to promote an increase of the API gravity from an original 11.1 °API to a maximum of 16.6 °API for a 30 mole % oxygen concentration. Similar apparent upgrading can be observed in **Fig. 6.4**, in which oil viscosity at 60°C, originally 568 cp, is reduced to a minimum of 46.3 cp at a 30 mole % oxygen concentration. Such apparent oil upgrading may be the result of distillation and thermal cracking occurring ahead of the combustion zone.

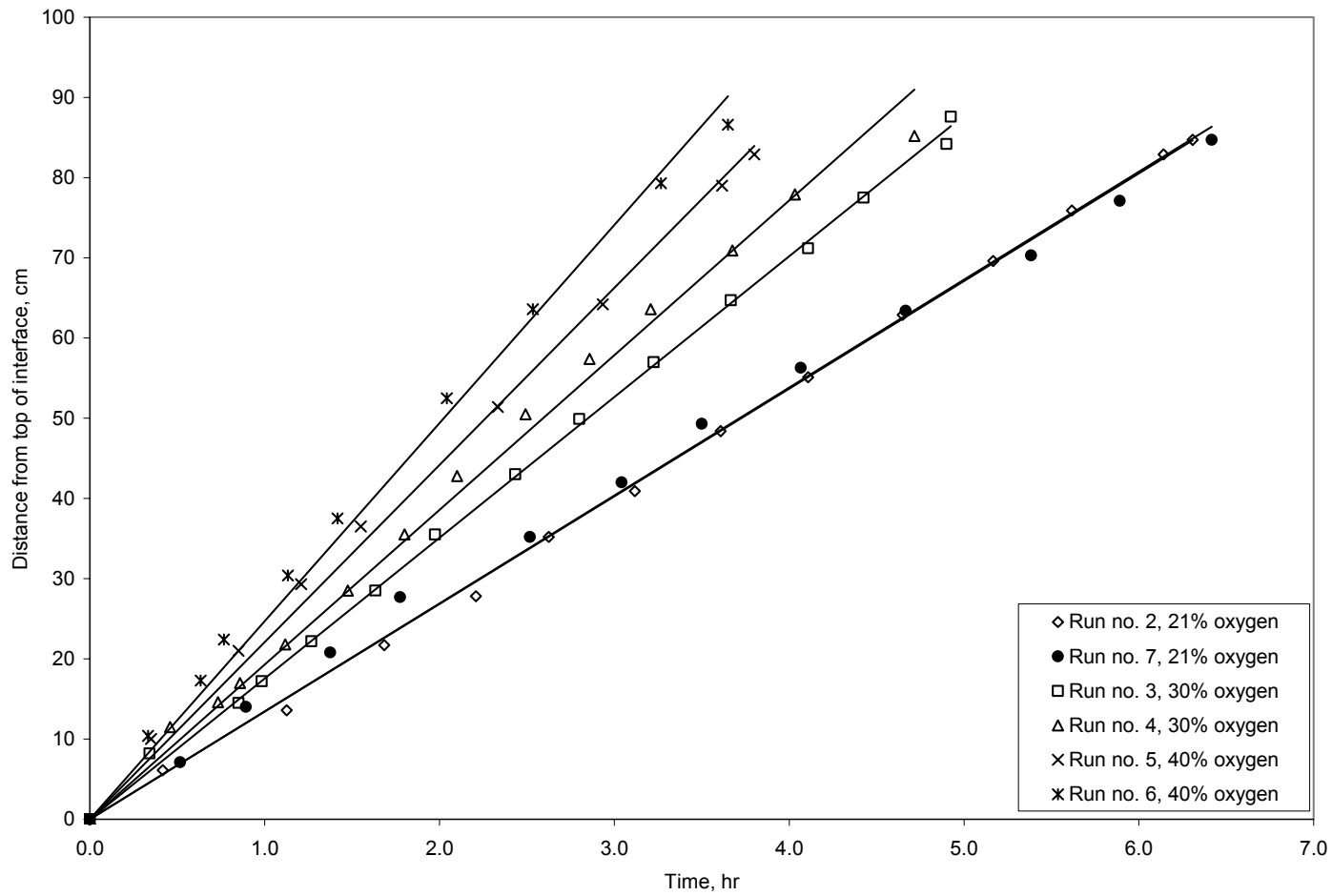


Fig. 6.1—Combustion front velocity for all runs.

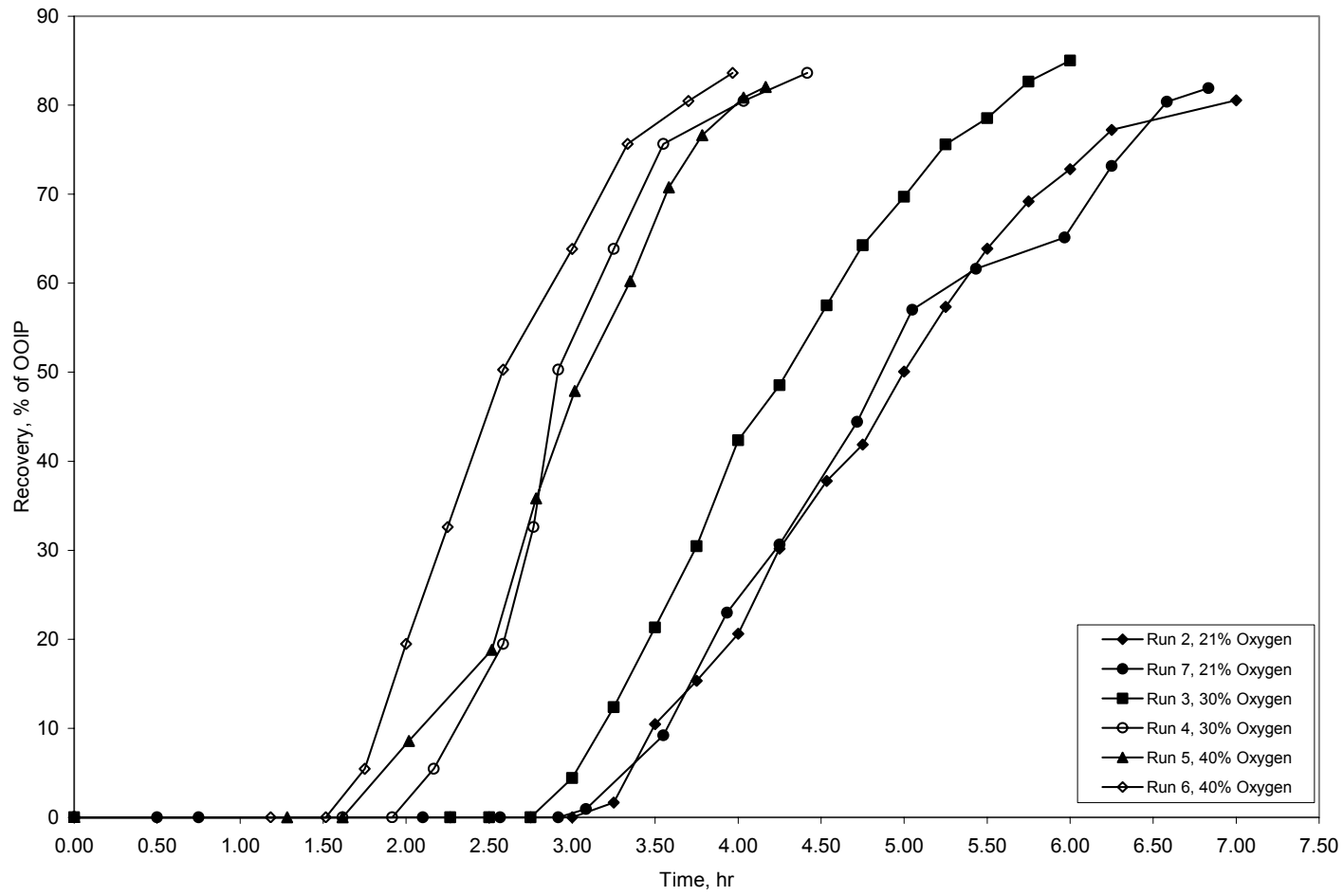


Fig. 6.2—Oil recovery for all runs.

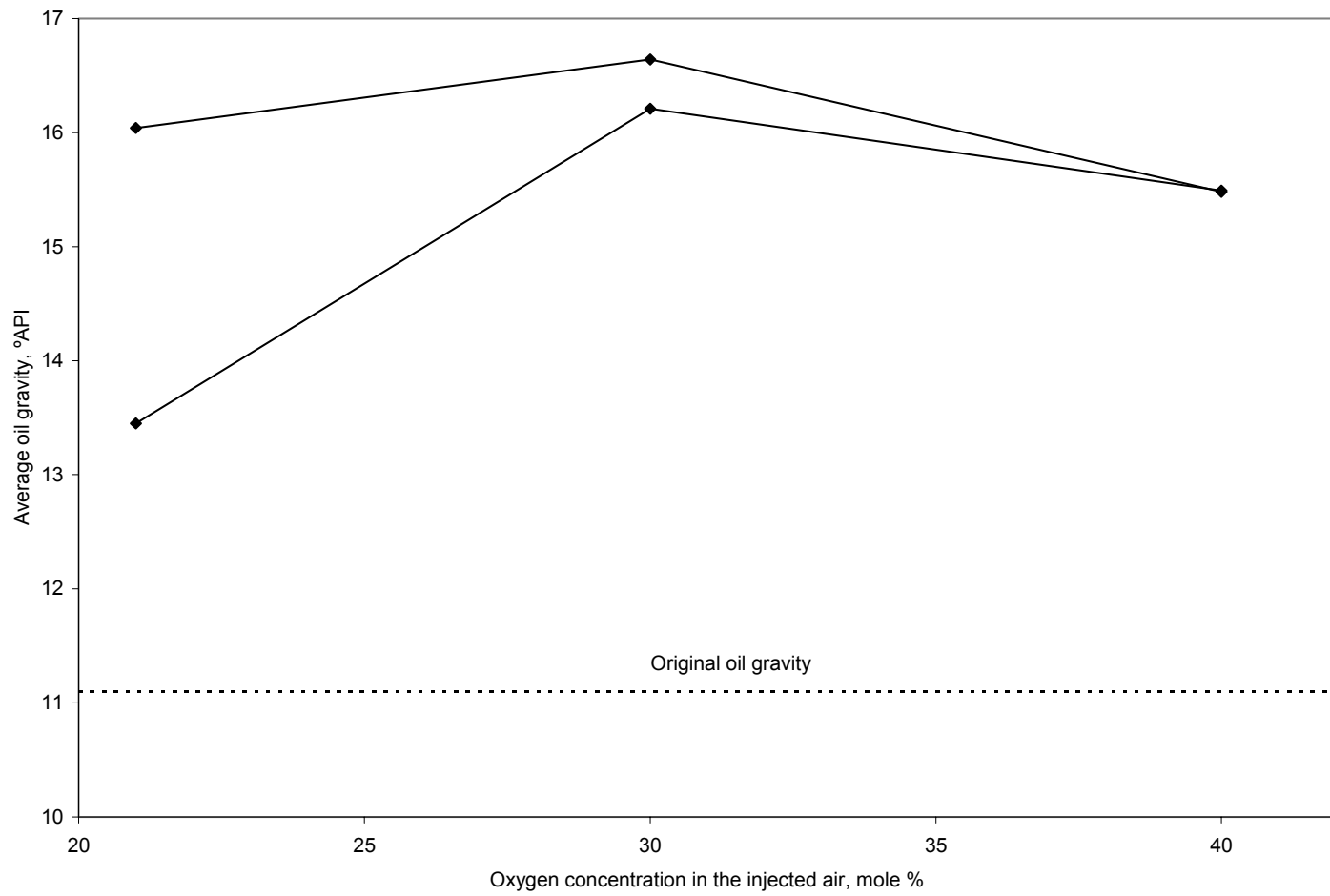


Fig. 6.3—Average API gravity of produced oil for all runs.

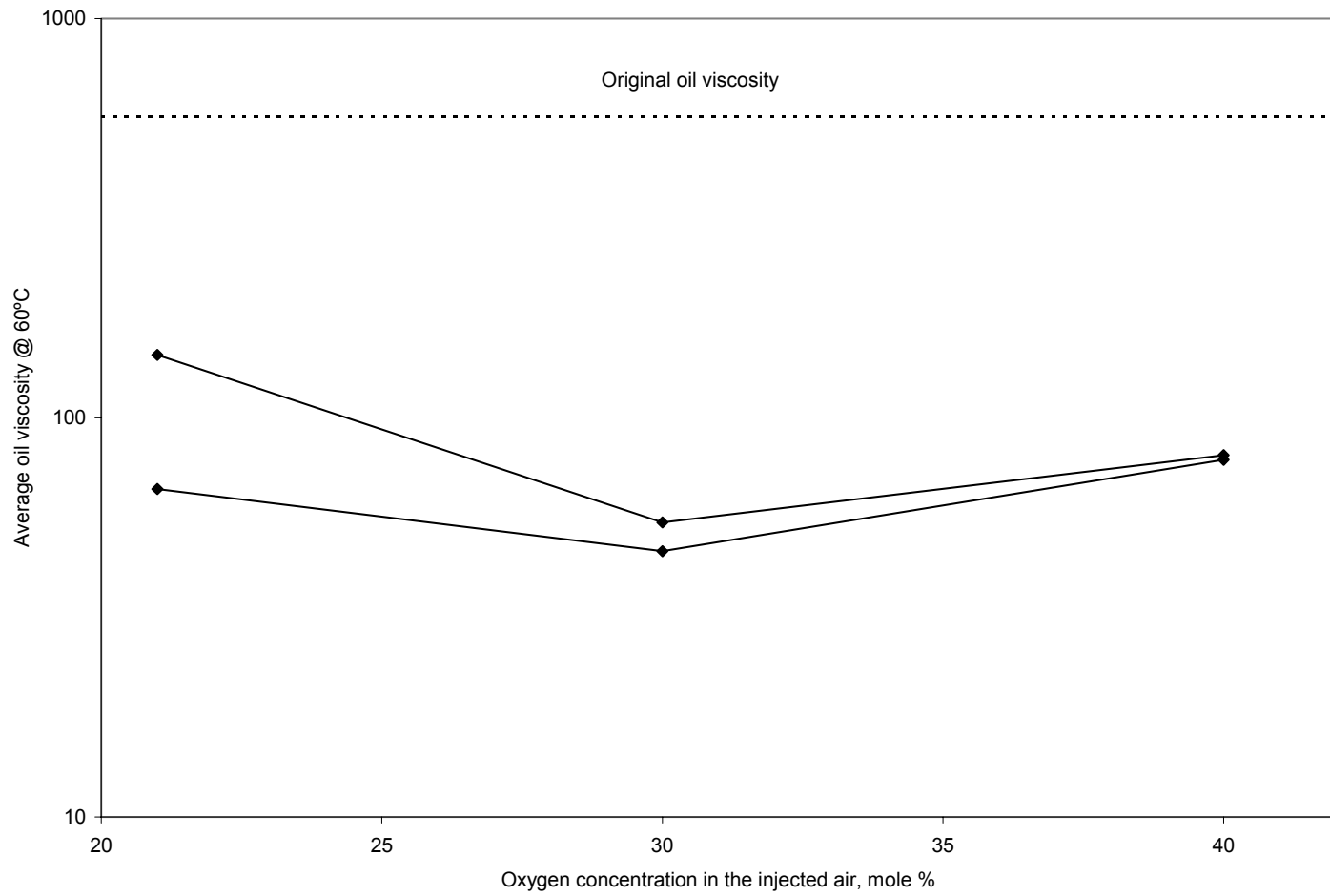


Fig. 6.4—Average produced oil viscosity at 60°C for all runs.

CHAPTER VII

SUMMARY, CONCLUSIONS, AND RECOMMENDATIONS

The main objective of my research was to develop an analytical model to estimate the combustion zone temperature on combustion stoichiometry with increase in oxygen concentration in the injected air.

7.1 Summary

Six combustion tube runs were performed with Jobo crude oil (9-11°API) from the Orinoco Belt in Venezuela. These runs were carried out with air containing three values of oxygen concentration, 21%, 30%, and 40%. The weight percentage of sand, clay, water, and oil in the sand mix was kept constant in all runs. Injection air rates (3 L/min) as well as the production pressure (300 psig) were kept constant in all runs. Stoichiometric analysis of the produced combustion gas, combustion front temperatures, temperature profiles behind and ahead of the combustion front, and fuel concentration were determined to help verify the new analytical model of the combustion zone.

A new analytical model of the combustion zone has been developed. The model consists of a combustion zone of known thickness, which is divided into elements of equal thickness. The amount of fuel burned in each element is based on oxidation reaction kinetics, while the amount of oxygen consumed in each element is based on combustion stoichiometry. The fuel concentration and produced gas composition may then be estimated. Using the model fuel concentration, the amount of heat generated in the combustion zone may be estimated. Using a heat balance that includes heat loss from the combustion zone and heat conducted and convected behind and ahead of the combustion front, the combustion front temperature may then be calculated.

7.2 Conclusions

Based on the experimental results, the following conclusions may be drawn.

1. The new combustion zone analytical model has been verified. The calculated combustion zone temperatures and temperature profiles are in good agreement with the experimental data, for the range of oxygen concentration in the injected air.

2. The model combustion zone temperature varied from 450°C in a 21 mole % O_2 concentration to a maximum of 475°C for air with 40 mole % O_2 concentration, in line with the experimental results.
3. The use of a higher oxygen concentration in the injected air slightly increased the combustion front temperature. However, the oxygen utilization efficiency decreased from 89% for (21% oxygen) to 81% (for 40% oxygen), as a result of the excess oxygen which increased the average O_2 concentration in the produced gas from 2.2% at an injected 21 mole % O_2 concentration to 8.1% for an injected 40 mole % O_2 concentration.
4. With oxygen-enriched air injection, the combustion front velocity increased from 13.4 cm/hr (for 21% oxygen) to 24.7 cm/hr (for 40% oxygen), and thereby reduced the start of oil production from 3.3 hours (for 21% oxygen) to 1.8 hours (for (40% oxygen). In the field, the use of oxygen-enriched air injection could translate into earlier oil production compared to with unenriched air injection.
5. Oxygen-enriched in-situ combustion does not increase the oil recovery, which averaged 83% of the original oil placed in the combustion tube for all runs.
6. Higher oxygen concentration in the injected air appears to increase the average produced oil gravity, from an original 11.1°API to a low of 13.5 °API (for 21 % oxygen) up to a maximum of 16.6 °API (for 30% oxygen). At the same time, oil viscosity (originally at 568 cp at 60°C), appears to decrease to a minimum of 46.3 cp for a 30 mole % oxygen concentration in the injected air.

7.3 Recommendations

1. In the new combustion zone analytical model, the combustion front thickness has to be specified. It is therefore recommended to follow up with research that aims at an independent determination of the combustion zone thickness. This probably would require more extensive use of reaction kinetics.
2. Further research is necessary to establish a better relationship between oxygen-enriched in-situ combustion and oil upgrading.

NOMENCLATURE

$a_R =$	air requirement, scf/ft ³
$A =$	cross-sectional area of the sand mix in the combustion tube, ft ²
$A_r =$	pre-Arrhenius constant
$C =$	dimensionless heat loss constant
$C_g =$	specific heat of the injected air, Btu/lbm-°F
$C_m =$	specific heat of the matrix, Btu/lbm-°F
$CH_{FHC} =$	hydrocarbon fuel
$CO =$	produced mole % of carbon monoxide
$CO_2 =$	produced mole % of carbon dioxide
$dm =$	mass of fuel burned in an element of the combustion zone, lbm fuel
$dt =$	time period, hrs
$dx =$	length of elements in the combustion zone, ft
$E =$	activation energy, btu/mole
$E_{O_2} =$	oxygen utilization efficiency, fraction
$F_C =$	fuel concentration, lbm fuel/ft ³
$F_{HC} =$	hydrogen-carbon ratio
$\Delta H_c =$	heat generated in the combustion zone, Btu/lbm fuel
$k =$	thermal conductivity of the matrix, Btu/(hr-ft-°F)
$L =$	length of the sand mix in the combustion tube, ft
$L_{cz} =$	combustion zone thickness, ft
$m =$	moles of CO_2 produced per mole of CO produced during in-situ combustion or reaction order with respect to P_{O_2}
$m_f =$	mass of burned fuel, lbm fuel
$m' =$	ratio of $CO/(CO + CO_2)$ in the combustion gas
$n =$	reaction order with respect to F_C or number of elements in the combustion zone
$n_p =$	moles of produced gas, mole
$N_2 =$	produced mole % of nitrogen

$O_2 =$	produced mole % of oxygen
$O_{2c} =$	consumed mole % of oxygen
$O_{2i} =$	injected mole % of oxygen
$O_{2p} =$	produced mole % of oxygen during the combustion run
$P_{O_2} =$	oxygen partial pressure, psia
$q =$	volumetric flow rate, scf/hr
$r_t =$	radius of the combustion tube, ft
$R =$	universal gas constant
$S_g =$	percentage of initial gas saturation in the combustion tube
$S_o =$	percentage of initial oil saturation in the combustion tube
$S_w =$	percentage of initial water saturation in the combustion tube
$t =$	time, hr
$t_D =$	dimensionless time variable
$T =$	absolute temperature, °R
$T_a =$	ambient temperature, °F
$T_{ah} =$	temperature at a distance dx of the combustion zone, °F
$T_c =$	combustion front temperature, °F
$T_D =$	dimensionless temperature variable
$T_{ext} =$	exterior temperature, °F
$U =$	overall heat transfer coefficient with respect to the radius of the combustion tube, Btu/(hr-ft ² -°F)
$U_a =$	injected air flux, scf/hr-ft ²
$V_f =$	combustion front velocity, ft/hr
$x =$	distance from the burning front, ft
$x_D =$	dimensionless distance variable
$\alpha =$	thermal diffusivity, ft ² /hr
$\beta =$	convection wave velocity, ft/hr
$\gamma =$	heat loss constant
$\Phi =$	porosity of the sand mix in the combustion tube, percentage

Subscripts

$i =$ time level

$n =$ time or location in the combustion zone

REFERENCES

1. White, P.D.: "In-Situ Combustion Appraisal and Status," *JPT* (November 1985) 1943.
2. Kuhn, C.S. and Koch, R.L.: "In-Situ Combustion—Newest Method of Increasing Oil Recovery," *Oil & Gas J.* (August 1953) **52**, 92.
3. Grant, B.F. and Szasz, S.E.: "Development of Underground Heat Wave for Oil Recovery," *JPT* (May 1954) 23; *Trans.*, AIME, **201**.
4. Moss, J.T., White, P.D., and McNeil, J.S.: "In-Situ Combustion—Results of a Five-Well Field Experiment in Southern Oklahoma," *JPT* (April 1959) 55; *Trans.*, AIME, **216**.
5. Gates, C.F., and Ramey, H.J. Jr.: "Field Results of South Belridge Thermal Recovery Experiment," *Trans.*, AIME (1958), **213**, 236.
6. Koch, R.L.: "Practical Use of Combustion Drive at West Newport Field," *Pet. Eng.* (January 1965) **37**, No. 1, 72.
7. Gates, C.F., and Sklar, I.: "Combustion as a Primary Recovery Process—Midway Sunset Field," *JPT* (August 1971) 981; *Trans.*, AIME, **251**.
8. Vogel, L.C., and Krueger, R.F.: "An Analog Computer for Studying Heat Transfer During a Thermal Recovery Process," *Trans.*, AIME (1955), **204**, 208.
9. Ramey, H.L. Jr.: "Transient Heat Conduction During Radial Movement of a Cylindrical Heat Source—Applications to the Thermal Recovery Process," *Trans.*, AIME (1959), **216**, 115.
10. Bailey, H.R., and Larkin, B.K.: "Conduction-Convection in Underground Combustion," *Trans.*, AIME (1960), **219**, 320.
11. Chu, C.: "Two-Dimensional Analysis of a Radial Heat Wave," *JPT* (October 1963) 1137.
12. Thomas, G.W.: "A Study of Forward Combustion in a Radial System Bounded by Permeable Media," *JPT* (October 1963) 1145.
13. Penberthy, W.L., and Ramey, H.J. Jr.: "Design and Operation of Laboratory Combustion Tubes," *SPEJ* (June 1966) 183.

14. Penberthy, W.L.: "An Investigation of the Fundamentals of Combustion Recovery," Ph.D. dissertation, Texas A&M University, College Station, TX (1967).
15. Agca, C., and Yortsos, Y.C.: "Steady-State Analysis of In-Situ Combustion," paper SPE 13624 presented at the 1985 California Regional Meeting, Bakersfield, CA, 27-29 March.
16. Millour, J.P, Moore, R.G., Bennion, D.W., Ursenbach, M.G., and Gie, D.N.: "A Simple Implicit Model for Thermal Cracking of Crude Oils," paper SPE 14226 presented at the 1985 SPE Annual Technical Conference and Exhibition, Las Vegas, NV, 22-25 September.
17. Belgrave, J.D.M., Moore, R.G., Ursenbach, M.G., and Bennion, D.W.: "A Comprehensive Approach to In-Situ Combustion Modeling," paper SPE 20250 presented at the 1990 SPE/DOE Symposium on Enhanced Oil Recovery, Tulsa, 22-25 April.
18. Crookston, R.B., Culham, W.E., and Chen, W.H.: "A Numerical Simulation Model for Thermal Recovery Processes," *SPEJ* (February 1979) 37.
19. Youngren, G.K.: "Development and Application of an In-Situ Combustion Reservoir Simulator," *SPEJ* (February 1980) 39.
20. Coats, K.H.: "In-Situ Combustion Model," *SPEJ* (December 1980) 533.
21. Burger, J.G., and Sahuquet, B.C.: "Laboratory Research on Wet Combustion," *JPT* (October 1973) 1137.
22. Martin, W.L., Alexander, J.D., and Dew, J.N.: "Process Variables of In-Situ Combustion," *Trans., AIME* (1958), **213**, 28.
23. Wu, C.H., and Fulton, P.F.: "Experimental Simulation of the Zones Preceding the Combustion Front in an In-Situ Combustion Process," *SPEJ* (September 1963) 127.
24. Alexander, J.D., Martin, W.L., and Dew, J.N.: "Factors Affecting Fuel Availability and Composition During In-Situ Combustion," *JPT* (October 1962) 1154.
25. Nelson, T.W., and McNeil, J.S. Jr.: "How to Engineer an In-Situ Combustion Project," *Oil & Gas J.* (June 1961) 58.

26. Bousaid, I.S., and Ramey, H.J. Jr.: "Oxidation of Crude Oil in Porous Media," *SPEJ* (June 1968) 137.
27. Dabbous, M.K., and Fulton, P.F.: "Low-Temperature Oxidation Reaction Kinetics and Effects on the In-Situ Combustion Process," *SPEJ* (June 1974) 253.
28. Thomas, G.W., Buthod, A.P., and Allag, O.: "An Experimental Study of the Kinetics of Dry, Forward Combustion-Final Report," Report No. BETC-1820-1, distributed by DOE (February 1979).
29. Moss, J.T., and Cady, G.V.: "Laboratory Investigation of the Oxygen Combustion Process for Heavy Oil Recovery," paper SPE 10706 presented at the 1982 SPE California Regional Meeting, San Francisco, 24-26 March.
30. Hansel, J.G., Benning, M.A., and Fernbacher, J.M.: "Oxygen In-Situ Combustion Oil Recovery: Combustion Tube Tests," *JPT* (July 1984) 1139.
31. Shahani, G.H., and Hansel, J.G.: "Oxygen Fireflooding: Combustion Tube Tests with Light, Medium, and Heavy Crude Oils," *JPT* (November 1987) 583.
32. Petit, H.J.M.: "In-Situ Combustion with Oxygen-Enriched Air," paper SPE 16741 presented at the 1987 Annual Technical Conference and Exhibition, Dallas, 27-30 September.
33. Benham, A.L., and Poettmann, F.H.: "The Thermal Recovery Process—An Analysis of Laboratory Combustion Data," *Trans.*, AIME (1958), **213**, 406.
34. Mamora, D.D.: "Kinetics of In-Situ Combustion," Ph.D. dissertation, Stanford University, Stanford, CA (1993).
35. Mamora, D.D.: "New Findings in Low-Temperature Oxidation of Crude Oil," paper SPE 29324 presented at the 1995 Asia Pacific Oil and Gas Conference, Kuala Lumpur, Malaysia, 20-22 March.
36. Mamora, D.D., and Brigham, W.E.: "The Effect of Low-Temperature Oxidation on the Fuel and Produced Oil During In-Situ Combustion," *In Situ* (1995), **19**, No. 4, 341.
37. Greaves, M., Ren, S.R., and Xia, T.X.: "New Air Injection Technology for IOR Operations in Light and Heavy Oil Reservoirs," paper SPE 57295 presented at the

1999 Asia Pacific Improved Oil Recovery Conference, Kuala Lumpur, Malaysia, 25-26 October.

38. Turta, A.T., and Singhai, A.K.: "Reservoir Engineering Aspects of Light-Oil Recovery by Air Injection," *SPEERE&E* (August 2001) 336.

APPENDIX

Public Sub Front()

```
Dim Cfc(1400) As Double, massf(1400) As Double, O2in As Double, _
    nO2c(1400) As Double, nO2out(1400) As Double, N2in As Double, _
    nCO2p(1400) As Double, nCOp(1400) As Double, nO2f(1400) As Double, _
    nCO2f(1400) As Double, nCOf(1400) As Double, nN2f(1400) As Double, _
    Dist(1400) As Double, molfuel(1400) As Double, Tmassf(1400) As Double, _
    O2out As Double, Fmass(1400) As Double, Tcc(1400) As Double
```

```
Dim x(1000) As Double, xd(1000) As Double, xx1(1000) As Double, xx6(1000) As
Double, _
xx2(1000) As Double, xx3(1000) As Double, xx4(1000) As Double, xx5(1000) As
Double, _
xx As Double, erfxx1(1000) As Double, erfxx2(1000) As Double, erfxx3(1000) As
Double, _
erfxx5(1000) As Double, Theta(1000) As Double, Tempb(1000) As Double,
Tempa(1000) As Double, _
axx As Double, axx1 As Double, axx11 As Double, axx2 As Double, axx3 As Double,
axx4 As Double, _
axx5 As Double, Temp(1000) As Double, _
erfxx4(1000) As Double, erfxx6(1000) As Double, erfcxx1(1000) As Double, _
erfcxx2(1000) As Double, erfcxx3(1000) As Double, _
erfcxx4(1000) As Double, erfcxx5(1000) As Double, erfcxx6(1000) As Double
```

```
Worksheets("Data").Select
With Worksheets("Data")
Range("A22:M1358").Select
Selection.ClearContents
```

End With

Worksheets("Table").Select

With Worksheets("Table")

Range("C5:F1500").Select

Selection.ClearContents

End With

With Worksheets("Data")

Range("D11").Select

O2i = .Cells(3, 2) 'Mole Percentage of O2 in injected air

CO2 = .Cells(4, 2) 'Average Mole Percentage of CO2 in produced gas

O2 = .Cells(5, 2) 'Average Mole Percentage of O2 in produced gas

N2 = .Cells(6, 2) 'Average Mole Percentage of N2 in produced gas

CO = .Cells(7, 2) 'Average Mole Percentage of CO in produced gas

C = .Cells(16, 2) 'Heat Loss Factor, dimensionless

Text = .Cells(3, 7) 'Ambient temperature, °C

Tr = .Cells(4, 7) 'Initial pack temperature, °C

Ts = .Cells(5, 7) 'Steam Plateau temperature, °C

Pres = .Cells(6, 7) 'Pressure, psi

Por = .Cells(7, 7) 'Porosity in combustion tube cell, frac

Length = (40 + 1 / 8) 'Total Length of Combustion Tube, in

Diam = .Cells(3, 4) 'Dia of combustion tube, in

wth = .Cells(4, 4) 'wall thickness of combustion tube, in

clsand = .Cells(5, 4) "Clean Sand height = Reference zero, cm

L = (Length * 2.54 - clsand) / 30.48 'Filled Length with mixture, ft

.Cells(18, 7) = L

Qinj = .Cells(6, 4) * 1000 / 30.48 ^ 3 * 60 'Injection Gas rate, scf/hr

Qprod = .Cells(2, 7) * 1000 / 30.48 ^ 3 * 60 'Produced Gas rate, scf/hr

rt = .Cells(7, 4) 'Run time, hr

t = .Cells(8, 4) 'Analysis time, hr

```

.Cells(13, 11) = Qinj
Trf = Tr * 1.8 + 32 'Initial pack temperature, °F
Tsf = Ts * 1.8 + 32 'Steam Plateau temperature, °F
T0 = Tr 'Reference Temperature, °C
T0f = 1.8 * T0 + 32 'Reference Temperature, °F
Tsf = Tsf - T0f
Textf = Text * 1.8 + 32 'Ambient temperature, °F
Ta = Tr - Text
Taf = 1.8 * Ta + 32 '- T0f
tdc = 100 'dimensionless time
Sw = .Cells(14, 11) 'Initial Water Saturation in combustion cell,frac
API = .Cells(15, 11) 'Initial Oil API gravity in combustion cell
Area = 3.1416 / 4 * (Diam / 12 - 2 * wth / 12) ^ 2 'Area of Combustion cell, ft2
.Cells(17, 7) = Area
radt = (Diam) / 24 ' Radius of combustion cell, ft - 2 * wth
MWO2 = 2 * 15.9994 'Molecular Weight of O2
MWCO2 = 12.01115 + 2 * 15.9994 'Molecular Weight of CO2
MWCO = 12.01115 + 15.9994 'Molecular Weight of CO
MWN2 = 2 * 14.0067 'Molecular Weight of N2
MW = (O2 * MWO2 + CO2 * MWCO2 + CO * MWCO + N2 * MWN2) / 100 _
'Molecular Weight of Combustion gas
' Calculations
mp = CO / (CO + CO2)
m = CO2 / CO
FHC = 4 * (O2i / (100 - O2i) * N2 - (CO2 + 0.5 * CO + O2)) / _
      (CO2 + CO) 'Apparent Molecular Weight of fuel
molprod = Qprod * rt / 379 'lbmol of fuel, lbmolf
mfuel = (12 + FHC) * (m + 1) * CO / 100 * molprod 'mass of fuel burned, lbmfuel
Cf = mfuel / (Area * L) 'Fuel Concentration, lbmfuel/ft3 pore volume

```

```

EO2 = 1 - (100 - O2i) / O2i * (O2 / N2)      'Oxygen Efficiency
Ua = Qinj / (Area)  'Air flux, scf/(hr-ft2)
aR = 379 / (O2i / 100 * EO2) * _
      ((2 * m + 1) / (2 * m + 2) + FHC / 4) * (Cf / (12 + FHC)) 'Air Requirement, scf/ft3
Vf = Ua / aR  'Combustion Front velocity, ft/hr
Faf = 379 * N2 * 100 / _
      ((100 - O2i) * (CO + CO2) * (12 + FHC))  'Air-Fuel Ratio, scf/lbmfuel
DeltaHf = 1800 / (12 + FHC) * _
      (94# - 67.9 * mp + 31.2 * FHC) 'Heat released per unit mass of fuel, Btu/lbmfuel
' PRINT TO WORKSHEET DATA
.Cells(3, 11) = mp  'CO/(CO+CO2) ratio
.Cells(4, 11) = m  'CO2/CO ratio
.Cells(5, 11) = FHC  'Apparent Molecular Weight of fuel
.Cells(6, 11) = Qprod  'Produced Gas rate, scf/hr
.Cells(7, 11) = molprod 'lbmol of fuel, lbmolf
.Cells(3, 14) = mfuel  'mass of fuel burned, lbmfuel
.Cells(4, 14) = Cf  'Fuel Concentration, lbmfuel/ft3
.Cells(5, 14) = Ua  'Air flux, scf/(hr-ft2)
.Cells(6, 14) = EO2  'Oxygen Efficiency
.Cells(7, 14) = aR  'Air Requirement, scf/ft3
.Cells(8, 14) = Vf  'Combustion Front velocity, ft/hr
.Cells(9, 14) = Faf  'Air-Fuel Ratio, scf/lbmfuel
.Cells(12, 14) = DeltaHf  'Heat released per unit mass of fuel, Btu/lbmfuel
Imass = .Cells(11, 4) ' Assumed Initial Fuel Mass, lbmf
n = .Cells(13, 7)  'Number of segments in the combustion zone
With Worksheets("Calc_Temp")
Range("A5:J100").Select
Selection.ClearContents
Range("A1").Select

```

End With

'Initializing

Tig = 300 'Ignition Temperature, °C

Tigf = Tig * 1.8 + 32 'Ignition Temperature, °F

Tigk = Tig + 273 'Ignition Temperature, °K

Tigr = Tigf + 460 'Ignition Temperature, °R

Z = 1# 'Gas Compressibility Factor, dimensionless

Rhor = 2.65 * 62.4 'Density of Formation, lbm/ft³

fq = 0.85 'Quartz fraction in formation, dimensionless

Rhog = (Pres + 14.7) * (MW) / _
(10.73 * Z * (Tigr)) 'Density of Gas, lbm/ft³

CgO₂ = (7.16 + 0.001 * Tigk - 0.0000004 * Tigk ^ 2) / MWO₂

CgCO₂ = (10.57 + 0.0021 * Tigk - 0.00000206 * Tigk ^ 2) / MWCO₂

CgCO = (6.79 + 0.00098 * Tigk - 0.00000011 * Tigk ^ 2) / MWCO

CgN₂ = (6.83 + 0.0009 * Tigk - 0.00000012 * Tigk ^ 2) / MWN₂

Cg = (O₂ * CgO₂ + CO₂ * CgCO₂ + CO * CgCO + N₂ * CgN₂) / 100
'Specific Heat Capacity of the Gas, Btu/(lbm °F)

Cr = (Tigf + 2000) / 10000 + _
(Tigf - Textf) / 20000 'Specific Heat Capacity of the Formation, Btu/(lbm °F)

kk = 0

Tmassf(0) = 0 ' Initialization total fuel mass in the combustion zone, lbmf

' Estimate of thermal conductivity, k, of the matrix

khs = 4.45 * fq + 1.65 * (1 - fq)

KHR = 0.735 - 1.3 * Por + 0.39 * khs * Sw ^ 0.5

k = khr - 0.00028 * (Tigf - 125) * (khr - 0.82)

' Thermal conductivity of the matrix, Btu/(ft-hr-°F)

alpha = k / (Rhor * Cr) ' Thermal diffusivity, ft²/hr

Ua = (Qinj * 14.7 * Tigr / ((60 + 460) + (Pres + 14.7)))
'Air flux in the combustion zone, scf/(hr-ft²)


```

beta = Vf - (Rhog * Cg * Ua * Por) / (Rhor * Cr)
      'Convection wave velocity, ft/hr
gamma = C * beta ^ 2 / alpha 'Heat loss constant
U = gamma * (Rhor * Cr * radt) / 2 'Overall heat transfer coefficient, Btu/(ft2-hr-°F)
bda = beta / alpha 'constant for use in temperature model
bcda = beta ^ 2 / alpha 'constant for use in temperature model
*** PRINT TO SHEET DATA ***
.Cells(13, 2) = k ' Thermal conductivity of the matrix, Btu/(ft-hr-°F)
.Cells(14, 2) = alpha ' Thermal diffusivity, ft2/hr
.Cells(15, 2) = beta ' Convection wave velocity, ft/hr
.Cells(18, 2) = U ' Overall heat transfer coefficient, Btu/(ft2-hr-°F)
.Cells(17, 2) = gamma ' Heat loss constant
*** END OF PRINT TO SHEET DATA ***
Lcz = .Cells(12, 7) ' Estimated combustion length interval, in
dx = Lcz / n ' Length of each element dx
rt = (dx / 12) / ((Vf) / 3600) ' residence time or injection time in dx, sec
dt = rt / 3600 ' time period, hrs
nO2out(0) = (Qinj / 3600) / 379 * (O2i / 100) * rt 'moles O2 entering element dx, lbmol
N2in = (Qinj / 3600) / 379 * (100 - O2i) / 100 * rt 'moles N2 entering element dx, lbmol
nCO2p(0) = 0 'initial moles CO2
nCOp(0) = 0 'initial moles CO
nO2f(0) = O2in / 100 'initial moles O2
*** INITIALIZATION OF DATA ***
Cfc(0) = 0
.Cells(22, 1) = 0
.Cells(22, 2) = rt
.Cells(22, 3) = 0
.Cells(22, 4) = 0
.Cells(22, 5) = nO2out(0)

```

```
.Cells(22, 6) = nO2out(0)
.Cells(22, 7) = nO2out(0) / (nO2out(0) + N2in)
.Cells(22, 8) = nCO2p(0)
.Cells(22, 9) = nCOp(0)
.Cells(22, 10) = N2in / (nO2out(0) + N2in)
.Cells(22, 11) = 0
.Cells(22, 12) = 0
.Cells(22, 13) = 0
'*** END OF INITIALIZATION OF DATA ***
```

```
'*** COMBUSTION ZONE THICKNESS MODEL ***'
```

```
nO2f(0) = nO2out(0) / (nO2out(0) + N2in)
i = 1
O2p = 0
Do While Abs(O2p - O2 / 100) > 0.00001
If i = 1 Then
massf(1) = Imass
Else
massf(1) = massf(1) * (O2i / 100 - O2 / 100) / ((O2i / 100 - O2p))
.Cells(11, 4) = massf(1)
End If
For j = 1 To n
Emass = massf(1)
molfuel(j) = massf(j) / (12 + FHC) 'moles of fuel to burn
nO2c(j) = molfuel(j) * ((2 * m + 1) / (2 * m + 2) + FHC / 4) 'moles O2 required to burn
massf
nO2out(j) = nO2out(j - 1) - nO2c(j)
nCO2p(j) = nCO2p(j - 1) + (m / (m + 1)) * molfuel(j) 'moles CO2 produced in dx
nCOp(j) = nCOp(j - 1) + (1 / (m + 1)) * molfuel(j) 'moles CO produced in dx
```

```

nO2f(j) = nO2out(j) / _
      (nO2out(j) + nCO2p(j) + nCOp(j) + N2in) ' moles fraction O2 out entering next
element
nCO2f(j) = nCO2p(j) / _
      (nO2out(j) + nCO2p(j) + nCOp(j) + N2in) ' moles fraction CO2 out entering next
element
nCOf(j) = nCOp(j) / _
      (nO2out(j) + nCO2p(j) + nCOp(j) + N2in) ' moles fraction CO out entering next
element
nN2f(j) = N2in / _
      (nO2out(j) + nCO2p(j) + nCOp(j) + N2in) ' moles fraction N2 out entering next
element
Tmassf(j) = Tmassf(j - 1) + massf(j) 'Total fuel mass burned
Fmass(j) = Fmass(j - 1) + Tmassf(j - 1) + massf(j)
Cfc(j) = Tmassf(j) / ((dx / 12) * Area) 'Fuel concentration, lbmfuel/ft3* (1 - Por)
massf(j + 1) = massf(j) * nO2f(j) / nO2f(j - 1) ' mass in next dx, lbm fuel
O2p = nO2f(j)      'Assign value for comparisson purposes
'LastFuel = massf(j) 'Assign value for future use
TotalFuel = Tmassf(j) 'Assign value for future use
'Fc = Cfc(j)      'Assign value for future use
Next j
i = i + 1
Imass = Emass      'Assign value for future use
Loop
'*** END OF COMBUSTION ZONE THICKNESS MODEL ***

'*** BEGINNING OF HEAT GENERATED AND LOST IN THE COMBUSTION
ZONE ****
q = 1

```

$T_{cc}(q - 1) = 300 * 1.8 + 32$ 'Assumed initial combustion front temperature, °F

Do While $Abs(T_c - T_{cc}(q - 1)) > 0.01$

$$T_c = (T_{cc}(q - 1) - 32) / 1.8$$

$$T_{c_{ff}} = T_c * 1.8 + 32 - T_{0f}$$

$i = 1000$ 'Temporary index

$td1 = 0.000000000001$ 'Very short time ahead of the front

$$a1 = -T_{af} * \text{Exp}(-C * td1) / (T_{c_{ff}} - T_{af})$$

$$a2 = T_{af} * \text{Exp}(-C * td1) / (2 * (T_{c_{ff}} - T_{af}))$$

$$x(i) = (dx / 2) / 12 \text{ 'feet}$$

$$xd(i) = bda * x(i)$$

$$xx1(i) = xd(i) / (2 * td1^{0.5}) - 0.5 * td1^{0.5}$$

$$\text{erfxx1}(i) = \text{Erfa}(xx1(i))$$

$$\text{erfcxx1}(i) = 1 - \text{erfxx1}(i)$$

$$xx2(i) = xd(i) / (2 * td1^{0.5}) + 0.5 * td1^{0.5}$$

$$\text{erfxx2}(i) = \text{Erfa}(xx2(i))$$

$$\text{erfcxx2}(i) = 1 - \text{erfxx2}(i)$$

$$xx3(i) = \text{Exp}(-0.5 * (xd(i) * (1 + (1 + 4 * C)^{0.5})))$$

$$xx4(i) = xd(i) / (2 * td1^{0.5}) - 0.5 * ((1 + 4 * C) * td1)^{0.5}$$

$$\text{erfxx4}(i) = \text{Erfa}(xx4(i))$$

$$\text{erfcxx4}(i) = 1 - \text{erfxx4}(i)$$

$$xx5(i) = \text{Exp}(-0.5 * (xd(i) * (1 - (1 + 4 * C)^{0.5})))$$

$$xx6(i) = xd(i) / (2 * td1^{0.5}) + 0.5 * ((1 + 4 * C) * td1)^{0.5}$$

$$\text{erfxx6}(i) = \text{Erfa}(xx6(i))$$

$$\text{erfcxx6}(i) = 1 - \text{erfxx6}(i)$$

$$\begin{aligned} \text{Theta}(i) = & a1 + a2 * (\text{Exp}(-xd(i)) * \text{erfcxx1}(i) + \text{erfcxx2}(i)) _ \\ & + 0.5 * (xx3(i) * \text{erfcxx4}(i) + xx5(i) * \text{erfcxx6}(i)) \end{aligned}$$

$T_{ahf} = \text{Theta}(i) * (T_{c_{ff}} - T_{af}) + T_{af} + T_{0f}$ 'Temperature ahead at a distance dx, °F

$T_{ah} = (T_{ahf} - 32) / 1.8$ 'Temperature ahead at a distance dx, °C

```

Cr = (Tahf + 2000) / 10000 + _
(Tahf - Textf) / 20000
AAA = DeltaHf * TotalFuel
BBB = 2 * 3.1416 * (Lcz / 12) * U * (dx / 12) / Vf
ZZZ = (1 - Por) * Cr * Rhor * Area
Tcc(q) = (AAA - BBB * (Tcc(q - 1) - Textf) + _
ZZZ * ((Lcz / 12) * Tcc(q - 1) + (dx / 12) * Tahf)) / _
(ZZZ * (Lcz / 12 + dx / 12))
With Worksheets("Calc_Temp")
.Cells(5 + q, 5) = AAA
.Cells(5 + q, 6) = BBB
.Cells(5 + q, 7) = Tahf
.Cells(5 + q, 8) = Cr
End With
Tc = Tcc(q - 1)
Tcf = Tc
kk = kk + 1
With Worksheets("Calc_Temp")
.Cells(4 + kk, 1) = massf(1)
.Cells(4 + kk, 2) = Lcz * kk
.Cells(4 + kk, 3) = (Tcc(q - 1) - 32) / 1.8
.Cells(4 + kk, 4) = (Tcc(q) - 32) / 1.8
End With
With Worksheets("Data")
.Cells(13, 14) = (Tcc(q - 1) - 32) / 1.8
.Cells(14, 14) = (Tcc(q) - 32) / 1.8
.Cells(15, 14) = q
End With
q = q + 1

```

```

Worksheets("Data").Select
Range("D11").Select
Loop
*** END OF HEAT GENERATED AND LOST IN THE COMBUSTION ZONE ****
j = j + 1
*** END OF PRINT TO WORKSHEET DATA COMBUSTION ZONE THICKNESS
RESULTS ***
For ww = 1 To n
.Cells(22 + ww, 1) = massf(ww)
.Cells(22 + ww, 2) = rt
.Cells(22 + ww, 3) = molfuel(ww)
.Cells(22 + ww, 4) = nO2c(ww)
.Cells(22 + ww, 5) = nO2out(ww - 1)
.Cells(22 + ww, 6) = nO2out(ww)
.Cells(22 + ww, 7) = nO2f(ww)
.Cells(22 + ww, 8) = nCO2f(ww)
.Cells(22 + ww, 9) = nCOf(ww)
.Cells(22 + ww, 10) = nN2f(ww)
.Cells(22 + ww, 11) = Tmassf(ww)
.Cells(22 + ww, 12) = Cfc(ww)
.Cells(22 + ww, 13) = ww * dx
Next ww
*** END OF PRINT TO WORKSHEET DATA COMBUSTION ZONE THICKNESS
RESULTS ***
***** BEGINNING OF TEMPERATURE PROFILE (PENBERTHY'S
MODEL)*****
Tcff = Tcf - T0f
td = bcda * t
xf = Vf * t

```

```

L2 = (xf) / 30
a1 = -Taf * Exp(-C * td) / (Tcff - Taf)
a2 = 0.5 * Taf * Exp(-C * td) / (Tcff - Taf)
  For i = 0 To 30 Step 1  'BEHIND THE FRONT
    x(i) = (xf - L2 * i)
    If x(i) < 0 Then x(i) = 0
    xd(i) = bda * (L2 * i)
    If td > tdc Then
      Theta(i) = Exp(-xd(i) / 2 * (-1 + (1 + 4 * C) ^ 0.5))
      Temp(i) = Theta(i) * (Tcff - Taf) + Taf + T0f
    Else
      xx1(i) = (xd(i) / (2 * td ^ 0.5) - 0.5 * td ^ 0.5)
      erfxx1(i) = Erfa(xx1(i))
      erfcxx1(i) = 1 - erfxx1(i)
      xx2(i) = (xd(i) / (2 * td ^ 0.5) + 0.5 * td ^ 0.5)
      erfxx2(i) = Erfa(xx2(i))
      erfcxx2(i) = 1 - erfxx2(i)
      xx3(i) = Exp(-0.5 * xd(i) * (-1 + (1 + 4 * C) ^ 0.5))
      xx4(i) = xd(i) / (2 * td ^ 0.5) - 0.5 * ((1 + 4 * C) * td) ^ 0.5
      erfxx4(i) = Erfa(xx4(i))
      erfcxx4(i) = 1 - erfxx4(i)
      xx5(i) = Exp(0.5 * xd(i) * (1 + (1 + 4 * C) ^ 0.5))
      xx6(i) = xd(i) / (2 * td ^ 0.5) + 0.5 * ((1 + 4 * C) * td) ^ 0.5
      erfxx6(i) = Erfa(xx6(i))
      erfcxx6(i) = 1 - erfxx6(i)
      Theta(i) = a1 + a2 * (erfcxx1(i) + Exp(xd(i)) * erfcxx2(i)) _
        + 0.5 * (xx3(i) * erfcxx4(i) + xx5(i) * erfcxx6(i))
      Temp(i) = Theta(i) * (Tcff - Taf) + Taf + T0f
    End If
  
```

```

With Worksheets("Table")
    .Cells(35 - i, 3) = xd(i)
    .Cells(35 - i, 4) = x(i) * 30.48 + clsand 'cm
    .Cells(35 - i, 5) = (Temp(i) - 32) / 1.8    °C
End With
Next i
'AT THE COMBUSTION FRONT
For i = 1 To n
    x(i) = (xf + dx / 12 * i)
    xd(i) = beta * (dx / 12 * i) / alpha
    With Worksheets("Table")
        .Cells(35 + i, 3) = xd(i)
        .Cells(35 + i, 4) = x(i) * 30.48 + clsand 'cm
        .Cells(35 + i, 5) = (Tcf - 32) / 1.8 °C
    End With
Next i
'END OF THE COMBUSTION FRONT
L1 = ((L - xf - Lcz / 12)) / 50
For i = 1 To 50 'AHEAD OF THE FRONT
    x(i) = (xf + L1 * i)
    xd(i) = bda * (L1 * i)
    If td > tdc Then
        Theta(i) = Exp(-xd(i) / 2 * (1 + (1 + 4 * C) ^ 0.5))
        Temp(i) = Theta(i) * (Tcff - Taf) + Taf + T0f
    Else
        xx1(i) = 0.5 * (xd(i) / td ^ 0.5 - td ^ 0.5)
        erfxx1(i) = Erfa(xx1(i))
        erfcxx1(i) = 1 - erfxx1(i)
        xx2(i) = 0.5 * (xd(i) / td ^ 0.5 + td ^ 0.5)
    End If
Next i

```



```

erfxx2(i) = Erfa(xx2(i))
erfcxx2(i) = 1 - erfxx2(i)
xx3(i) = Exp(-0.5 * xd(i) * (1 + (1 + 4 * C) ^ 0.5))
xx4(i) = 0.5 * (xd(i) / td ^ 0.5 - ((1 + 4 * C) * td) ^ 0.5)
erfxx4(i) = Erfa(xx4(i))
erfcxx4(i) = 1 - erfxx4(i)
xx5(i) = Exp(-0.5 * (xd(i) * (1 - (1 + 4 * C) ^ 0.5)))
xx6(i) = 0.5 * (xd(i) / td ^ 0.5 + ((1 + 4 * C) * td) ^ 0.5)
erfxx6(i) = Erfa(xx6(i))
erfcxx6(i) = 1 - erfxx6(i)
Theta(i) = a1 + a2 * (Exp(-xd(i)) * erfcxx1(i) + erfcxx2(i)) _
          + 0.5 * (xx3(i) * erfcxx4(i) + xx5(i) * erfcxx6(i))
Temp(i) = Theta(i) * (Tcff - Taf) + Taf + T0f
End If

With Worksheets("Table")
    .Cells(35 + i + n, 3) = xd(i)
    .Cells(35 + i + n, 4) = x(i) * 30.48 + clsand + Lcz * 2.54 'cm
    .Cells(35 + i + n, 5) = (Temp(i) - 32) / 1.8 '°C
End With

Next i
'***** END OF TEMPERATURE PROFILE (PENBERTHY'S MODEL)*****

End
End With
End Sub
' ***** ERROR FUNCTION ROUTINE *****

Function Erfa(axx As Double) As Double
cc1 = 0.254829592
cc2 = -0.284496736
cc3 = 1.421413741

```

```
cc4 = -1.453152027
cc5 = 1.061405429
If axx < 0 Then
  axx = Abs(axx)
  tp = 1 / (1 + 0.3275911 * axx)
  Erfa = -(1 - (cc1 * tp + cc2 * tp ^ 2 + _
    cc3 * tp ^ 3 + cc4 * tp ^ 4 + cc5 * tp ^ 5) * Exp(-axx ^ 2))
Else
  tp = 1 / (1 + 0.3275911 * axx)
  Erfa = (1 - (cc1 * tp + cc2 * tp ^ 2 + _
    cc3 * tp ^ 3 + cc4 * tp ^ 4 + cc5 * tp ^ 5) * Exp(-axx ^ 2))
End If
End Function
```

VITA

Name: Jose Ramon Rodriguez

Permanent Address: Universidad de Oriente
Núcleo de Anzoátegui
Departamento de Ingeniería de Petróleo
Barcelona, Anzoátegui, 6001, Venezuela
Phone: (01158281) 2623259-60
Email: moncho00@yahoo.com

Education: Universidad de Oriente
Barcelona, Anzoátegui, Venezuela, Petroleum Engineering
B.S. Petroleum Engineering, 1990

Texas A&M University
College Station, Texas
M.S. Petroleum Engineering, 2001

Texas A&M University
College Station, Texas
Ph.D. Petroleum Engineering, 2004

Experience: Instructor Professor 1995-1998
Universidad de Oriente, Barcelona, Anzoátegui, Venezuela

Production Engineer 1989-1995
Simupet C.A., Petroleum Engineering Consulting Company
Barcelona, Anzoátegui, Venezuela